1968

MECHANICAL EFFECTS OF ACOUSTIC TRANSIENTS ON TOBACCO MOSAIC VIRUS

Philip Edward Hamrick

Abstract of MECHANICAL EFFECTS OF ACOUSTIC TRANSIENTS ON TOBACCO MOSAIC VIRUS by Philip Edward Hamrick, Department of Biophysics, Medical College of Virginia, June 1968

The mechanical breakage of tobacco mosaic virus (TMV) due to the action of acoustic transients has been investigated. The acoustic transients were produced by transient heating of a Prussian blue dye solution (attenuation coefficient of 1000 per cm) when a ruby laser light (20×10^6 watts) was incident on the dye surface. A quartz piezoelectric transducer was used to determine the amplitude and form of the acoustic wave. The production of acoustic waves by transient heating is discussed, and the theoretical form of the acoustic wave determined for various boundary and initial conditions are compared to the experimentally measured values.

The electron microscope was used to compare particle length distributions of control TMV solutions and solutions exposed to the acoustic transients. Two conditions of exposure have been studied by varying the boundary conditions of the TMV solutions. In one case the TMV solution was exposed to a single acoustic transient whereas in the other case the solution was exposed to an acoustic transient which was reflected within the solution. Significantly greater breakage was produced in the latter case demonstrating the importance of boundary conditions in the biological effects of pressure transients.

Calculations were made of the magnitude of hydrodynamical forces producing tensions in the TMV particle. A laser intensity of 1.6×10^8 watts per cm^2 incident on the absorbing dye solution was found to be sufficient to cause significant breakage at the 5 percent

level (Kolmogorov-Smirnov test). The corresponding tension on the TMV particle was calculated to be 6.3×10^{-5} dynes.

MECHANICAL EFFECTS OF ACOUSTIC TRANSIENTS ON TOBACCO MOSAIC VIRUS

by

Philip Edward Hamrick

B.S., North Carolina State College, 1961

M.S., North Carolina State College, 1962

Thesis

submitted in partial fulfillment of the requirements for the

Degree of Doctor of Philosophy in the Department of

Biophysics at the Medical College of Virginia

Richmond, Virginia

June, 1968

This thesis by Philip Edward Hamrick

is accepted in its present form as satisfying the thesis requirement

for the degree of Doctor of Philosophy

Date:

10/3/67

Approved:

[redacted]

Advisor, Chairman of Graduate Committee

3 Oct 1967

10/3/67

10/3/67

[redacted]

APPROVED: [redacted]

Dean of the School of Graduate Studies

VITA

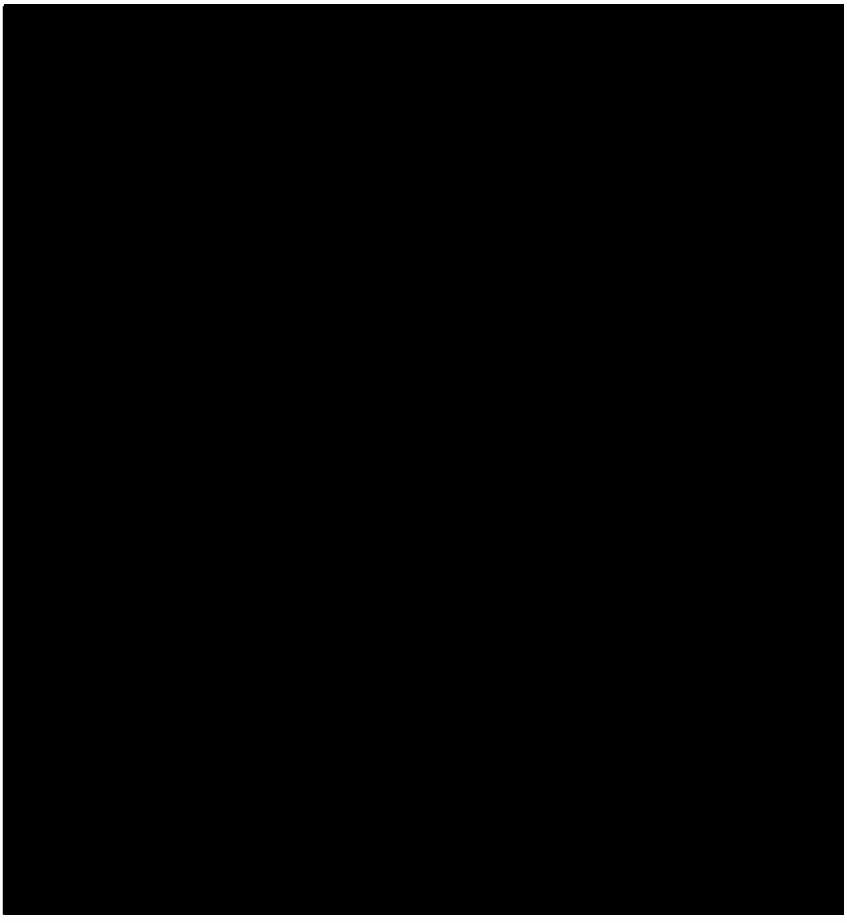

ACKNOWLEDGEMENTS

The author wishes to express his thanks to Dr. William T. Ham, Jr., chairman of the Department of Biophysics at the Medical College of Virginia, for leadership in providing an intellectually stimulating department in which to do research. The author thanks all members of the Department of Biophysics for their help and particularly Mr. Raymond Ruffin and Mr. Harold Mueller for aid in construction and calibration of the laser system used in this study.

Special acknowledgement and gratitude is expressed to Dr. Stephen F. Cleary of the Department of Biophysics for his patient guidance and for the genuine interest he has shown for the author.

The author wishes to thank Dr. Robert H. Brownson, chairman of the Department of Anatomy, for use of the electron microscope and Mrs. Shirley Craig also of the Department of Anatomy for technical assistance. For support as a graduate student, recognition is given to the National Institutes of Health and to the United States Army Medical Research and Development Command, Office of the Surgeon General.

Sincere appreciation is expressed to the author's wife, Caroline, for long hours spent in typing and for understanding and encouragement.

TABLE OF CONTENTS

TABLE OF CONTENTS (continued)

LIST OF TABLES

LIST OF FIGURES

LIST OF FIGURES (continued)

CHAPTER I - INTRODUCTION

A. INTRODUCTORY STATEMENT

The effects of intense dynamic pressures on biological systems have been the object of numerous investigations since 1927 when Wood and Loomas (1) first described the effects of a high frequency (300 kilocycles per second) pressure field on protozoa. The biological effects of pressure have been noted most often in the range of frequencies from just above the audible limit, approximately 17 kilocycles per second, to several megacycles per second (ultrasonic frequencies). The times employed in the ultrasonic irradiation of biological systems usually range from a few seconds to several hours. Thus, even the shortest irradiation times used would subject an organism to many thousands of oscillations from negative to positive pressures. In contrast to studies utilizing many thousands of pressure oscillations, the use of single pressure transients has received little attention.

The present study is directed toward an analysis of the mechanical effects of short duration pressure transients on a biological system. Tobacco mosaic virus (TMV), because of its well characterized geometrical shape and because it is one of the better understood viral systems, has been chosen as the biological model for study.

The recent development and application of physical systems capable of producing intense transient pressures has focussed attention on the possible biological effects of such pressure transients. One such system, the ruby laser first developed by Maiman (2), is a

source of high intensity monochromatic coherent electromagnetic radiation in the visible spectrum produced by light amplification by stimulated emission of radiation (LASER). Intense, short duration, pressure transients are produced by the absorption of this light in a material with a high optical attenuation coefficient (i.e., approximately 1000 cm^{-1}) at the wavelength of the laser. The widespread use of laser systems in modern technology has increased the need for a better understanding of the biological effects of pressure transients which might be induced in the human body by exposure to laser beams.

B. BIOLOGICAL ASPECTS

1. Effects of Continuous Wave Ultrasonic Irradiation

As noted in the introductory statement, the frequencies most often employed in examining the effects of pressure waves on biological systems have been in the ultrasonic region. Oscillating pressures in this frequency range are generated by means of magnetostrictive or piezoelectric transducers (3). An alternating voltage supply operated at its resonant frequency is employed in driving such a transducer so that the maximum output power is realized. The usual mode of irradiation is continuous wave (CW) irradiation. However, a transducer may be driven only during certain intervals of the irradiation period, thus producing a pulsed form of irradiation in which a specific period of time is required for the resonant circuit to reach its peak and to decay. The pulse length is thus chosen so that the rising and falling portions of the pulse can be neglected in comparison with the main

part of the pulse which is at the resonant frequency and amplitude of the driving oscillator. Typical rise and decay times are of the order of 10 microseconds so that pulses of one millisecond and longer are normally used (4). Therefore, even in pulsed operations, the biological specimen undergoes numerous pressure oscillations. Since most investigators of the biological effects of pressure have utilized continuous and/or pulsed oscillations rather than transients, it is useful to consider some of the findings in this field in order that comparisons may be made between the two types of irradiation.

Observed biological effects of ultrasonic irradiation are usually attributed either to thermal, chemical, or mechanical processes (5). The phenomenon of hydrodynamical cavitation which can give rise to all of these processes is believed to be the major factor leading to the observed biological effects of ultrasonic irradiation. It is appropriate therefore to consider cavitation and some of its more important effects.

Cavitation is a term applied to the process or processes by which cavities are formed in liquids. The lifetime of the cavity may vary from approximately 1 microsecond to several seconds, depending on the type of cavitation and the frequency of the applied ultrasonic field (6). In a liquid exposed to ultrasound, the type of cavity that is formed is dependent on the intensity of the pressure field, the state of the liquid with respect to dissolved gases, and the intrinsic hydrodynamical properties of the liquid such as surface tension forces, shear modulus and viscosity. Liquids under normal conditions contain trapped gases in the form

of bubbles as well as dissolved gases. These bubbles usually are finely dispersed and may be so small (i.e., on the order of 1 micron or less) that they cannot be seen with the unaided eye (7). These small bubbles constitute weak spots in the liquid and serve as nuclei for the production of cavities.

The van der Waals equation may be employed to demonstrate that a liquid undergoing cavitation must contain vacuoles of phase discontinuity or weak spots:

$$(p + av^{-2})(v - b) = RT \qquad \text{(I-1)}$$

where

p = pressure,

v = volume,

T = absolute temperature,

R = gas constant, and

a,b = van der Waals constants.

Although the van der Waals equation is usually applied to gases, Briggs (8) has applied it to liquids to get an approximate value of the cohesive forces which must be overcome in order that cavities may be produced in the liquid. The usual interpretation of van der Waals equation considers the terms av^{-2} and b as corrections to the ideal gas law with av^{-2} as the effective pressure due to the attractive forces between molecules and b as the effective volume of the molecules. If it is assumed that the liquid is incompressible, then the volume and the term av^{-2} are constants. The term av^{-2} may now be viewed as the internal pressure, P_i, arising from the attractive forces between the molecules that hold the volume of the liquid constant. The magnitude of this internal pressure may be

estimated from the known compressibilities of liquids (about 10^{-4} per atmosphere of pressure. If P_i, the internal pressure, is assumed to be large compared to P, then

$$\Delta P/P_i = -\Delta v/v \qquad \text{(I-2)}$$

or

$$P_i = -v\Delta P/\Delta v$$

which is the reciprocal of the compressibility. Therefore the cohesive forces in liquids are of the order of 10^4 atmospheres. Consequently, only at very high negative pressures would cavities be expected to form during ultrasonic irradiation. However, as noted below, cavities do appear at much lower negative pressures.

Hueter and Bolt (9) have reviewed the types of cavitation expected as a function of the ultrasonic pressure. In a liquid saturated with gas and exposed to a pressure field with a frequency of 60 kilocycles, for example, cavitation sets in at sound pressures of about 0.25 atmospheres. Large visible bubbles are formed which remain after the sound field is shut off. These gaseous cavities are formed by diffusion of dissolved gases out of the liquid into the small nuclei bubbles. The process by which this occurs is called rectified diffusion. It involves alternating diffusion into and out of the cavity as the pressure oscillates in response to the sound source, there being a net inward diffusion because the cavity surface is larger when the diffusion is inward. If the liquid is not saturated with gas, steady diffusion out of the cavity competes with the rectified diffusion, so that the cavity grows only if the sound pressure exceeds a threshold value which may be as high as several atmospheres.

In carefully degassed water a second type of cavitation occurs. As the sound pressure amplitude is raised to about four atmospheres (at 60 kilocycles per second) transient cavities are formed which collapse violently, giving rise to intense pressure waves. These transient cavities occur when the instantaneous pressure in the liquid falls so low that the original gas-filled bubble nucleus cannot remain stable simply by increasing its volume to a new equilibrium size. The resulting instability leads to a cavity filled primarily with vapor since gas diffusion is too slow to fill the rapidly expanding cavity. The cavity collapses as the vapor condenses during the positive portion of the pressure cycle. During collapse of the bubble, the walls of the bubble rush inward until the cushioning action of the gas within the bubble stops the radial motion. At the end of the collapse the contents of the bubble are highly compressed, resulting in high instantaneous temperatures which may lead to ionization effects as evidenced by luminescence and the formation of H and OH radicals and hydrogen peroxide (10). This mechanism of radical formation is believed to be responsible for the observed chemical effects that occur when biological materials are irradiated ultrasonically under conditions which lead to cavitation. However, the predominant biological effect is caused by the intense pressure waves that emanate from the cavitation centers. At 10 kilocycles per second, an initial bubble radius of 100 microns, and with a sound pressure of one atmosphere, shock waves having a peak pressure of 200 to 500 atmospheres at a distance of 0.1 centimeter from the bubble center have been observed (11).

The occurrence of cavitation thus appears to require the

presence of small, usually invisible, gas bubbles in the liquid. Strasberg (12) has noted that the smaller the bubbles, the larger the internal pressure. The internal pressure is given by:

$$P_i = P_o + 2sR^{-1} \qquad \text{(I-3)}$$

where

P_o = hydrostatic pressure,

s = surface tension, and

R = bubble radius.

Thus, it is expected that unless a liquid is supersaturated with gas, it cannot contain gas in the form of stable bubbles since the high internal pressure of the bubbles tends to force the gas within the bubble into solution in the liquid. However, experimental evidence indicates that small nuclei bubbles do remain in water that has been aged (i.e., allowed to remain undisturbed long enough for all visible bubbles to diffuse into the liquid)(13). Dust particles, container walls and other impurities may act as stabilizing agents by entrapping gases on their surfaces in the form of bubbles.

In order to predict theoretically when and where cavitation will take place on applying a given pressure field to a liquid, a knowledge of the nuclei bubble size and location throughout the liquid is needed. This is usually not known, so that the exact prediction of cavitation thresholds is difficult. However, approximate empirical thresholds have been determined as noted previously in the discussion of gaseous and vaporous cavitation. Since cavitation tends to degas the liquid, thresholds will increase with the duration of the irradiation. Cavitation thresholds also

increase as the frequency of the sound source increases. For example, Willard (14) has found that negative pressures of 120 atmospheres were required before cavitation could be produced at a frequency of 5 megacycles per second. His data indicate that an initiation phase involving the growth of nuclei bubbles is necessary before cavitation can begin. He concludes that cavitation cannot be produced in a single pressure cycle. Even if the bubble does expand and collapse during one cycle of pressure, the effect at high frequencies should be small since the magnitude of the pressure wave created by the collapsing bubble depends on the change in bubble radius from its largest to its smallest size (15). The time for expansion at high frequencies is less than for low frequencies, so that the maximum bubble radius is small.

Another phenomenon occurring in liquids exposed to ultrasonic pressure which is closely related to cavitation and occurs concomitantly with cavitation is bubble resonance. At the resonant frequency the expansion and collapse of the bubble becomes unstable and the bubble breaks into smaller bubbles which then grow to resonant size and start the process anew. The presence of many such resonating bubbles, colliding with other bubbles, collapsing, and forming smaller bubbles, will enhance the mechanical effects associated with liquids undergoing cavitation.

The above observations concerning the conditions which must exist when cavitation is produced in liquids undergoing continuous wave irradiation are also pertinent to liquids exposed to pressure transients. The duration of the pressure transients considered in the present study are of the order of 10^{-7} seconds which is also the

duration of the positive or negative portion of one cycle of pressure at a frequency of 5 megacycles per second. Under these conditions the transient is said to have an equivalent frequency of 5 megacycles per second. The maximum negative pressures employed in this study are believed to be less than the 120 atmospheres which Willard found to be required for cavitation. Consequently, it is expected that the importance of cavitation as a mechanism for the production of the observed biological effects will become negligible when a biological system is exposed to pressure transients of the amplitude and time duration used in this study.

Biological specimens suspended in a liquid undergoing cavitation will be exposed to many processes which tend to alter function and structure. The principal chemical effect on biological materials is that of oxidation. As mentioned previously, hydrogen peroxide is formed in cavitating liquids and is believed to be the principal agent causing oxidation. The intense local temperatures produced upon the collapse of a bubble may also give rise to other types of chemical changes. The combination of oxidation and thermal processes may give rise to complex chemical reactions. For example, El'piner (16) reports that succinic, citric and malic acid irradiated in alkaline media are transformed into substances with absorption spectra characteristic of molecules of the cyclic series or of molecules with conjugated double bonds.

Cavitating liquids also generate various mechanical forces which are important in the degradation of biological particles. As previously noted, the collapsing bubbles give rise to intense pressure waves in addition to those produced by the ultrasonic

transducer. These expanding pressure waves may lead to velocity gradients across the biological particles, producing viscous tensions which tend to break them. On the other hand, if a particle is exposed to the surface of a collapsing or expanding bubble, the surface tension forces will probably lead to breakage. Also resonating bubbles near cell or bacterial walls may cause displacement and disorganization of the cell contents and eventual death of the cell (17). If the cell is of the proper size it may undergo resonance itself, with the walls of the cell expanding and collapsing in phase with the impressed ultrasonic radiation frequency, leading to eventual rupture of the cell membrane (18).

Many of the above mentioned effects such as resonance phenomena and temperature increases in ultrasonically irradiated solutions will be absent or negligible in solutions exposed to a single acoustic transient. It therefore appears that the principal biological effects of acoustic transients result from mechanical processes. As this study is concerned with the mechanical aspects associated with biological damage by pressure transients, the results of several investigations in which a mechanical disruption has been postulated for the observed biological effects will be presented.

In studies on a molecular level, Hawley, Macleod and Dunn (19) have reported degradation of deoxyribose nucleic acid (DNA) by intense noncavitating sonic waves under conditions such that thermal effects of irradiation were minimized. The breakage was believed to be due to the viscous forces produced by the relative motion between the molecules and the surrounding liquid medium. Polymers of polymethyl methacrylate and polystyrene were degraded under both

cavitating and noncavitating conditions (20). Although the polymers were broken in both cases, the breakage was more pronounced under cavitating conditions. It was also observed that the molecules of high molecular weight (500,000 to 700,000) were broken more easily than those of lower molecular weight (100,000 to 200,000), as would be expected if the breakage were produced by the presence of a pressure gradient across the molecule.

Freifelder and Davidson (21), using the ultracentrifuge, compared the sonic degradation of DNA with random degradation by x-rays and DNAase. Their results were consistent with a hydrodynamic-type shearing force leading to preferential breakage near the center of the molecule. This is in contradiction to a study by Doty (22) in which he reported random breakage of the DNA molecules based on data obtained by electron microscopy. Freifelder and Davidson suggest that the difference in the results of these experiments is due to the time period of sonic irradiation and to the initial method of preparation of the DNA which led in Doty's experiment to DNA that was broken in more than one place, resulting in a wider distribution of breaks. Other investigations have shown that when DNA is denatured sonically the viscosity is lowered but that the intensity of the absorption spectrum is essentially unchanged. In typical DNA the intensity of the absorption may be 40 percent less than in a mixture of the corresponding nucleotides. This reduction in intensity is known as the hypochromic effect and is due to the interaction of the bases when in helical array. Only at high intensities of sonic irradiation is an increase in the optical density noted. The decrease in viscosity is believed to be due to shearing across the phosphate

sugar backbone, whereas a change in the hypochromicity is produced by the free radical attack of the hydrogen bonding between the bases, leading to a disordering of the helix (23). Although cavitation can produce OH radicals and other chemical effects (as mentioned previously, page 6), the fact that the hypochromicity of the DNA is unchanged indicated that the principal effect on DNA is of a mechanical nature (24). For example, collagen macromolecules exposed to ultrasonic waves are broken along their length, but the helical configuration is essentially unaltered (25). In contrast to these studies, Melville (26) has shown that monomeric styrene may be polymerized when exposed to sonic irradiation.

The action of ultrasonic irradiation on viruses was noted as early as 1934 by Takahashi and Christensen (27), who observed the virucidal action of ultrasound (450 kilocycles per second) on TMV. The infectivity of the TMV on Nicotiana glutinosa was found to decrease with the time period of irradiation, the infectivity becoming essentially zero after two hours of exposure to the acoustic waves. This work was soon confirmed by Stanley (28) who also noted that if the virus were sealed under vacuum to reduce cavitation, almost no inactivation of the virus occurred. In neither of the above studies was the pressure amplitude of the acoustic waves determined. More detailed studies of the effects of ultrasonic waves on TMV were made by Oster (29) who used an estimated acoustic intensity of 100 watts and a frequency of 9 kilocycles per second for the irradiation of the particles. Using an electron microscope, he studied the lengths of the virus particles as a function of the time of irradiation. When the TMV was exposed to the sonic field for 64 minutes, the

infectivity decreased to less than 1 percent of its value for the unexposed virus. The original length of 3,000 angstroms (A^{o}) for the viral particles appeared to be broken into halves, fourths and eighths. For short periods of irradiation the majority of broken particles were one-half the length of the original particles. As the time of irradiation was increased, the particles of one-half of the original length were broken down into particles of one-fourth the original length. For very long periods of irradiation, only small fragments of the original particles remained. Decrease in infectivity was correlated with decrease in the number of normal virus particles of approximately 3,000 A^{o} length and this decrease was exponential with the time of irradiation. The number of halves, fourths and eighths showed an increase and then a decrease with time of irradiation. Since the infectivity showed only a decrease with time of irradiation, Oster cites this as evidence that the 3,000 A^{o} rod shaped particle is the infective unit in TMV disease.

Studies of the effect of ultrasonic irradiation of TMV at a frequency of 7 megacycles per second were made by Newton(30). He found that the infectivity was reduced by 95 percent in 3.3 minutes. The amplitude of the pressure wave was not reported. Newton states that at the lower transducer intensities, the TMV particle is fractured at a constant distance from the end of the particle, indicating a structural weakness at one definite point in the viral rod. At higher intensities he reports random breakage. The random breakage observed may be due to the fact that the initial TMV solution was not monodisperse. The author has not found any other references supporting the presence of a structural weakness at one

definite point in the TMV particles.

Anderson, Boggs and Winters (31) have studied the effects of ultrasonic irradiation on the seven T-series Escherichia coli bacterial viruses. The sensitivity of the viruses to loss of infectivity when irradiated was found to be a function of the size and shape of the virus. The most sensitive of the bacteriophages (T-2, T-4, T-6, T-5) are the largest of the series, with T-2, T-4 and T-6 having tadpole shaped heads of the order of 600 A^{o} by 800 A^{o}, and with the T-5 having a round head of about 900 A^{o} diameter. The most resistant bacteriophages T-1, T-3 and T-7 have smaller heads of the order of 450 A^{o} diameter.

The breakage of macromolecules and viruses is either generally ascribed to the production of viscous forces arising from the relative velocity between the suspending medium and particles or to a velocity gradient along the particle. These forces may be produced under cavitating (32) or noncavitating (33) conditions. The hydrodynamic forces occurring in liquids undergoing irradiation depend on the size and shape of the particle. The fact that TMV particles and DNA were observed to be preferentially broken near the center is also consistent with mechanical breakage of the particles by hydrodynamical forces. The production of these forces and their magnitudes under various conditions will be considered in more detail in Chapter II. This section has presented some of the more important effects on ultrasonically irradiated biological specimens. It appears that use of pressure transients will permit the study of some of the mechanical processes occurring in acoustically irradiated biological materials without many of the complicating effects

of continuous wave irradiation.

2. Effects of Pressure Transients

The study of the biological effects of pressure transients requires systems capable of producing intense pressures of short duration. The methods used to produce these intense pressure rises have been restricted generally to those employing the detonation of explosives or to those using a shock tube in which a membrane under high static pressure is ruptured. Many experiments have been conducted in which a whole animal or a large part of it has been exposed to blast waves produced by one of these methods (34). As these experiments have been performed on large organisms, the concern has been with macroscopic effects such as bruises, rupture of blood vessels, and displacement of organs. These experiments are more pertinent to blast damage from nuclear weapons than to the study of pressure effects on microscopic particles.

Another method used to generate intense transient pressures is that of underwater spark production. Intense pressure waves are produced by increasing the voltage difference between two electrodes until a spark discharge takes place. Spark discharges that have been used in some sterilization procedures are designed usually to give periodically occurring pulses. In the sterilization of milking machines a repetition rate of 5 to 15 sparks per second has been found suitable with voltages of 4 to 8 kilovolts and capacitance values of 0.05 to 0.1 microfarad (35). The pressure amplitudes produced by these spark discharges range from 900 to 2,000 atmospheres as measured at seven centimeters from the spark source.

Allen and Soike (36) have investigated the relative effect of

spark discharges on suspensions of Escherichia coli, spores of Bacillus subtilis, Saccharomyces cerevisiae, and bacteriophage T-2. With arc discharge repetition rates of from 0.8 to 30 times per second, all of the types of organisms studied were completely killed within one minute. They found the rate of kill to be essentially a linear function of input energy. S. cerevisiae was found to be the most resistant with about four times as much energy being required for 100 percent kill as for E. coli, the most sensitive of the organisms studied. Allen and Soike point out that the cell wall of E. coli is left intact. They believe that free radicals produced by the electrical discharge penetrate the cell walls to produce cell death. These results may also be explained on the basis of purely mechanical effects. If the rod shaped bacteria E. coli are exposed to intense velocity gradients, as in the above experiment, they would be subjected to forces rapidly orienting them to a position of least resistance to the velocity gradients (see Appendix B, page 48). This rapid turning could conceivably disrupt the internal structure of the bacteria without breaking the cell wall. The mechanical forces on rod shaped particles in viscous flow are discussed in Chapter II.

The investigations with spark discharges employed very high pressures, and it is important to note that from 10 to 15 pressure transients were sufficient for sterilization purposes (37). The pressures employed in the present study are not expected to lead to such dramatic effects, but by using lower pressures and applying the results of hydrodynamics, a model to explain the action of pressure transients on biological particles such as viruses and

macromolecules may be developed.

The method used to produce pressure transients in this investigation is by the absorption of laser light pulses in optically dense media. Therefore, it is worthwhile to consider those biological effects produced by laser light which have been ascribed to the production of pressure transients.

Ham, et. al. (38) have studied the effects of intense white light and laser light pulses on the retina of the rabbit. Their data for Q-switched laser pulses of 30 nanosecond duration, producing power densities on the rabbit retina ranging from 3-5 megawatts/cm^2, indicate that pressure transients may play a role in the observed biological damage. Retinal bubbles and choroidal hemorrhages at slightly higher power density levels are caused by these pulses, whereas thermal injury is the principal biological effect for longer, non-Q-switched pulses which do not produce appreciable pressure transients. In this regard Amar, et. al. (39) have used a piezoelectrical crystal to detect acoustic waves produced when a laser beam was focused by the eye of the rabbit. These results indicated that the Q-switched laser might be a good device for producing short, intense pressure transients. In 1964 Carome, Clark and Moeller (40) showed that, indeed, pressure transients could be produced with the Q-switched laser and that the shape of the pressure pulse depended to some extent on the boundary conditions. That is, depending on whether the surface on which the laser light was absorbed was free or rigid, the pressure transient produced had a negative component or was predominantly positive (see Appendix A).

Fine, et. al. (41) have demonstrated hemorrhaging in tissues

distant from the site of laser impact. They suggest that pressure transients may be formed due to a volume expansion either with or without a liquid to gas phase transition when transient heating occurs. For tissue in which much of the energy of the laser beam is absorbed below the surface, entrapped water may be vaporized and the resulting volume expansion may be the primary cause of biological damage. However, when most of the energy is absorbed on the surface of the tissue, the volume expansion without phase change is probably of more importance in the production of pressure transients.

Little research has been performed on the biological effects of pressure transients. The author believes that a study of the effects of pressure transients is valuable in elucidating important aspects of biological damage to living systems. Since the presence of cavitation complicates the study of the biological effects of pressure, the elimination or minimization of cavitation simplifies the analysis of the mechanism of sonic damage. Positive pressure transients eliminate any possibility of cavitation. The complicating effects of high temperature are also minimized since there is a negligible temperature rise associated with the transmission of a single transient pressure wave through aqueous media.

3. Characteristics of Tobacco Mosaic Virus

The desirability of selecting a geometrically well defined system to study the biological effects of pressure transients has already been emphasized in the Introductory Statement, page 1. The tobacco mosaic virus (TMV), because of its well known physical and biological characteristics has been chosen as the biological

model. TMV has been the subject of numerous investigations since it was isolated and purified by Stanley in 1935 (42). TMV is not only the first virus to be purified, it is also the first virus for which sufficient x-ray diffraction data have been collected to give a detailed representation of its structure. Bernal and Fankuchen (43) were able to show by x-ray diffraction of oriented gels that the virus has a mean diameter of 152 A^{o} and a length of 3,000 A^{o}. Franklin and Klug (44), also using x-ray diffraction methods, determined that the TMV particle was neither a smooth cylinder nor a hexagonal prism as had been previously postulated, but rather it was a rod bearing a helical array of protuberances. The pitch of the helix was found to be 23 A^{o} with an axial repeat distance of 69 A^{o}. Klug and Caspar (45) list additional structural parameters for TMV as determined by x-ray diffraction analysis. The molecular weight of the fundamental TMV particle is 39 million with 2.06 million of the total accounted for by ribonucleic acid (RNA) and the remainder by protein. Each protein protuberance or subunit has a molecular weight of about 18,000, there being about 2,100 of these units in the TMV particle.

The TMV rod may be chemically degraded in alkaline solution and the protein subunits separated from the RNA by precipitation or electrophoresis (46). The protein, even when freed from the RNA, has the remarkable property of polymerizing spontaneously into a rod similar to the intact virus (47). However, polymerization of the protein in the absence of RNA does not produce infective particles. Stevens and Lauffer (48) have shown that the polymerization is thermodynamically reversible. Positive increments of temperature,

ionic strength and protein concentration favor polymerization. They have shown that protein in 0.1 percent solution buffered at pH 6.5 and 0.1 ionic strength sodium phosphate exists predominantly in the polymerized state at room temperature (21° centigrade) and is depolymerized at 2° centigrade. The subunits which form the repolymerized particle have a molecular weight of 18,000 as determined by ultracentrifugation; this agrees with the molecular weight found by x-ray diffraction.

Franklin (49) has taken repolymerized protein containing no RNA and compared its cross sectional electron density with that of TMV. He found that in particles containing RNA, the electron density had it maximum peak at a distance of 40 A° from the axis of the rod, whereas the electron density of the particles containing no RNA had a minimum at this location. He concluded that the RNA chain was located at a position of 40 A° from the axis of the rod. From this information and a knowledge of the amount of RNA in the TMV particle, it is concluded that the TMV particle consists of a single strand of RNA held in a helical configuration by the protein subunits which make up the rod (see Figure 1, page 21). Hart (50) has shown that not only can a part of the protein be removed from the TMV particle while leaving the RNA intact and preserving infectivity, but also that the RNA exposed to this treatment is covered again when more TMV protein is supplied. Thus, it would seem that the RNA does not run throughout the protein subunits but that the subunits pack, leaving a vacant space for the RNA.

Phosphorous analysis of the RNA indicates that there are three nucleotides per protein subunit. It is believed that the RNA chain

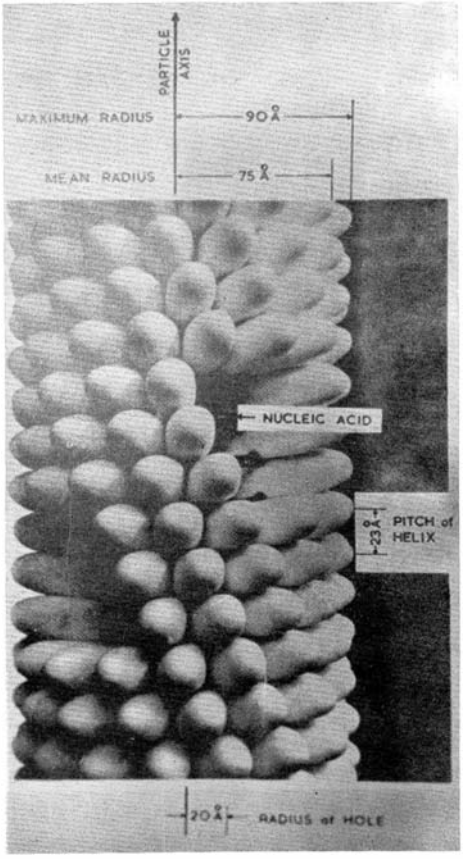

Fig. 1. Model of TMV from Klug and Caspar (45).

helps to hold the protein subunits together in a more stable configuration than would be found in the absence of RNA. This is supported by x-ray diffraction analysis of rods containing no RNA (51). It is found that these rods may change dimensions by as much as 5 A° between protein layers when going from a dry to a wet gel, whereas for RNA stabilized rods the change is negligible. The x-ray pattern also fades out more quickly at high scattering angles, indicating a more disordered structure in the repolymerized protein (52). This indicates that the bonds holding the protein subunits together are weak compared to the stability attained in the presence of the RNA chain.

Electron microscopy has substantiated the results of x-ray diffraction analysis. Using phosphotungstic acid as a negative stain, Williams and Steere (53) have shown that the length of the particle is 2,980 $A^{\circ} \pm 100\ A^{\circ}$ with 96 percent of the particles either in the form of monomers or dimers. Preparation for electron microscopy results in drying with some breakage of particles and a broader distribution of particle lengths than would be observed for the intact particle in solution (see Chapter III, page 82). However, it is still observed that most of the particles are about 3,000 A° long. It is also observed that the phosphotungstic acid fills the center axis of the particle, indicating a hollow rod in agreement with the 40 A° diameter hole predicted by x-ray diffraction analysis. Adjacent rods are never observed nearer than 170 A° to 180 A° to each other, indicating that they do not ordinarily interlock (54). This again agrees with the x-ray data of 150 A° average diameter, the electron density of the x-ray pattern falling off gradually up to

180 A° (55).

Attempts have been made to characterize TMV by various hydrodynamical methods in order to determine the dimensions of TMV in solution. One of the most recent and most thorough of these studies is that of Boedtker and Simmons (56). In these studies they have determined the length and diameter of the TMV particles by flow birefringence, sedimentation and viscosity studies. All of these hydrodynamical methods lead to particle dimensions of about 3,700 A° by 157 A°. However, the hydrodynamical calculations were made on the assumption of an ellipsoidal particle. If this hydrodynamically equivalent ellipsoid is equated to the volume of a cylinder 3,000 A° long, a diameter of 149 A° is obtained. Therefore, there is good agreement between the dimensions of the solvated and non-solvated TMV particle.

The dimensions assumed for the TMV particle in the present study are those of the hydrodynamically equivalent ellipsoid since an ellipsoidal form is used to determine the hydrodynamical stress on the particle.

C. PHYSICAL ASPECTS

1. Production and Propagation of Pressure Waves and Transients

The term pressure transient as used throughout this study designates a single acoustic pulse with an amplitude distribution of only one or two peaks. If the mechanical disturbance caused by the propagating pressure transient results in molecules being displaced from their equilibrium position, parallel to the direction of propagation, the disturbance is termed compressional or longitudinal. The particle displacement may also be perpendicular or transverse to

the direction of propagation of the disturbance. These transverse motions occur in solids and in liquids to some extent. It is generally assumed that there is no propagation of transverse motion in gases and liquids since the resistance to shear in liquids and gases is so small. However, in considering the force on particles submerged in a liquid, it will be necessary to include the fact that a viscous liquid can support a shear.

The Q-switched laser is capable of delivering a powerful pulse of energy over a very short period of time (20 to 50 nanoseconds). If the irradiated material has a high coefficient of absorption for laser light, rapid heating will occur. The generation of pressure transients by this mechanism has been demonstrated by Carome (57) as mentioned previously (see page 17). In the theoretical work of White (58) it is shown that transient temperature rises can lead to the production of acoustic transients. Thermal expansion of material due to a temperature rise $T(x,t)$ will produce a strain

$$\frac{\partial \xi(x,t)}{\partial x} = aT(x,t) \qquad \text{(I-4)}$$

where

$\xi(x,t)$ = the particle displacement as a function of position and time,

$T(x,t)$ = the temperature rise as a function of position and time, and

a = the coefficient of linear thermal expansion.

The ratio of stress to strain in liquids is given by the bulk modulus. In the presence of both heating and elastic stresses, the stress-strain relationship is altered such that

$$S = c \frac{\partial \xi}{\partial x} - BaT \qquad \text{(I-5)}$$

where

c = the elastic constant,

S = the stress, and

B = the bulk modulus.

Applying Newton's second law to the stress-strain equation for a material of density ρ:

$$\rho \frac{\partial^2 \xi}{\partial t^2} = c \frac{\partial^2 \xi}{\partial x^2} - Ba \frac{\partial T}{\partial x}. \qquad \text{(I-6)}$$

This equation is the wave equation with a forcing function proportional to the temperature gradient. Thus if the temperature is given as a function of position and time, a solution may be found for the pressure transient. Appendix A includes a more detailed explanation of how this equation is solved, making use of the variation of parameters technique. The difficulty that arises in determining the form of the pressure transient is due principally to a proper choice of the temperature distribution. Given an explicit function that describes the spatial and time variation in light intensity, the spatial and time dependent temperature rise may be determined by solving the heat equation, viz.:

$$\frac{\partial^2 T(x,t)}{\partial x^2} - \frac{1}{k} \frac{\partial T(x,t)}{\partial t} = - \frac{A(x,t)}{K} \qquad \text{(I-7)}$$

where

k = the thermal diffusivity,

K = the thermal conductivity, and

A = the heat production per unit volume per unit time.

The resulting temperature function may in some cases be of such a nature that the wave equation cannot be solved in closed form. Therefore it is necessary that simplifying assumptions be introduced.

If it is assumed that the distribution of the power density (watts/cm^2) versus time for the laser pulse is rectangular and that the instantaneous temperature is directly proportional to the total photon energy absorbed at a particular time, then the time distribution of the temperature will be in the form of a linear rise which levels off to a plateau at the end of the laser pulse. The spatial distribution of the temperature within the absorber will exhibit an exponential decrease if the electromagnetic energy is assumed to be exponentially absorbed. This temperature distribution is not a solution to Fourier's law of heat diffusion for absorption of heat on a plane surface. However, the form of the acoustic pulse obtained from the solution of the wave equation using the above form of temperature distribution is in fair agreement with Carome's (59) and the author's results. This will be discussed further in Chapter III, page 65. Michaels (60) has also used an approximate temperature function with a linear rise time in discussing thermally induced elastic wave propagation in slender bars.

Ready (61) determined the temperature distribution produced in metals by the absorption of a typical laser pulse of about 30 nanoseconds duration and from 10^6 to 10^9 watts per cm^2 by numerically integrating the heat equation. His solution indicates that the temperature on the absorbing surface rises to a maximum in about 10 nanoseconds. Ready predicts temperature gradients as high as 10^6 degrees centigrade per centimeter and temperature rates of change of

10^{10} degrees centigrade per second. The solution to the heat equation shows that the temperature in the absorbing material is dependent on the ratio of the thermal diffusivity to the thermal conductivity (62). A dye (Prussian blue) in water was used as an absorber in this study. However, it is found that the ratios of the thermal diffusivity to the thermal conductivity in water and tungsten are of the same order of magnitude so that the above values should be approximately correct for water also. The production of pressure transients is directly related to the temperature gradient; therefore, very steep pressure gradients are expected. For materials with a high coefficient of absorption for laser light, the temperature rise may be sufficient to cause vaporization of the material. However, the unfocused energy output (approximately 0.4 joules per cm^2) of the laser used in this study is not sufficient to cause vaporization if an attenuation coefficient of 1000 per centimeter is assumed. Even if all the energy is assumed to contribute to vaporization, only about a milligram of water could be vaporized. Therefore, it is felt that any effects due to vaporization will be small when using unfocused laser light.

In order to describe the propagation of acoustic phenomena mathematically, it is assumed that the stress, S, tending to displace a particle from its equilibrium position is proportional to the displacement. That is

$$S = c \frac{\partial \xi}{\partial x} \qquad \text{(I-8)}$$

where

ξ = the particle displacement in the x direction, and

c = the elastic constant.

From Newton's second law, one has that

$$\rho \frac{\partial^2 \xi}{\partial t^2} = \frac{\partial S}{\partial x} \tag{I-9}$$

where

ρ = the density at time, t.

Combining these two expressions gives the wave equation

$$\frac{\partial^2 \xi}{\partial t^2} = v^2 \frac{\partial^2 \xi}{\partial x^2} \tag{I-10}$$

where

$v^2 = \frac{c}{\rho}$ is the square of the wave velocity.

The solution of interest is of the form

$$\xi = Ae^{i\omega(t - xv^{-1})} + Be^{i\omega(t + xv^{-1})} \tag{I-11}$$

where

ω = the angular frequency of the waves.

The first term in this equation represents a wave traveling in the positive x direction; and the second term, a wave traveling in the negative x direction. The application of boundary values determines the constants A and B.

The specific acoustic impedance which is important in determining the relative amounts of acoustic power transmitted or reflected at boundaries and interfaces is defined as follows:

$$Z_{sp} = p/(\frac{\partial \xi}{\partial t}) \tag{I-12}$$

where

Z_{sp} = the specific acoustic impedance, and

p = the pressure.

Assuming the pressure to be a simple harmonic function of time, let

$$p = p_+ e^{i\omega(t - xv^{-1})} + p_- e^{i\omega(t + xv^{-1})} \qquad \text{(I-13)}$$

where

p_+ = amplitude of the pressure wave traveling in the positive x direction, and

p_- = amplitude of the pressure wave traveling in the negative x direction.

Making use of Newton's law and the fact that the pressure is defined as the negative of the stress, then

$$\frac{\partial p}{\partial x} = -i\rho\omega\frac{\partial \xi}{\partial t} \qquad \text{(I-14)}$$

and

$$Z_{sp} = \rho v \phi \qquad \text{(I-15)}$$

where

$$\phi = \frac{p_+ e^{-i\omega x v^{-1}} + p_- e^{i\omega x v^{-1}}}{p_+ e^{-i\omega x v^{-1}} - p_- e^{i\omega x v^{-1}}} \qquad \text{(I-16)}$$

and

ρv = the characteristic impedance of the medium.

In the above solution for the particle displacement, all losses were neglected. Sound attenuation and consequently absorption in fluids is determined primarily by viscosity, heat conduction and the molecular characteristics of the fluid in question. These various absorption processes become important only at high frequencies. For frequencies below 10 megacycles per second the intensity of the sound field is reduced less than 3 percent for a path length of 1

centimeter (63). Since the equivalent frequencies employed in this study are less than 10 megacycles per second and since the acoustic path lengths are short (i.e., order of 1 centimeter or less), the absorption of the acoustic waves is negligible.

For large amplitude waves the particle displacement is not a linear function of the stress as was assumed in deriving the wave equation. As a result the wave velocity is no longer constant but is dependent on the particle displacement, with the velocity being greater in the regions of greatest particle displacement. The wave form will become steeper as the wave propagates since the regions of greatest particle displacement will travel faster than those of small particle displacement. This steepening of the wave front leads to the production of higher frequencies. Lester (64) has discussed the generation of harmonic frequencies as a function of propagation distance for large amplitude waves using an equation of state for liquids of the form

$$P = P_o + A\left(\frac{\rho - \rho_o}{\rho_o}\right) + 1/2\ B\left(\frac{\rho - \rho_o}{\rho_o}\right)^2 \qquad \text{(I-17)}$$

where

A and B are empirical constants, and

P and P_o are the pressures when the density is ρ and ρ_o respectively.

The propagation velocity is found to depend linearly on the particle velocity up to pressures of the order of 1000 atmospheres, viz.,

$$v' = v + (B/2A + 1)\frac{\partial \xi}{\partial t}$$

where

v' = the propagation velocity for waves of large amplitude and

v = the propagation velocity for waves of small amplitude.

Lester's graphs, showing the relative magnitudes of the harmonics as a function of distance, show that for water (B/A is assumed to be = 5) the amplitude of the second harmonic is only 10 percent of the fundamental frequency (1 megacycle per second) for a distance of propagation of about 7 centimeters and for an initial pressure of 10 atmospheres. Since distances of propagation of the order of 1 centimeter are used in this study, the effects of large amplitude distortion will be small and have thus been neglected.

CHAPTER II - TOBACCO MOSAIC VIRUS BREAKAGE

A. PROPOSED MECHANISMS

Various mechanisms have been proposed to account for the observed breakage of macromolecules and viruses exposed to ultrasonic irradiation. Some of these were mentioned previously in discussing the effects of ultrasonic irradiations on biological materials (Chapter I, pages 9-14). However, it is the purpose of this chapter to consider in greater detail those mechanisms which have been proposed to account for the mechanical breakage of long, rod-shaped particles. Only those mechanisms which appear to be applicable to the study of transient phenomena will be analyzed. These will be analyzed to determine the magnitude of the forces tending to rupture rod-shaped particles.

Two principal approaches have been made in considering the breakage of macromolecules. The first approach assumes that the particles under consideration do not interact and that each particle is completely isolated from all other particles. The second approach assumes that the particles form aggregates or entanglements. Aggregates may conceivably be present in dilute solutions if the particles tend to adhere to one another. For the case where the TMV particle is assumed to be isolated (i.e., not in an aggregate), the inertia of the particle is generally so small that the particle is assumed to move with the fluid so that there is no net force acting on the particle (65). In other words, the center of mass of the particle will move with a velocity that is equal to the average velocity of the solvent (see Appendix B, page 146). When an acoustic pulse is propagated through the medium, the

molecules will undergo compression and expansion. During compression the molecules of the solvent will be packed closer together along the TMV particle. As the positive pressure begins to decrease, there will be an expansion or separation of the molecules of the solvent resulting in a viscous tension along the TMV particle. The rupture of particles is attributed to this viscous tension. Frenkel (66) has used this mechanism to discuss the orientation and rupture of linear macromolecules. In particular he has focused attention on the forces tending to break a linear array of spheres with connecting links.

Mostafa (67) in considering the occurrence of breakage of polystyrene under noncavitating conditions has concluded that the forces are not of sufficient magnitude to break the particles if it is assumed that the polystyrene particles are isolated from each other in solution. He concludes that the molecules must become entangled to an extent sufficient to increase their effective mass so that they do not move relative to the solvent. With an increased effective mass the molecules may be assumed to be fixed at one end or both ends due to the entanglements. The velocity relative to the macromolecule is thus much greater than if the polystyrene were assumed to be free and able to follow the undulatory motion of the applied acoustic field.

Mark (68) has made similar comments in attempting to explain the breakage of polystyrene and nitrocellulose under noncavitating conditions. He suggests that "most of the macromolecules will join the vibrational motion of the solvent and only rarely, here and there, will considerable friction develop." He says this explains

the very low degree of degradation (only 5 bonds broken in 1000), obtained when the particles were irradiated from 20 minutes to over an hour at 10 watts per cm^2 and at 100 kilocycles frequency. He estimates that the force exerted on the molecules is about 4 or 5 times the strength of a carbon-carbon bond for molecules which are assumed to be stationary with respect to the solvent. However since millions of oscillations of the pressure field are required to produce significant breakage, Mark postulates that the effective force rupturing the molecules is much less than the force calculated on a basis that the molecules are considered stationary with respect to the solvent.

Gooberman (69) has studied the breakage of polystyrene under cavitating conditions in benzene. He concluded that no significant breakage can occur except under cavitating conditions. Under these conditions breakage is possible even for a single isolated molecule since the molecule may be adjacent to a collapsing cavity where pressures greater than 1000 atmospheres may be experienced.

The above mechanisms possibly may explain the observed breakage of TMV particles that have been exposed to transient acoustic pressure waves. Before considering these mechanisms further, the hydrodynamical forces experienced by a rod-shaped cylinder in a field of solvent flow must be considered.

B. HYDRODYNAMICAL CONSIDERATIONS

1. Limits of Applicability

The study of viscous forces exerted on a cylinder in a one dimensional field of flow is complicated by the fact that the cylinder perturbs the flow. Therefore, it is necessary to con-

sider a three dimensional field of flow around the cylinder. The complete three dimensional equation of motion as given in standard texts on hydrodynamics (70) is

$$\rho \frac{D\vec{q}}{Dt} = \rho\vec{F} - \nabla p - \mu\nabla\wedge(\nabla\wedge\vec{q}) + \frac{4}{3}\mu\nabla(\nabla\vec{q}), \qquad \text{(II-1)}$$

where

ρ = density,

$\vec{q}$ = velocity (the arrow denotes a vector quantity),

p = pressure,

$\vec{F}$ = external forces,

μ = viscosity coefficient,

$\wedge$ denotes the cross product, and

D denotes the total derivative, i.e.,

$$\frac{D\vec{q}}{Dt} = \frac{\partial\vec{q}}{\partial t} + \vec{q}\nabla\vec{q}.$$

Making use of the equation of continuity and assuming that the fluid is incompressible, then $\nabla\vec{q}$ must be zero and equation (II-1) becomes:

$$\rho \frac{D\vec{q}}{Dt} = \rho\vec{F} - \nabla p - \mu\nabla\wedge(\nabla\wedge\vec{q}). \qquad \text{(II-2)}$$

The form of this equation may be modified with the aid of the vector identity:

$$\nabla^2\vec{q} = \nabla(\nabla\vec{q}) - \nabla\wedge(\nabla\wedge\vec{q}).$$

The equation (II-2) may now be written as:

$$\rho \frac{D\vec{q}}{Dt} = \rho\vec{F} - \nabla p + \mu\nabla^2\vec{q} \qquad \text{(II-3)}$$

which is recognized as the time dependent Navier-Stokes equation. Expanding the total derivative and neglecting external body forces such as gravitational forces, equation (II-3) becomes:

$$\rho\left(\frac{\partial \vec{q}}{\partial t} + \vec{q}\nabla\vec{q}\right) = -\nabla p + \mu\nabla^2\vec{q}. \qquad \text{(II-4)}$$

Equation (II-4) is a difficult equation to solve and has been solved successfully only through the use of various approximation schemes. The problem becomes even more difficult at sufficiently high velocities because turbulence develops in the flow. The velocity and pressure then become discontinuous at various points and motion is better described in terms of stochastic processes. Even with simplifications, it has not proved possible to solve the equations of motion for flow past finite bodies when turbulence is present.

In order to determine the conditions under which turbulence is not induced so that equation (II-4) may be simplified, use will be made of the Reynolds number. The Reynolds number is a dimensionless quantity that depends on the ratio of inertial to viscous forces, and is often used as a measure of the turbulence expected for a given system (71). The Reynolds number depends on the characteristic parameters of the system under consideration, such as the diameter of the particle, the velocity, viscosity, and density of the medium. For low Reynolds numbers (i.e., < 1) the flow is essentially laminar, the importance of turbulence rising as the Reynolds number approaches 1.

For flows characterized by low Reynolds numbers, equation (II-4) may be simplified. In order to justify the simplification, a transformation to dimensionless variables is made. Let

$t' = t/\tau$ - dimensionless time,

$\vec{q}' = \vec{q}/U$ - dimensionless velocity vector, and

$\vec{r}' = \vec{r}/\lambda$ - dimensionless position vector, and

$p' = \rho\lambda/U\mu$ = dimensionless pressure

where τ, U, and λ are characteristic values of the time, velocity and length of the system under investigation. Under this transformation, equation (II-4) becomes:

$$\frac{\rho\lambda^2}{\mu\tau}\frac{\partial\vec{q}'}{\partial t'} + \frac{\lambda\rho U}{\mu}\vec{q}'\nabla'\vec{q}' = -\nabla'p' + (\nabla')^2\vec{q}' \qquad \text{(II-5)}$$

or

$$N_1\frac{\partial\vec{q}'}{\partial t'} + N_2\,\vec{q}'\,\nabla'\vec{q}' = -\nabla'p' + (\nabla')^2\vec{q}'$$

where N_1 and N_2 are the Reynolds numbers defined by:

$$N_1 = \rho\lambda^2/\mu\tau \qquad \text{and} \qquad N_2 = \rho U\lambda/\mu. \qquad \text{(II-6)}$$

These numbers may be evaluated for an acoustic pulse of 10^{-7} seconds duration and with a pressure amplitude of 10 atmospheres. The equations (A-21) and (A-28) derived in Appendix A can be used to obtain an estimate of the solvent velocity, U, of about 1 meter per second. The equivalent radius of the TMV particle (the radius of a sphere with the same volume as the TMV particle) may be taken as approximately 2.33×10^{-8} meters. Using these values gives $N_1 = 5.4 \times 10^{-3}$, and $N_2 = 2.3 \times 10^{-2}$; N_1 and N_2 are small enough so that the terms on the left side of equation (II-5) may be neglected. Changing back to untransformed variables, the simplified equation may now be written as:

$$\mu\nabla^2\vec{q} - \nabla p = 0. \qquad \text{(II-7)}$$

Although this equation is identical in form to the steady state Stokes equation, it is, in fact, dependent on the time implicitly, since p and $\vec{q}$ are functions of time. It is called, therefore, the

quasi-steady Stokes equation (72). It is the solution of this equation for the transient case that is to be investigated.

The approximation involved in the use of equation (II-7) becomes more accurate the smaller the Reynolds numbers involved, these numbers being a measure of the ratio of inertial forces to viscous forces exerted on the particle by the surrounding fluid. The order of the approximation involved in using equation (II-7) may be investigated by comparing the forces on the particle as calculated from this formula with the known force experienced by an infinitely long cylinder oriented with its long axis perpendicular to a uniform flow velocity, U. The force experienced by a particle in a field of uniform flow is dependent on the Reynolds number of the flow and on the shape of the particle. A dimensionless number, the drag coefficient, is generally employed in discussing the forces on bodies of various shapes. The drag coefficient as a function of the Reynolds number for an infinitely long cylinder is well known and is given in Perry's Chemical Engineer's Handbook (73). The drag force in terms of the drag coefficient is

$$F = \frac{CA\rho U^2}{2} \qquad \text{(II-8)}$$

where

C = the drag coefficient,

A = the projected area of the particle perpendicular to the direction of fluid flow,

ρ = the density, and

U = the flow velocity in the absence of the suspended

particle.

Since steady flow has been assumed in arriving at values for the drag coefficients, the Reynolds number N_2 of equation (II-6) is the one that must be considered. All of the parameters of N_2 are fixed except the velocity. As an upper limit consider a pressure of about 1000 atmospheres. Calculations based on formulas (A-21) and (A-28) in Appendix A show the expected value of U to be of the order of 100 meters per second, and N_2 to be about 2.3. The drag coefficient for a Reynolds number of 2.3 for an infinite cylinder is about 7.5 and the force is found to be 1.7×10^{-7} newtons. The force calculated using the solution to equation (II-7) is 1.8×10^{-7} newtons.

The solution to equation (II-7) is given in Appendix B, page 140 and is discussed below. The surprisingly close agreement between these forces is probably misleading since the comparison was made for the drag coefficient of an infinitely long cylinder. The actual drag coefficient, and consequently the drag force, may be 15 to 20 percent lower than indicated above. The drag coefficients for cylinders vary with the length to diameter ratio, the coefficient for a length to diameter ratio of one being about half that for an infinitely long cylinder. Even for a length to diameter ratio of 40 the coefficient is only about 85 percent of that for an infinitely long cylinder (74). Since the pressures employed in this study are below 1000 atmospheres, it appears that there is good justification for disregarding the inertial term $\vec{q} \cdot \nabla \vec{q}$ in equation (II-4).

The Reynolds number associated with the term $\frac{\partial \vec{q}}{\partial t}$ in equation (II-4) is independent of the fluid velocity but is inversely related to the time. Unless characteristic times of 10^{-9} seconds or

less are considered, the magnitude of this number is still less than one and therefore, the term $\frac{\partial \vec{q}}{\partial t}$ can also be disregarded. In order to estimate the order of approximation involved when the term $\frac{\partial \vec{q}}{\partial t}$ is neglected, consider the solution of the equation in which this term is not neglected. Lamb (75) gives the solution of the equation for the case of a sphere undergoing oscillations in a fluid. If, as in the case in the present calculations, an equivalent frequency of 5 megacycles is assumed for the transient pressure, then the force calculated for a sphere of 150 A^{o} is found to be about 6 percent greater than it would be if the force were calculated on the basis of the usual Stokes equation:

$$\vec{F} = 6\pi \mu a \vec{U} \qquad \text{(II-9)}$$

where

a = the radius of the sphere,

μ = the viscosity of the solution, and

$\vec{U}$ = the flow velocity in the absence of the suspended particle.

In the above case it was assumed that the particle was stationary with respect to the flow field. If the particle is assumed to move with the flow field, then the Reynolds number, N_2, will be even less, since the relative velocity of the solvent to the particle is the important parameter. Having justified the use of the quasi-steady equation of motion, it is now necessary to consider the solution of the equation (II-7) and how it is used in determining the stress on the TMV particle produced by a pressure transient.

2. Solutions

The flow past spheres has been studied extensively both

theoretically and experimentally. Equation (II-7) was first solved for spheres in a steady uniform field of flow by Stokes (76). It is also of interest to note that Einstein (77) studied the motion of spheres suspended in a liquid with respect to their effect on the viscosity of the liquid. The solution of equation (II-7) for the case of an ellipsoid of revolution undergoing translation is given in Appendix B, page 140. The method of solution follows one given by Lamb (78) in his treatise, Hydrodynamics. Lamb based his solution on the original work of Oberbeck. Jeffery (79) extended the solution along the lines followed by Einstein in order to determine the effect of a suspension of translating or rotating ellipsoids on the viscosity of the suspensions. Attempts have been made to partially correct for inertial effects neglected in using equation (II-7). One such attempt, made by Oseen, involves approximating the term $\vec{q}(\nabla\vec{q})$ in equation (II-4) by $\vec{U}(\nabla\vec{q})$, where $\vec{U}$ is the uniform velocity of flow at large distances from the particle. This method is discussed by Burgers (80)(81) for bodies of various geometric shapes, including the ellipsoid. This method gives results which are more consistent with experimental values at large distances from the particle. However, in the region near the particle where the viscous forces tending to rupture the particle are greatest, $\vec{q} \neq \vec{U}$, and the solution to equation (II-7) gives results as valid as those obtained using Oseen's approximation. Burgers applies Oseen's method to find the approximate solution for cylinders immersed in a uniform, steady flow. He finds that the solution for the force on a cylinder with its axis perpendicular to the direction of flow is given by the same formula that the exact solution of equation (II-7) provides for

an ellipsoid (see equation B- 63 of Appendix B). For the resistance of a cylinder with its axis along the direction of flow, he finds that

$$\vec{F} = \frac{4\pi\mu\vec{U}a}{\ln 2\left(\frac{a}{b}\right) - 0.72} \qquad \text{(II-10)}$$

where

a = major semi-axis of an ellipsoid of revolution, and

b = minor semi-axis of an ellipsoid of revolution

as compared with the solution of equation (II-7) for an ellipsoid of revolution, where

$$\vec{F} = \frac{4\pi\mu\vec{U}a}{\ln 2\left(\frac{a}{b}\right) - 0.5}. \qquad \text{(II-11)}$$

Since the solution for a cylinder by Oseen's method of approximation gives essentially the same results as the exact solution of equation (II-7), and, since this equation appears to be applicable in the range of pressures employed in this study, the form of the particle will be assumed to be that of an elongated ellipsoid of revolution. It is useful to make this assumption, since in all of the hydrodynamical methods employed to determine the properties of tobacco mosaic virus, it has been assumed that the particle was in the form of an ellipsoid of revolution. As previously mentioned (Chapter I, page 23) the parameters that will be assumed for the tobacco mosaic virus particle are those determined by Boedtker and Simmons using hydrodynamical methods. That is, the length of the major axis will be assumed to be 1850 A^{o}, and that of the minor axis, 78 A^{o}.

The solution to equation (II-7) for the force on a particle

undergoing translation can be put in the form

$$\vec{F} = \mu\tilde{K}\vec{U} \qquad \text{(II-12)}$$

where $\tilde{K}$ is a translation dyadic which depends only on the geometry of the particle and $\vec{U}$ is the value which the velocity field would have at the origin if the particle were not present (82). This form of the solution is discussed in more detail in Appendix B, page 141. For small distances, corresponding to the length of the TMV particle, the solvent velocity, $\vec{U}$, may be assumed to vary linearly along the direction of propagation. For the case where the TMV particle is assumed to move with the flow field, the maximum tensile stresses will be developed when the velocity gradient is a maximum.

There will be a torque, associated with this force, tending to align the particle with the flow field. For the case where the particle is free to move under the influence of the applied flow field, the resultant torque will be zero and will not tend to rupture the particle. For the case where one or both ends of the particle are assumed to be rigidly fixed, the torque may play an important role. Even for the case where the particle is assumed to be free, the torque will tend to align the particles in the field so that its effect must be considered in determining the orientation of the particles. The magnitude of this orienting effect must be known before a calculation can be made of the average force exerted on the particle during exposure to a given pressure transient. If it is assumed that the long axis of the particle lies along the x-axis, then the torque experienced by a particle in the x-y plane will be given by

$$\vec{L} = \int_{-a}^{a} \vec{i}x \wedge d\vec{F} = \vec{k}\mu K \int_{-a}^{a} x(\partial U'/\partial x)dx \qquad \text{(II-13)}$$

where

$U' = U \sin\theta$,

θ = angle the particle makes with the direction of propagation of the pressure wave,

$\vec{i}$ = unit vector in the x direction, and

$\vec{k}$ = unit vector in the z direction.

The magnitude of the torque and the time required for the particle to rotate is considered in Appendix B, pages 146-8 . For typical values of the velocity gradient, it is found that the time required for complete orientation of the particle, even for large velocity gradients, is quite long, so that it may be assumed that the particles are oriented randomly as in an undisturbed solution.

Since the incident pressure wave is assumed to be a plane wave, the velocity gradient is along the direction of propagation of the wave. Therefore, in considering the viscous tensions on the particle, only the orientation with respect to the direction of propagation need be considered. As before, the x-axis is taken along the long axis of the particle and the angle this axis makes with the direction of propagation of the pressure wave is designated by θ. The particles are assumed to be randomly distributed with respect to θ, where θ varies from 0^{o} to 90^{o}, and the probability of a particle having an angle θ will be equal for all values of θ. The average force exerted on the particle will be

$$\langle \vec{F} \rangle = \frac{\int_{o}^{\pi/2} \vec{F} d\theta}{\int_{o}^{\pi/2} d\theta} = \frac{2}{\pi}\int_{o}^{\pi/2} \vec{F} d\theta. \qquad \text{(II-14)}$$

The force $\vec{F}$ is the resultant force over the entire particle.

However, since the velocity is assumed to vary with position along the axis of the particle, it is necessary to consider a force, f(x)dx, distributed along the axis of the particle. The form of the distributed force (83) (see Appendix B, page 144) is given by

$$f(x) = \frac{4\pi\mu U}{\ln 2\left(\frac{a}{b}\right) - 0.5}. \qquad \text{(II-15)}$$

The average tension exerted at a point x on the particle in a field of flow U can then be expressed as

$$\langle \vec{F} \rangle = \frac{8\mu}{\ln \frac{2a}{b} - 0.5} \int_0^{\frac{\pi}{2}} \int_x^a \vec{U} dx d\theta . \qquad \text{(II-16)}$$

The velocity gradient across a particle which is assumed to move with the average velocity of the suspending medium may be written

$$U = \alpha u_o x' \qquad \text{(II-17)}$$

where

x' is along the direction of propagation of the acoustic wave,

α is the absorption coefficient at wavelength 6943 A^o (see Appendix A, page 118), and

$u_o = \alpha v \xi_o$ (Defined in Appendix A, page 123).

Substituting this value of U into equation (II-16), the force becomes

$$\langle \vec{F} \rangle = \frac{4\mu u_o \alpha (a^2 - x^2)}{\ln \frac{2a}{b} - 0.5} \qquad \text{(II-18)}$$

The tension tending to rupture the particle is seen to be greatest at the center of the particle where x is zero.

For the case where the particle is assumed to be fixed relative

to the motion of the medium, and no other assumptions are made regarding the boundary conditions, the force tending to produce breakage will be found to be much greater than in the previous case. That is, if it is assumed that conditions such as aggregations which increase the inertia of the particles do not perturb the flow pattern, then the force on the entire particle is given by equation (II-16), where U can be replaced by the space average of the velocity, U_o, such that

$$\langle \vec{F} \rangle = \frac{16\mu U_o a}{\ln \frac{2a}{b} - 0.5} . \qquad \text{(II-19)}$$

If U_o is taken to be the maximum velocity produced in the liquid by the pressure transients, then the force calculated by using equation (II-19) will be the maximum force possible leading to breakage of the particles. The actual velocity field will be modified considerably by the presence of a large aggregate of TMV particles. The shape, as well as the size, will also influence the velocity field. Consider, for example, how the velocity varies near the surface of a sphere. The velocity in the x' direction is approximately

$$u = U(1 - a/r) \qquad \text{(II-20)}$$

where

a = the radius of the sphere, and

r = the distance from the center of the sphere (84).

At the surface of the sphere, the velocity is zero and becomes equal to one-half of U at a distance of 2a from the center of the sphere. For a large sphere, the velocity will increase slowly with distance from the sphere, whereas for small spheres the velocity

will increase more rapidly. Calculations in Appendix B, page 146 show that the smallest sphere which could be assumed stationary with respect to the applied field has a radius of about 5000 A^{o}, or a mass equivalent to about 10^{4} TMV particles. The particles could be arranged conceivably in an elongated form rather than in a spherical form. The effective radius at the ends of such elongated aggregations could be small, so that the maximum force given by equation (II-19) would be realized. The position of breakage of the particle would depend on how it was fixed relative to the aggregate. Breakage would probably occur near the center portion of the particle, since a portion of the particle would necessarily have to be attached or embedded in the aggregate in order to hold the particle stationary.

The realization of the maximum forces discussed above is dependent on the occurrence of aggregations in the medium. Experimental evidence to be discussed in Chapter IV indicates that aggregations were not present to an appreciable extent in this study.

C. STABILIZING FORCES

The magnitude of the force necessary to rupture a virus particle or a macromolecule is dependent on the nature of the molecular bonds holding the particle or macromolecule together. The 3000 A^{o} length TMV particle is composed of a single strand of RNA and about 2100 protein subunits held together by van der Waals forces, salt linkages, hydrophobic bonds and hydrogen bonds. The nature and magnitude of the forces holding the virus in the rod-shaped configuration has been explained to some extent by the experiments of Stevens and Lauffer (Chapter I, page 19). Their work showed that the bonding between molecular subunits in the absence of RNA was

strongly dependent on the pH of the suspending medium, changing reversibly from the depolymerized state at pH 7.5 to a polymerized state at pH 5.5. The stability of the TMV particle is dependent to a large extent on the interaction of the RNA with the protein subunits. Such RNA stabilized particles may be degraded reversibly, but only at pH values of 10.5 or greater (85).

The solutions of TMV used in this study were adjusted to pH 7.5 to prevent the formation of dimers. The research of Stevens and Lauffer regarding the dissociation of the TMV particles demonstrates that the bonding which gives stability to the rod is primarily due to the presence of the RNA at this pH. The position of the RNA with respect to the subunits was discussed in Chapter I, page 20. It was noted that there are three nucleotides per protein subunit. Assuming that each base can form only one hydrogen bond per subunit, then a total of about 16 hydrogen bonds should be involved between the RNA chain and a radial cross section of the TMV rod. The bonding in the direction of the axis may be less, since some of the bonds will be directed at various angles to the axis. The energy of the hydrogen bond formed depends on many factors such as the chemical constitution of the bonded groups, steric effects, and the solvent. For aqueous protein solutions Kauzmann (86) indicates that the bond energy is from 1 to 2 kilocalories per mole. If 2 kilocalories per mole is taken as the energy of the hydrogen bond, the energy stabilizing the bonding between radial sections of the TMV rod is of the order of 32 kilocalories per mole (87). This energy is less than that of a carbon-carbon bond in accordance with the experimental evidence that the viral RNA and its subunits may be

separated without breaking the primary bonds in either the protein subunits or the RNA.

A stretching force of sufficient magnitude to break the TMV particle into two parts must be able to rupture at least the hydrogen bonding between the RNA and the protein subunits before rupturing the primary bonding in the RNA chain. The ultimate strength to resist breakage will depend on the weakest primary bonding link in the RNA chain. If the RNA chain remains intact, any broken hydrogen bonds will probably reform quickly. Thus, an estimate of the force necessary to break a TMV particle into two parts can be made if the force necessary to rupture primary chemical bonds can be established.

The force between two interacting atoms is defined as the first derivative of their potential energy with respect to the distance separating them. Morse (88) has shown that the potential energy expressed in the form

$$V = De^{-2a(r - r_o)} - 2De^{-a(r - r_o)} \qquad \text{(II-21)}$$

where

a is a constant,

D is the dissociation energy of the chemical bond, and

r_o is the equilibrium distance of separation of the two atoms

is in good agreement with spectroscopic data. The dissociation energy for a diatomic molecule is equal identically to the bond energy (89). However, for polyatomic molecules the situation is not quite so simple. The energy needed to dissociate the molecule into its separate atoms may be measured, but the distribution of

Table 1

Average Bond Energies

Bond	Bond Energy (kilocalories per mole)
Carbon-Carbon	66.2
Carbon-Oxygen	77.1
Phosphorous-Oxygen	80.0

(90) Cottrell, T. L., The Strengths of Chemical Bonds, pp 275-277. Academic Press, New York (1954).

the energy between the various bonds is not known usually. Table 1 (90) lists average values for the bond energies of primary bonds occurring in the RNA backbone; however, the strength of any particular bond may be greater or less than this, depending on the bond angles and neighboring molecules. Spectroscopy also reveals that the force necessary to distort a molecule depends upon the nature of the force--that is, whether it is a stretching, bending or twisting force. For example, force constants determined for benzene show that for small linear displacements or stretching the force constant is about 7.6×10^5 dynes per centimeter. For deformation of the benzene ring by displacements of the carbon atoms in the plane, so that alternate angles will become greater and less than 120°, the force constant is about 0.7×10^5 dynes per centimeter, and for torsional, out-of-plane, vibration the constant in approximately 0.06×10^5 dynes per centimeter (91).

De Boer (92) has used a Morse potential to calculate the in-

fluence of the carbon-carbon bond on the tensile strength of the artificial resins, phenol-formaldehyde and m-cresol-formaldehyde. He states that the value of the tensile force calculated in this manner is always greater than the experimentally determined forces (for example, the theoretical tensile stress of m-cresol-formaldehyde when all possible carbon-carbon bonds are taken into account is found to be 4000 kg per mm^2). Even if van der Waals forces are the only forces assumed to be operative, the theoretical values are about an order of magnitude greater than the experimentally determined values. The explanation usually offered for these discrepancies is that there are flaws or weak spots in the material (93).

The above discussion indicates that if a Morse potential is used to estimate the tensile strength, the breaking force obtained should be an upper limit to the force observed experimentally. While this type of argument may hold for polymers, the concept of "flaws" in a single molecular chain, such as the RNA found in TMV or the protein subunits of this virus, may not be valid.

The force required to break the carbon-carbon bond (weakest listed in Table 1) may be estimated from the Morse potential by differentiating equation (II-21) and obtaining the force,

$$F = - 2aDe^{-2a(r - r_o)} + 2aDe^{-a(r - r_o)}. \qquad \text{(II-22)}$$

The maximum force required for rupture of the bond is determined by setting the derivative of the above expression equal to zero and solving for r_{max}.

$$\frac{\partial F}{\partial r} = 0 = 4a^2De^{-2a(r_{max} - r_o)} - 2a^2De^{-a(r_{max} - r_o)} \qquad \text{(II-23)}$$

and

$$r_{max} = \frac{ar_o + \ln 2}{a} .$$

Substituting r_{max} into equation (II-22) gives the maximum force

$$F = \frac{aD}{2} = 3.65 \times 10^{-9} \text{ newtons.} \qquad \text{(II-24)}$$

This value is obtained by using 66.2 kilocalories per mole for the dissociation energy of the carbon-carbon bond and assigning to the constant, a, a value of 1.59×10^{10}/m as determined by the relation, (94)

$a = 2\pi\nu\left(\frac{\mu}{2D}\right)^{1/2}$,

ν = bond frequency (2.43×10^{13} cycles per second),

μ = reduced mass, and

D = dissociation energy.

Bond dissociation energies are determined from enthalpy values; however, the free energy is really the energy term needed for the determination of the force (95). Of interest in this respect are the values for the free energy involved in the thermal inactivation of TMV (34.6 kilocalories per mole)(96). Using this value for D in equation (II-24), the force becomes 2.64×10^{-9} newtons.

Because of the nature of the approximation in the above derivation, the value of the tensile strength of the TMV particle is only valid to an order of magnitude. However, these values are useful for comparison with and evaluation of the experimental results of Chapter IV.

CHAPTER III. DESCRIPTION OF APPARATUS AND TECHNIQUES

A. THE LASER

The intense light pulse used for the production of the acoustic transients in this study was produced by a ruby laser. The first solid state laser was produced in 1959 by Maiman (97). He succeeded in obtaining stimulated emission at optical frequencies in a solid state substance, thus demonstrating experimentally the feasibility of producing very intense bursts of monochromatic and coherent electromagnetic radiation.

The ruby laser consists of a rod of aluminum oxide doped with approximately 0.05 percent chromium as a source of (Cr^{+3}) ions. The ends of the rod are ground optically flat and parallel. Capacitive discharge flash lamps placed near the rod and surrounded by a reflector provide energy for the operation of the laser. The energy level of the chromium ions (Cr^{+3}) is raised from the ground state to two higher levels with absorption bands centered at 5500 A^{o} and 4000 A^{o}. Lattice interactions rapidly depopulate these levels to two metastable intermediate energy levels. Normally, these metastable levels give rise to fluorescent emission of two spectral lines in the red region (6943 A^{o} and 6929 A^{o}) with half-lives of the order of several milliseconds. However, the oscillations of the emitted photons between the reflecting surfaces at the ends of the rod lead to stimulated emission in which the metastable state (6943 A^{o}) is depopulated in a short period of time (approximately 50 nanoseconds). Stimulated emission of the 6929 A^{o} level can be achieved also by using band pass filters to block out the 6943 A^{o} component. The time of depopulation of the metastable state is affected by the

intensity-time distribution of the radiation produced by the flash lamps and by the conditions of the reflecting surfaces at the ends of the rod. The laser may be operated with the back surface of the rod totally reflecting and the front surface partially reflecting. As the population of the metastable state builds up, stimulated emission will occur causing depopulation. The duration of the laser pulse is usually long enough to allow many oscillations. However, if the reflectance of the back surface of the rod is kept low during the major portion of the pumping pulse from the xenon lamps, the metastable states become heavily overpopulated. Now, if the reflectance is suddenly increased by any one of several means, such as a rapidly spinning prism or by the use of a Kerr cell (98), the heavily overpopulated metastable state will be stimulated to emit an intense single pulse of light with a duration of 10^{-8} to 10^{-7} seconds. Such systems are termed Q-switched systems. The resultant light beam produced by the laser has a low angle of divergence (usually a few milliradians). The frequency of the emitted light is highly monochromatic, having a much narrower line width than the fluorescent line width. The light emitted from the front surface of the laser rod is coherent both in space and in time (99).

The laser used in this study consists of a 6 and 3/4 inch long by 3/8 inch diameter ruby crystal mounted between FX-47 Edgerton, Germeshausen and Grier, Inc. (EG and G) xenon flash lamps. A double elliptical cavity serves as a reflector for the two lamps so that the light from each lamp is focused within the ruby rod.

Figure 2 is a block diagram of the components of the laser system; Figure 3 is a photograph of the laser and the schlieren

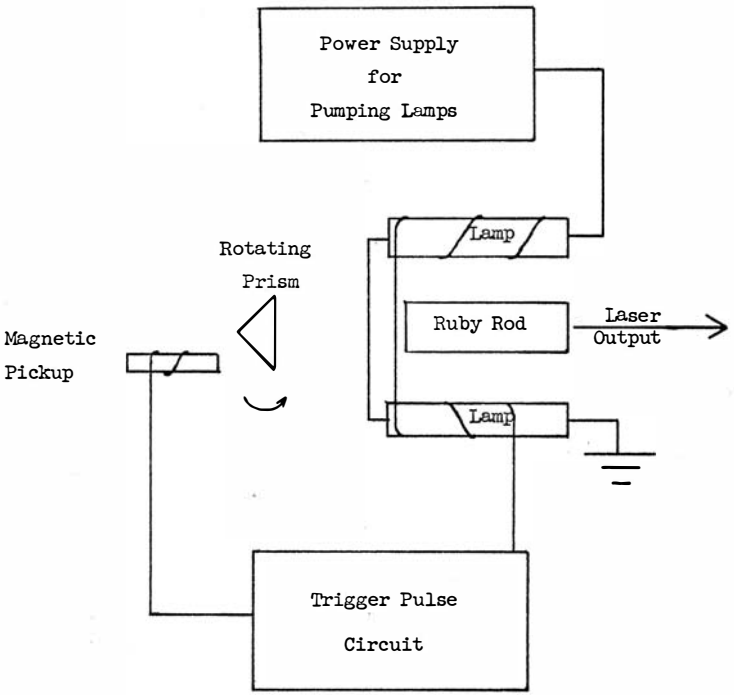

Figure 2. Diagram of Laser System

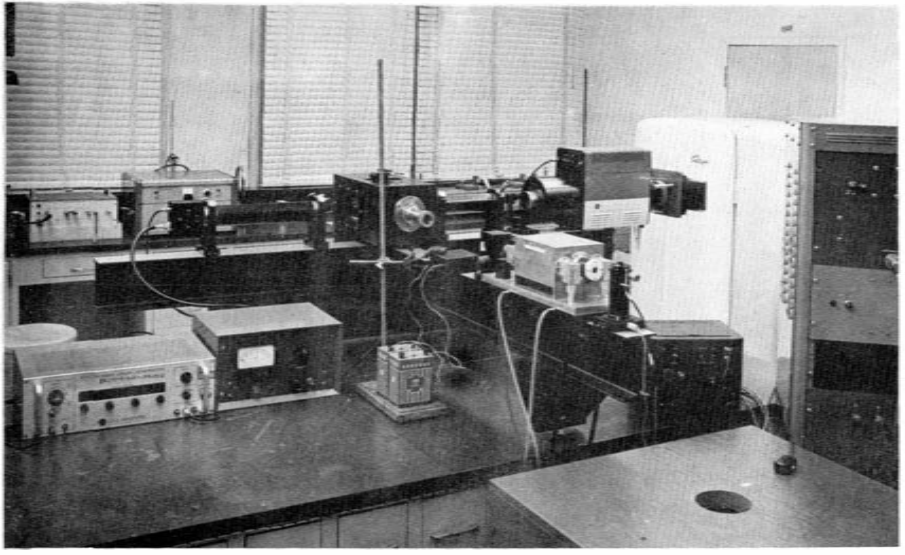

Fig. 3. Photograph of laser and schlieren system.

system. The energy source for the flash lamps which are connected in series consists of a condenser bank having a total capacitance of 1440 microfarads fed through a 550 microhenry choke. When the condensers are charged to 3200 volts the energy output to the lamps is about 7,400 joules. The duration of the light pulse from the flash lamps was 3 milliseconds as determined by a fast rise time diode (EG and G, SD-100).

The laser was operated in the Q-switched mode by means of a spinning, totally reflecting or (90^{o}) prism which served as the back reflector. A magnetic pickup on the spinning prism produced a trigger pulse which, after amplification, fired the lamps 3.5 milliseconds before the prism was in position for total reflection.

The ruby laser is sensitive to temperature changes, becoming more inefficient as the temperature of the rod increases after exposure to the flash lamps. This effect is minimized by cooling the rod with a solution of copper sulfate (10 gm/liter). Copper sulfate is used because it absorbs strongly in the region above 7,000 A^{o} while transmitting 90 percent of the light in the pump bands of the ruby laser.

The output of the laser was measured with a thermopile calorimeter (Technical Research Group, Inc., Model V2913B) as a black body receiver and found to be approximately one joule when operated at 3200 volts in the Q-switched mode. The calorimeter provided a measure of the total energy output in the pulse. The distribution of power density versus time was determined independently by using an F-4000 (International Telephone and Telegraph) light sensitive diode. A photograph of this distribution taken with a Tektronics 585

oscilloscope operated at a sweep speed of 50 nanoseconds/cm is shown in Figure 4. The pulse is seen to be approximately 50 nanoseconds wide at half maximum amplitude. In order to monitor the laser output an F-4000 diode was connected to an integrating capacitor and calibrated against the calorimeter. A small but constant fraction of the total energy in the pulse was reflected out of the main beam by means of a beam splitter and absorbed on the surface of the F-4000 diode, thus providing a means of monitoring the laser pulse used to produce the acoustic signals (100).

B. PRESSURE TRANSDUCER

Piezoelectric crystals were used to detect and measure the amplitude of the pressure transients. Since several materials possess piezoelectric properties suitable for the generation and detection of acoustic signals, preliminary studies of the response to pressure transients were made with barium titanate, lead metaniobate, and quartz. Quartz was selected for use in this study since the piezoelectric properties of quartz are stable over long periods of time and a wide range of temperatures and stress conditions, making it useful even as a frequency standard. For example, Cady (101) indicates that the piezoelectric constant d_{11} (see Appendix C) has a rate of variation of the order of 0.1 percent per degree over a range of several hundred degrees. He also points out that stresses as high as 1000 atmospheres cause only a 0.1 percent decrease in d_{11}. The piezoelectric properties of ceramics, however, such as barium titanate and lead metaniobate are found to vary with age, use, and temperature. The sound propagation velocity in barium titanate, for example, may vary as much as 15 percent over a

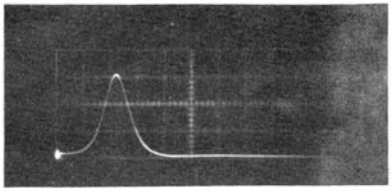

Fig. 4. Photograph of laser light intensity versus time.
Abscissa: 5×10^{-8} sec. per division.

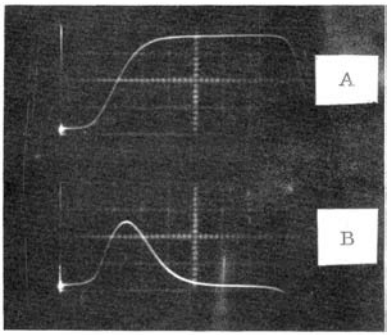

Fig. 5. Photograph of piezoelectric transducer output voltage resulting from laser-induced acoustic transient.
Ordinate: A - 40 volts per division (undifferentiated)
B - 4 volts per division (differentiated)
Abscissa: 5×10^{-8} sec. per division.

range of 50^{o} centigrade (102). The piezoelectric ceramics are advantageous for generating high pressures but for the detection of acoustic signals, quartz transducers are of equal sensitivity and are more stable than barium titanate.

In the calibration of the transducers use was made of Redwood's theoretical treatment of the response of piezoelectric crystals to plane wave pressure transients (103). This theory is treated in Appendix C. Both the pressure output for a given voltage applied to a piezoelectric crystal and the voltage output for a given pressure incident on the transducer are calculated by this method. The results were tested experimentally by using two opposed transducers (Figure 6) submerged in a tank of water. A Hewlett Packard square pulse voltage generator (model 214A) was used to produce the voltage pulse applied to the output or sending transducer. The voltage output of the receiving transducer was measured with a Tektronics 585 oscilloscope equipped with a P-80 probe. The response of a transducer to a pressure transient was tested by applying a single 50 nanosecond pulse from the pulse generator to the sending transducer. The results were in good agreement with Redwood's theory. Using two quartz transducers of the same size, an output voltage of 1.93×10^{-2} volts was expected for an input square pulse of 100 volts and 50 nanoseconds duration. The measured output voltage after correction for capacitive loading was 1.85×10^{-2} volts, or a difference of about 5 percent.

An x-cut quartz transducer, 1.5 cm in diameter and 2 mm thick, (Valpey Corporation) was used to study the pressure transients produced by the absorption of the laser light. This transducer was

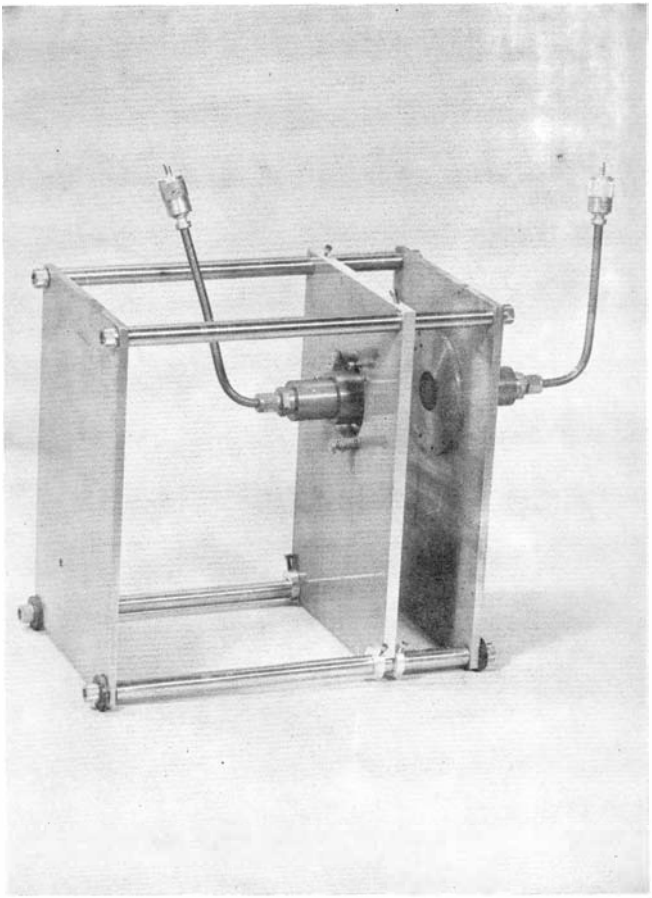

Fig. 6. Photograph of piezoelectric transducer calibration rack with opposed transducers.

mounted in a brass holder with nonconductive epoxy. Both front and back surfaces of the transducer were plated with gold to provide electrical contact. The front surface, connected electrically to the brass holder with conductive paint, was held at ground potential. The back surface of the transducer was connected to the signal conducter by a spring loaded gold contact. Swagelok connectors and brass co-axial tubing with teflon insulation (Micro-Coax UT250, Uniform Tubes, Inc.) were used to make watertight connections, enabling the entire transducer to be immersed in water for testing. Figure 7 is a diagram of the transducer and holder.

Redwood's theory (see Appendix C) predicts that the voltage output distribution with time will be in the form of the integral of the pressure versus time distribution. Since the pressure versus time distribution rather than its integral is desired, it was necessary to differentiate the output voltage. This was done electrically using a simple RC differentiator with a time constant of 8 nanoseconds. An impedance matching circuit was designed to match the transducer output to the differentiator (Figure 8). The overall response time of the transducer, impedance matching circuit and differentiator was of the order of 20-30 nanoseconds.

The expression for the stress, S, incident on the transducer in terms of the output voltage, V, is:

$$S = \frac{\epsilon(Z_d + Z_1)}{2e_d} \frac{dV}{dt}, \qquad \text{(III-1)}$$

where

$\epsilon = 3.94 \times 10^{-11}$ coul^2/Nt m^2, the clamped or high frequency

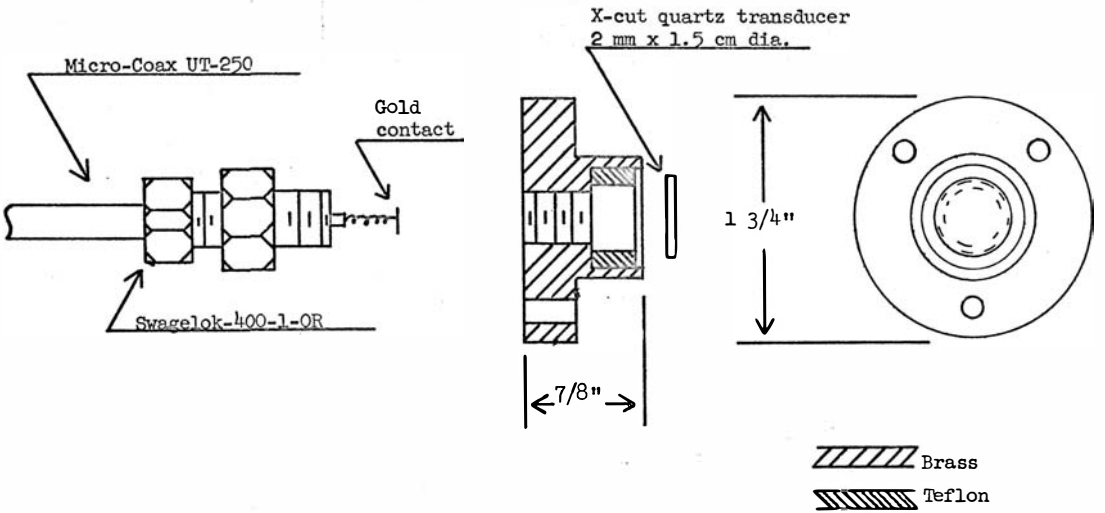

Fig. 7. Transducer mount.

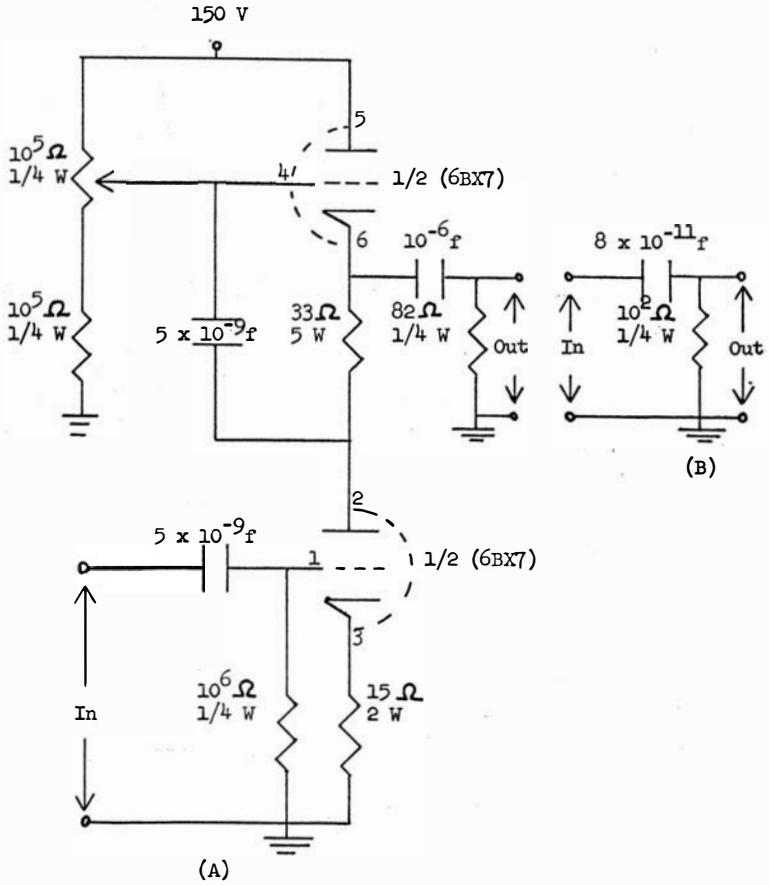

Fig. 8. Schematic of impedance matching circuit (A) and pulse differentiator (B).

dielectric constant of quartz (104),

Z_d = 1.5 x 10^7 Kg/m^2 sec., the characteristic impedance of quartz (105),

Z_l = 1.46 x 10^6 Kg/m^2 sec., the characteristic impedance of water,

e_d = 0.167 coulombs/m^2, the piezoelectric stress constant for quartz (106).

Using these values, S = 1.93 x 10^{-8} dV/dt, where V is in volts and S is in atmospheres.

Figure 5, page 59, is a photograph of the voltage output of the transducer produced by the absorption of an unfocused laser beam in a Prussian blue dye absorber (14.2 gm/liter). The upper trace corresponds to the voltage output as measured with a Tektronics 585 oscilloscope before differentiation and the lower trace to the voltage output after differentiation. The latter trace may be compared to Figures 22 and 23 of Appendix A which show the stress calculated using equation (A-24). The form of the voltage pulse is seen to correspond more nearly to negatives of the stress of Figure 23 than of Figure 22. Since there is almost no detectable negative voltage output, it may be assumed that because of the time necessary for heat conduction the form of the temperature distribution is approximated best by the case in which g = 1. It is noted that the rise and fall times of the calculated transient are steeper than those observed experimentally. This can be accounted for by the 20-30 nanosecond response time of the transducer system.

C. THE SCHLIEREN SYSTEM

A schlieren system was used to obtain a visual representation of the acoustic transient as it travels through an aqueous medium. Figure 3, page 56, is a photograph showing the schlieren system mounted on an optical bench with its optical axis perpendicular to the path of the laser light.

The irradiation tank (Figure 9) is large enough so that the entire irradiation cell containing an absorbing dye solution and the TMV (described on page 70) can be immersed in water. Various types of absorbers with variable optical density may be introduced into the irradiation tank for the production of the acoustic transients. Figure 9 shows the irradiation tank with a carbon coated mylar film in position for irradiation. The schlieren system may be used to observe a "shadow" of the pressure wave produced by the absorption of the laser light in the dye solution or in the black plastic film at various times after the laser is fired (from 5 microseconds to 100 microseconds) by using a Space Technology Laboratory (STL) trigger delay generator to trigger the STL image converter camera.

The principle of operation of the schlieren system is based on the detection of a change in the index of refraction of the medium as a result of a change in pressure or density in the medium. A pulsed zenon lamp serves as the light source for the schlieren system. The light passes first through a 0.01 inch aperture and is then collimated by means of a positive lens (focal length, 12 inches) before passing through the irradiation tank. After passing through the irradiation tank, the collimated light is then focused so that the light passes through another small aperture (i.e., 0.01 inch)

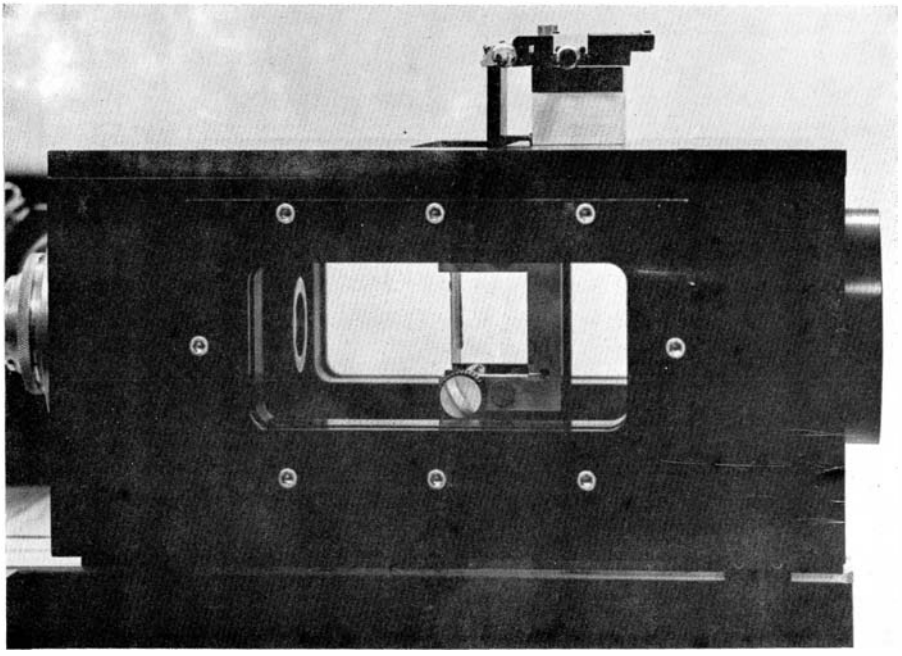

Fig. 9. Photograph of irradiation tank with plastic film absorber.

before reaching the STL image converter camera. A change in the index of refraction of the medium in the irradiation tank causes light passing through this region to be deviated due to refraction. The amount of deviation is directly proportional to the change in index of refraction. If the light is deviated to such an extent that it no longer passes through the exit aperture, a shadow will appear on the photographic film which corresponds to the location of the pressure pulse at that particular instant of time. An indication of the magnitude of the pressure wave is obtained by increasing the size of the exit aperture to the point where the deviated light passes through the aperture in such a way that no shadow is formed on the film (107).

Figure 10 shows the plane wave produced by the absorption of an unfocused beam of laser light (1 joule pulse of 50 nanoseconds duration over an area of 3.14 cm^2 or 6.4 x 10^6 watts/cm^2) on the Prussian blue solution. The time in microseconds between the absorption of the laser energy and the time of the photograph is indicated in the figure. Figure 11 shows the approach to and reflection from an air backed plastic membrane (Saran wrap) of an acoustic wave produced by the absorption of a focused laser beam on the Prussian blue solution. The profile of the acoustic pulse is curved because expansion of the medium occurs in all directions. It is also noted that the magnitude of the reflected wave is of about the same magnitude as the incident wave for the air backed case. For the water backed membrane (vertical line), Figure 12, the reflection is not discernable. However, the impedance mismatch producing reflection at a water-air interface causes the incoming

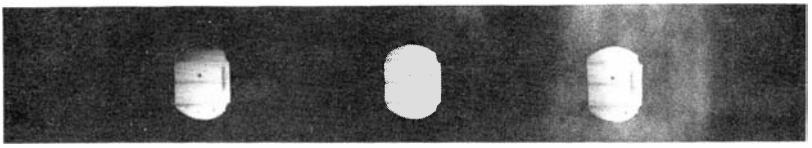

10 11 12

Fig. 10. Schlieren photograph of plane pressure wave resulting from the absorption of unfocused laser light in Prussian blue dye solution. (Numbers refer to time in microseconds after absorption of laser energy.)

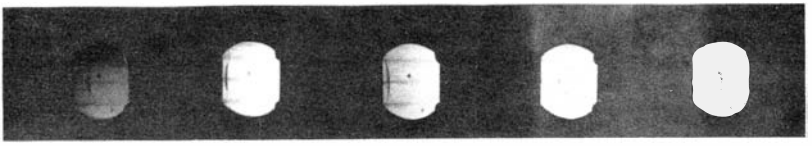

25 30 35 40 45

Fig. 11. Schlieren photograph of the reflection of a laser-induced pressure wave incident on an air backed plastic membrane located at left hand boundary of photograph. Direction of incident wave right to left.

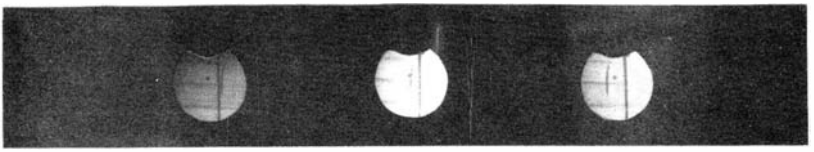

30 35 40

Fig. 12. Schlieren photograph of the transmission of a laser-induced pressure wave incident on a water backed plastic membrane located to the right of the center of photograph. Direction of incident wave right to left.

positive pressure pulse to be changed to a negative pressure so that conceivably cavitation may occur. Figure 11, however, shows that if cavitation does occur, pressure pulses of the same or greater order of magnitude as the original pulse are not produced within 10 microseconds after reflection from the surface. This result indicates that if cavitation is produced it does not lead to the production of pressure pulses of high amplitude.

D. THE IRRADIATION CHAMBER

The chamber used for the exposure of the virus suspension to the acoustic transients was a modified Rose chamber (tissue culture chamber)(108). The chamber as ordinarily used in tissue culture work consists of two metal retaining plates (3 x 2 x 1/8 inch) with a hole (1 inch diameter) in the center of each. The two plates are separated by a 1/8 inch silicon rubber gasket with a hole in the center of the same diameter as the metal plates. Microscope slide cover glasses serving as windows for the chamber are positioned between the rubber gasket and the metal plates. The cell is made air and water tight by bolting the two plates together with the gasket and cover glasses held in position. The absorbing dye or virus solutions are introduced into the chamber via syringes fitted with hypodermic needles (numbers 20-25).

Figure 13 is a photograph of the components of the modified chamber and the order of arrangement of the components in the assembled chamber is shown in Figure 14. The modified chamber contains two rubber gaskets (components 6 and 7) rather than the one usually used in the Rose chamber. The front window of the chamber was made of 1/16 inch thick plexiglass (component 3) and the rear

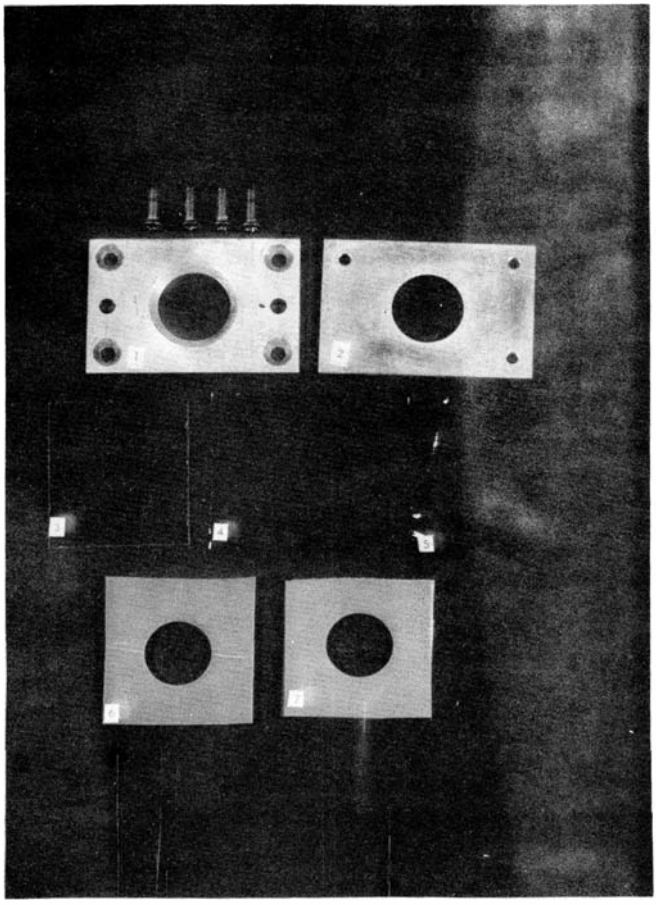

Fig. 13. Photograph of components of modified rose chamber for virus irradiation.

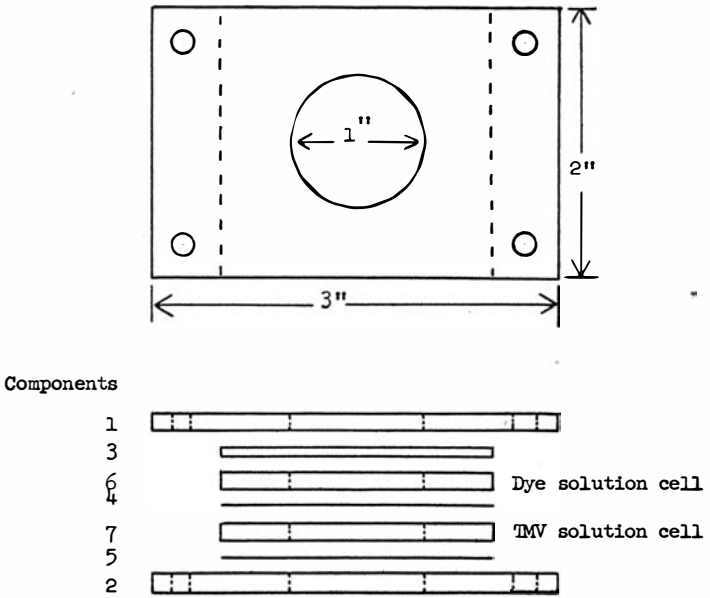

Fig. 14. Arrangement of components in modified rose chamber for TMV irradiation.

window of a thin plastic membrane of Saran wrap (component 4). An additional plastic membrane (component 5) was used to separate the chamber into two compartments. Plastic windows were necessary since glass was shattered by the acoustic transients. The plastic membranes were also used to permit the transmission of the acoustic wave with negligible reflection or attenuation when aqueous solutions were used on both sides of the membranes. No difference could be detected in the amplitude of the output of the pressure transducer when the membrane was inserted in the path of the acoustic pulse. Schlieren photographs (Figure 12) also show that the acoustic pulse passes through the water backed plastic membrane (the black line) with negligible reflection and distortion. The times given in Figure 12 refer to times after the absorption of the laser energy.

A concentrated dye solution (14.7 gm/liter Prussian blue) with an optical density of 1000/cm was introduced into the front compartment of the chamber to absorb the laser light and produce the acoustic transient. Alternatively, a black plastic membrane could be introduced between the front window and the first rubber gasket to serve as the absorber. The dye solution not only serves as a means of producing the acoustic pulse but it also serves as a thermal barrier isolating the virus solution from the high temperatures that may be produced on the surface of the dye. (In the case of the black plastic absorber, water is used in the front compartment to serve as the thermal barrier). The average temperature rise of the dye solution for an input energy of 1 joule is less than $0.2^{\circ}C$.

The chamber may be irradiated in air or in water. If the

chamber is irradiated in water, the thin plastic membrane will serve to transmit the acoustic pulse with little reflection and the solution will be exposed to essentially a single acoustic transient.

E. TOBACCO MOSAIC VIRUS PREPARATION

The tobacco mosaic virus (TMV) was obtained by infecting a suitable host (i.e., tobacco plant), allowing sufficient time for virus multiplication and then extracting the newly formed virus. The host may exhibit either a systemic infection in which the virus spreads throughout the plant, or it may exhibit a localized infection which is restricted to the area immediately surrounding the point of inoculation. Some plants may exhibit both types of infection (109). A plant exhibiting a systemic infection is desirable for the production of large quantities of virus particles (i.e., on the order of 0.1 to 1.0 gram per plant). The local lesion host is useful when an assay of virus infectivity is needed. The severity of the infection depends on the type of tobacco and the virus strain used. In some plant-virus combinations, growth is severely hampered and leaves are deformed and show the characteristic mosaic pattern of light and dark green. With other strains, the infection may be so mild that no reduction in growth or change in leaf pattern is discernable. However, even in these cases many virus particles may be isolated from the plant. The peak production of tobacco mosaic virus particles in an infected plant occurs from one to two weeks after inoculation (110). Commoner and co-workers (111) have found that the maximum production of TMV in infected leaf areas is attained about 200 hours after inoculation, there being an initiation period of 24 to 48 hours before any virus is detected. The quantities

of TMV produced reached a maximum of about 0.5 micrograms per square millimeter of leaf surface area. The host plants used in this study were of a variety of black cigar tobacco obtained from Dr. William Stepka at the Medical College of Virginia. The strain was originally obtained from the University of Kentucky.

Plants may be infected either from virus stored in dried or frozen tobacco leaves or in suspensions of purified virus (112). The virus was prepared for this study by rubbing the leaves of black cigar tobacco plants with a suspension of dried leaves known to be infected with virus. The suspension was made by grinding the dried infected leaves with a mortar and pestle in a small amount of buffer (pH 7.5). The suspension was then applied to one or two leaves of the plant to be infected by rubbing the leaves with a gauze pad dipped in the virus suspension. The virus used for the original infection was supplied by Dr. R. I. Steere of the United States Plant Virology Laboratory, Crops Research Division, of the Department of Agriculture at Beltsville, Maryland. The strain of the virus was the strain known as the common tobacco strain (ATC-2).

When the black cigar tobacco is inoculated with virus the infection spreads throughout the plant producing a systemic infection, the greatest virus infection occuring in the rapidly growing young leaves. TMV rods formed in plants are observed to vary in length from 150 A^{o} to 3,000 A^{o}. This variation in rod length is accentuated by the occurence of end-to-end aggregation which results in particle lengths of 6,000 A^{o} or more. In order to study the mechanical effects of acoustic pulses, a relatively monodisperse system of particle lengths is desired. Therefore the procedure used to

purify the virus was based on the procedure used by Steere to obtain fractions of essentially monodisperse virus particles of the length of 3,000 A^{o} (113). In order to minimize end-to-end aggregation Steere has found that the pH of the suspending medium must be held above pH 7.2, and that the ionic strength should be kept as low as possible, consistent with the maintenance of a pH of about 7.5. The presence of phosphate salts also tend to cause aggregations even above pH 7.5.

The following procedure was used to isolate the TMV. Leaves from infected plants were harvested about two weeks after infection and frozen until ready for isolation of the virus. The frozen leaves were weighed and 100 milliliters of buffer added to each 100 grams of leaves. The buffer used was 0.05 molar ethylenediamine tetraacetate (EDTA) adjusted to pH 9.5 with sodium hydroxide. The buffer soaked leaves were ground in a Waring blender for about 30 seconds. The juice was extracted from the ground tissue by filtering through gauze. The extract was then adjusted to pH 7.5 by the addition of sodium hydroxide. The extract was filtered using suction through a 1/4 inch pad of super-cel cellite (John Mansville). The filter cake was prepared with the 0.05 molar EDTA buffer used above. After the extract was filtered, additional virus particles were washed from the pad with about 40 milliliters of buffer. The virus suspension was then centrifuged at 50,000 g for 25 to 30 minutes. A clear pellet of virus particles was formed which was then resuspended in 0.001 molar EDTA at pH 7.5.

The particles produced by the above procedure are not monodisperse since some virus particles are inevitably broken in the

purification procedure. Steere has found that more nearly monodisperse suspensions may be produced by filtering the virus suspension through an agar-gel column before centrifuging. Steere (114) has been able to obtain suspensions of virus in which about 90 percent of the particles were 3,000 A^{o} long. His infectivity studies with this virus show that it is the 3,000 A^{o} length particle that is the infective unit.

Hulett and Loring (115) have made similar and more detailed studies of the infectivity of virus particles as a function of length. Their results also show that the infection is caused by the 3,000 A^{o} length particles, although they find some evidence indicating that the presence of shorter length particles enhances infectivity. They hypothesized that "the enhancement of infectivity found with the shorter rods is a specific effect possibly related to their nucleic acid content and their ability in multiple particle infections to supplement the genetic information carried by the standard particle." Hulett and Loring state that differences in concentrations of infectious material of the order of $\pm$ 20 percent can be detected by employing a local lesion host, but that there is not a one-to-one correlation between number of lesions and concentrations of virus. Their data were examined for significance using the t-test for paired variates. The control solution was spread on one half of the tobacco leaf and an irradiated solution was spread on the other half of the leaf. In this way leaf-to-leaf variation was eliminated. This method was applied in this study to the local lesion host, Nicotiana tobaccum, variety Xanthi, and the infectivity of control solutions was compared to the

infectivity of air backed solutions which had been exposed to 20 acoustic pulses produced by the absorption of an unfocused laser beam (see page 73). The obtained t value of 3.46 showed there was a significant difference at the 5 percent level (21 df) between the control and irradiated solution indicating that a decrease in concentration of infective material in the irradiated solution of 20 percent or more had occurred. This is in agreement with the 40 percent decrease estimated by electron microscopy.

Agar-gel column fractionation was used in this study to obtain a more monodisperse TMV preparation. A 1.5 centimeter diameter column 100 centimeters long was filled with agar-gel. The gel was broken into small particles and washed through 40 to 60 mesh screen seives (U. S. standard mesh series). Only those granules which passed through the 40 mesh but not the 60 mesh screens were saved for use in the column. The column was washed with 0.001 molar EDTA, pH 7.5, before adding the virus. The distribution of particle lengths was improved by the gel fractionation, there being about 60 percent of the particles in the range 2,750 to 3,250 A^{o}.

F. THE ELECTRON MICROSCOPE

Use of the electron microscope to study viruses began about 1940. The first virus to be studied was tobacco mosaic virus (116). The photomicrographs obtained during these early studies showed poor contrast, and consequently the study of viruses with the electron microscope was not widely used. In 1945 Williams and Wychoff (117) demonstrated the applicability of the newly developed shadowing technique to the photography of virus particles. Subsequently, many studies of TMV as well as other viruses have been made using this technique.

Shadowing of the virus particles is accomplished with the aid of an electron dense metal. The metal, evaporated under vacuum, provides contrast for the photomicrograph by providing regions of high and low electron density. The contrast is very high between areas covered with metal and those free from metal (in the shadow of the particle). Other than the obvious advantage of contrast, shadowing also provides a measure of the relative height of different areas of the specimen and allows a three dimensional contour of a geometrically simple object to be inferred from the shape of its shadow.

In 1959 another important contrast technique was developed by Brenner and Horne (118). This technique is referred to as negative staining. A solution of a high electron density material, phosphotungstic acid, is either mixed with the particles to be observed or placed over the particles on the supporting grid. The result is an electron dense background surrounding less electron dense particles. This method has several advantages over shadowing. One of the most important advantages is that the preparation time is shorter and that no vacuum evaporation system is needed. Another advantage is that some of the internal structure of the particle is revealed with phosphotungstic acid staining, whereas shadowing permits only the evaluation of external structure. For example, Brenner and Horne (119) were able to demonstrate the presence of the 40 A^{o} diameter hole along the long axis of the TMV rod as predicted by x-ray diffraction analysis. The resolution attainable by this method has been estimated by Brenner and Horne as about 15 A^{o}. The resolution (approximately 100 A^{o}) attained by the author does not approach this figure since instrumental magnifications of only 20,000 times were used,

whereas Brenner and Horne used magnifications up to 80,000 times.

The negative staining procedure used in this study is as follows. One-eighth inch copper wire grids (500 mesh) were coated with a 200-500 A° film of parlodion. The parlodion films were made by dipping a glass slide into a 2 percent solution of parlodion dissolved in amyl acetate. The thin film of parlodion formed on the glass slide was allowed to dry and then the film was floated off the glass slide onto a water surface. Several wire grids were placed carefully on the floating film. The film with grids attached was removed from the water surface with a piece of absorbant paper which became wet so that the film plus grids would adhere to the paper. The film and grids were allowed then to dry. Thus, each grid had a thin parlodion film over its surface and could be manipulated with forceps to perform the rest of the staining procedure. A drop of TMV solution was placed on the parlodion coated grid. The drop was allowed to remain on the grid about 15 to 20 seconds before it was removed by touching a piece of filter paper to one edge of the grid. Next, a drop of phosphotungstate solution (one to two percent at pH 7.5) was placed on the grid and removed in the same manner. The grid was now ready for placement in the electron microscope.

The microscope used was an RCA EMU-E operated at 50 KV. The particles were photographed on 3 1/4 x 4 inch Kodak projector slide plates (contrast). All photographs were made at the same magnification setting of 20,000 times. Particle lengths were measured directly from the photographic plates using a ruler and a magnifying glass. Particle lengths were measured to the nearest 0.5

millimeters (approximately 250 A^{o} at particle dimensions).

The measured lengths and widths of TMV particles stained with phosphotungstic acid are in excellent agreement with those obtained by x-ray diffraction analysis, indicating that any artifacts introduced by the method had little effect on these dimensions. Williams and Steere (120) have made detailed studies of the artifacts produced when TMV particles are prepared for electron microscopy. Their results indicate that except for a small amount of breakage, the electron micrographs give a true representation of the TMV particles as found in vivo. In support of these conclusions, Steere (121) has observed 3000 x 150 A^{o} particles in hair cells of infected Turkish tobacco. The particles were observed by freezing the cells and shadowing with heavy metal. A herringbone pattern of 3,000 A^{o} long particles lying parallel to each other was found in the cells. It should be noted that even in so-called monodisperse fractions of TMV particles, the particle length is not exactly 3,000 A^{o}. Hall (122) for example, found the lengths to be in good agreement with Steere's determination of 2,980 A^{o} with a 50 A^{o} standard deviation. However, he found that the monomer length varied as much as 8 percent (or about 250 A^{o}) and concluded that this was due to a real variation in the actual monomer length since the method used to determine the length was more precise than this. On this basis the monomer length may be expected to fall within the range of 2,750 to 3,250 A^{o}.

The most probable source of artifacts in applying this technique is the process of drying the prepared grids. In some systems where high salt concentrations are involved, the drying leads to further

concentrations of the salts which may affect the contrast due to high electron density. In the present work the salt concentration was kept low and no additional procedure such as washing the grids in distilled water after drying was required.

Other artifacts produced by air drying are those related to surface tension forces. As the solution of particles dries, particles will tend to concentrate in the last areas to dry. The form of the particles may be flattened or distorted. For counting particles of known shape and size this can sometimes be an advantage since many particles may be photographed simultaneously. Breakage of TMV rods which occurs during preparation is taken into account by using control solutions. The magnititude of the surface tension forces and a more detailed account of their actions has been discussed by Anderson (123). Horne and Wildy (124) have discussed the use of phosphotungstate on various viral preparations. They point out that several studies have indicated that even after the virus is mixed with phosphotungstate and dried, 100 percent infectivity is retained. Other viruses, however, appear to exhibit some distortion in drying in the phosphotungstate, depending upon the concentrations of the stain. It is therefore important to use phosphotungstate at concentrations and at pH's where artifacts are minimized. For TMV the use of 1 to 2 percent phosphotungstate at pH 7.5 has been found to be satisfactory.

CHAPTER IV. ANALYSIS AND RESULTS

A. PROCEDURE

The experimental procedure employed in the exposure of TMV to acoustic transients required the use of a modified Rose chamber described in Chapter III, page 70. A concentrated Prussian blue dye solution (14.2 gm/liter) or a carbon coated mylar film served as the absorber for the production of the acoustic transients. The chamber was irradiated both in air and in water in order to observe the effect of a reflection of the acoustic wave at the air-TMV solution boundary. The effects produced by focusing the laser beam to a small diameter (order of 1 to 4 mm) were also investigated. Specimen grids for use in the electron microscope were prepared by the procedure given in Chapter III, page 80. The particles were photographed using 3 1/4 x 4 inch projector slide plates (Kodak contrast). The length of each TMV particle was measured directly from the slide plates with the aid of a magnifying glass. Each time a specimen grid was prepared for an irradiated solution a grid was also prepared for a control solution which was treated in the same manner as the irradiated except that it was not exposed to acoustic transients.

The effects of the various exposure conditions on the distribution of particle lengths were compared graphically and evaluated statistically using the Kolmogorov-Smirnov goodness of fit test.

B. STATISTICAL CONSIDERATIONS

The Kolmogorov-Smirnov goodness of fit test can be used to determine if two independent samples have been drawn from populations

with the same distribution. Either one- or two-tailed tests may be made depending upon the statistical hypothesis to be tested. The two-tailed test is sensitive to any kind of difference in the distributions such as central tendency, dispersion, and skewness (125). The one-tailed test is used to test hypotheses concerning the displacement of the distribution of one population relative to another population. If breakage of the TMV particles occurs on exposure to acoustic transients the values of the particle lengths in the exposed materials would be expected to be less than in the control and the one-tailed test would be appropriate. However, since intra-comparisons of control solutions were also necessary using the Kolmogorov-Smirnov test, the more general two-tailed test was used throughout the study for comparisons of the samples and inferences regarding the nature of the differences produced in the samples by exposure to acoustic transients were made on the basis of the graphical data.

Samples of m and n observations respectively may be compared using the Kolmogorov-Smirnov test under the assumption that they are mutually independent random variables having a common (unknown) continuous cumulative distribution function F(x). If $S_m(x)$ and $T_n(x)$ are the corresponding empirical cumulative distribution functions, then a new variable, D, may be defined by

$$D = \text{maximum} \left| S_m(x) - T_n(x) \right|. \qquad \text{(IV-1)}$$

If the two samples are drawn from the same population, then the cumulative distribution of both samples should differ only slightly due to random deviations in the sampling procedure. Conversely,

large deviations between the two sample cumulative distributions is evidence for rejecting the hypothesis that the two samples were drawn from the same population. If it is assumed that n and m approach infinity in such a way that m/n approaches a constant, then it may be shown for fixed $z \geq 0$ that the

$$\text{probability of } D \leq N^{-1/2}z \rightarrow L(z) \qquad \text{(IV-2)}$$

where

$$L(z) = 1 - 2\sum_{v=1}^{\infty}(-1)^{v-1}e^{-2v^2z^2} \text{ and}$$

$$N = mn/(m + n). \quad (126)$$

D is completely distribution-free since it is simply the value of the largest vertical difference between $S_m(x)$ and $T_n(x)$. Any one-to-one transformation of x will affect only the horizontal differences in the distributions and vertical differences will remain unchanged. Table 2 gives a list of z values for various levels of significance (127). The 5 percent level of significance was used throughout this study as the level of significance for the rejection

Table 2

Critical values of z in the Kolmogorov-Smirnov two-sample test

(sample size > 40: two-tailed test)

Level of significance	z
0.1000	1.22
0.050	1.36
0.025	1.48
0.010	1.63
0.005	1.73
0.001	1.95

of the null hypothesis of no difference between the distributions.

C. RESULTS

The experimental results of exposure of TMV solutions to acoustic transients are summarized in Table 3, page 92. The original data as obtained from electron micrographs consisted of frequency distributions of the TMV particle lengths. Figure 15 is a photomicrograph of a control solution of TMV that has been mixed with Dow polystyrene latex spheres (880 A^{o} diameter) for size comparison. Figure 16 is a photomicrograph of a TMV solution that has been exposed 10 times to acoustic transients produced by an unfocused laser beam under air-backed conditions. Frequency distributions corresponding to control and irradiated solutions are shown in Figures 17 and 18. In this case the TMV solution was exposed 8 times to the acoustic transients produced by the focused laser beam (1 mm diameter) under water-backed conditions. In the particular cases chosen for illustration, it is readily apparent that exposure to acoustic transients has altered the particle length distribution. Cumulative distribtuions were calculated for each control and exposed sample. Figure 19 is a graph of the cumulative distributions for the same control and exposed sample used in Figures 17 and 18. The maximum difference in the ordinates of the two cumulative distributions is the D value used in equation (IV-1). Values of D were calculated for all exposed and control sample pairs. The values of D are listed in Table 3. The level of statistical significance associated with a given D value is given in the last column of Table 3. The 5 percent level of significance is used as the criterion for the rejection of the null

Fig. 15. Electron micrograph of control TMV solution.

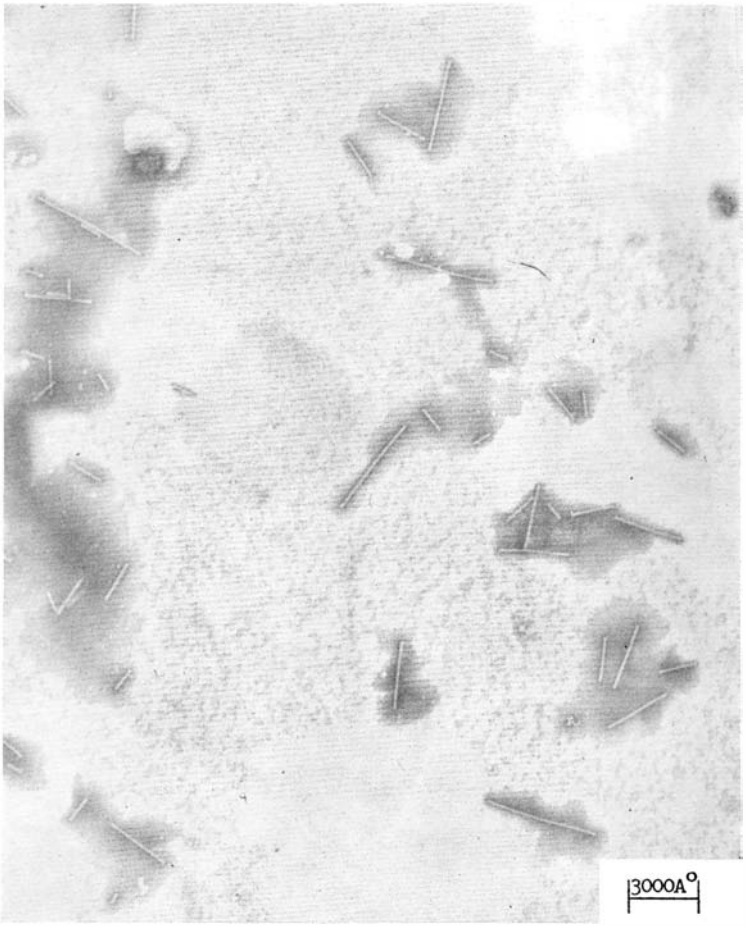

Fig. 16. Electron micrograph of exposed TMV solution. Air backed TMV solution exposed 10 times to acoustic transient produced by absorption of laser light (6.4×10^6 watts/cm^2) in Prussian blue dye solution.

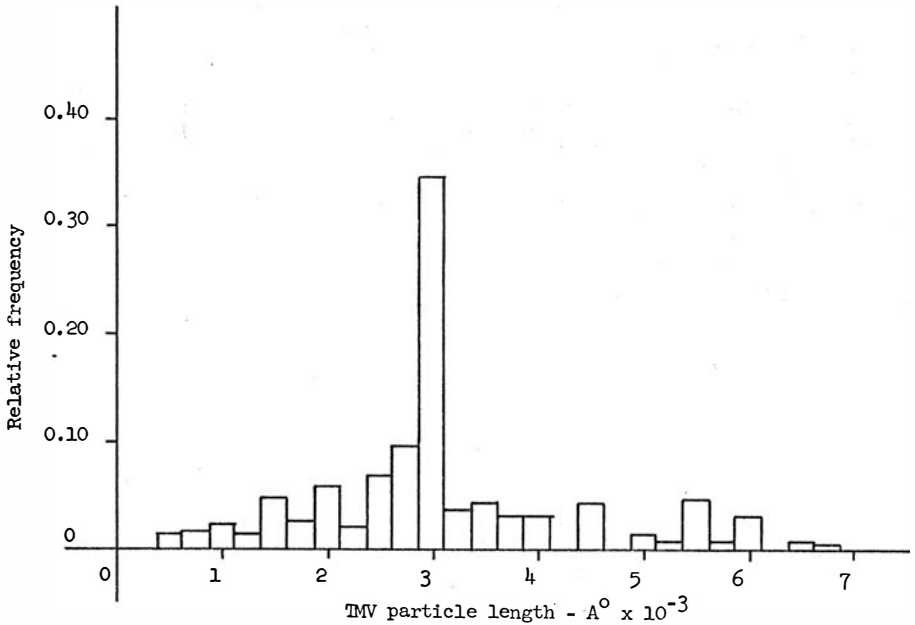

Fig. 17. Frequency distribution of control TMV particles (Fraction 4).

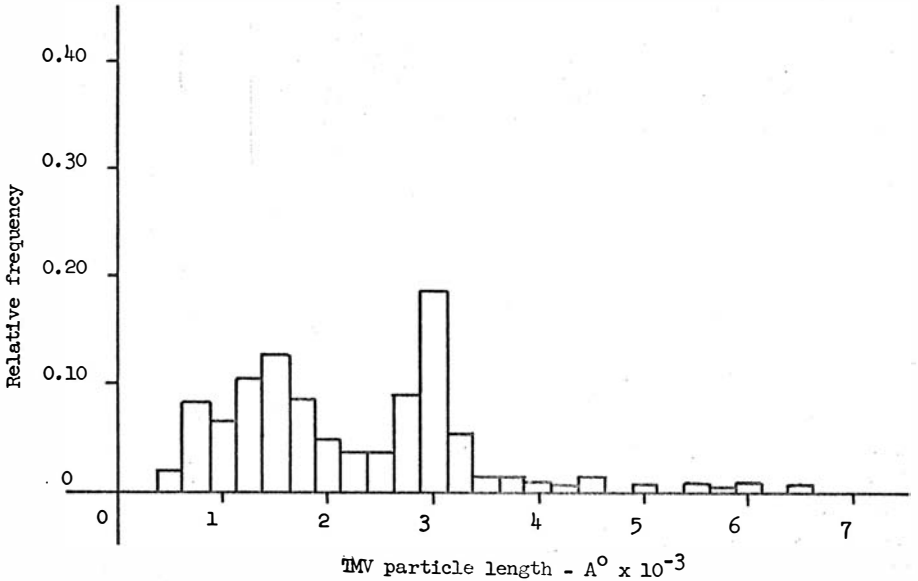

Fig. 18. Frequency distribution of exposed TMV particles. (Fraction 4; exposed 8 times; laser focused to 1 mm dia.; water backed TMV solution)

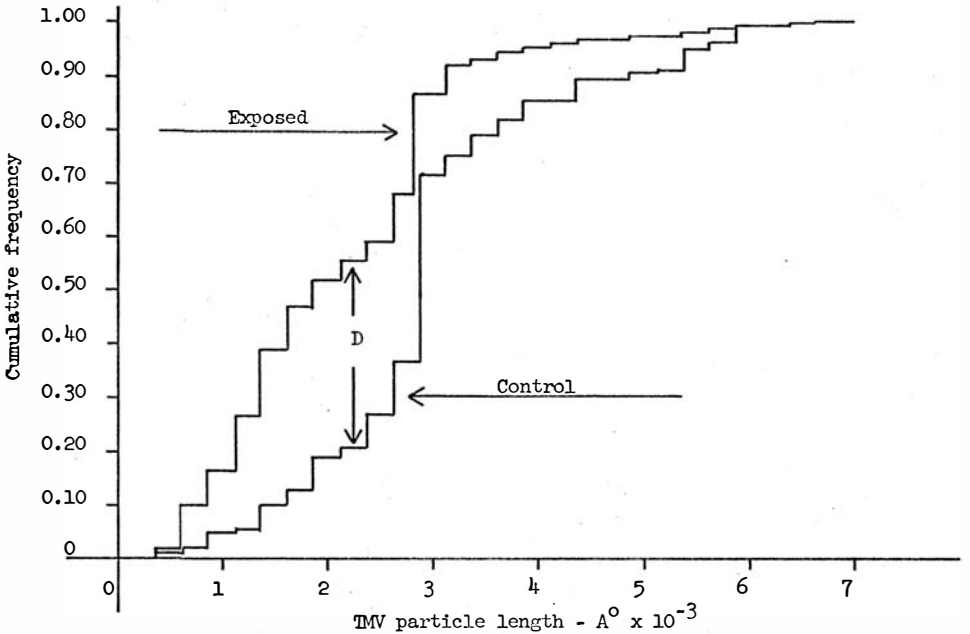

Fig. 19. Cumulative frequency distributions of control and exposed TMV particles. (Fraction 4; exposed 8 times; laser focused to 1 mm dia.; water backed TMV solution)

Table 3

Results of Kolmogorov-Smirnov Test

Fraction Number	Conditions of Exposure	Number of TMV Particles		D Value	Level of Significance
		Control	Exposed		
1*	air-backed sample laser unfocused				
	a. exposed 3 x	270	230	0.208	< 0.001
	b. exposed 6 x	270	230	0.379	< 0.001
	c. exposed 9 x	270	46	0.418	< 0.001
	d. exposed 12 x	270	190	0.391	< 0.001
2	air-backed sample laser unfocused exposed 10 x	119	144	0.494	< 0.001
3	air-backed sample laser focused to 2 mm dia. exposed 1 x	84	48	0.440	< 0.001
4	water-backed sample				
	A. laser focused to approximately 4 mm dia.				
	a. exposed 2 x	236	176	0.103	> 0.100
	b. exposed 4 x	236	80	0.156	> 0.100
	c. exposed 8 x	236	201	0.161	< 0.010
	B. laser focused to approxmiately 1 mm dia.				
	a. exposed 2 x	236	99	0.081	> 0.100
	b. exposed 4 x	236	208	0.218	< 0.001
	c. exposed 8 x	236	245	0.347	< 0.001
5	exposed to unfocused laser 10 x				
	A. air-backed sample	262	396	0.349	< 0.001
	B. virus suspension with intervening water layer between virus solution and water-air interface	262	265	0.070	> 0.100

*Carbon coated mylar film

hypothesis.

The laser pulse used to produce the acoustic transients had a total energy of one joule and a duration of 50 nanoseconds (see page 57). The absorber used was either a carbon coated mylar film or a Prussian blue dye solution (14.2 gm/liter). Since an estimate of the optical attenuation coefficient could be more easily attained for the dye solution than for the carbon coated film, it was decided to restrict most of the measurements to the latter system. The optical attenuation coefficient of the dye solution was obtained by diluting the dye and determining the attenuation coefficient and extrapolating according to Beer's law to the concentration of the dye solution used in the experiment. The attenuation coefficient was measured using a Beckman DK spectrophotometer fitted with a variable optical path length cell. The attenuation coefficient at the ruby laser wave length of 6943 A^{o} was found to be 1000 per cm.

The numbering of the fractions listed in Table 3 is unrelated to the order in which the fractions were obtained from the agar-gel column (see page 78). Only those fractions having the highest percentage of monomers were used in the experiments. The monomer was taken to be any particle that was measured to be 3000 ± 250 A^{o} (see page 81). Control samples obtained from the same fractions were compared with each other over a 2 day period to investigate the possible effect of aging of the virus suspension. No significant difference at the 5 percent level could be detected over this period. Since the same procedure was used in preparing the exposed and control samples, it is apparent that any significant difference in the frequency distributions of the control and exposed samples is

due to the effect of exposure to the acoustic transients.

As emphasized in Chapter II, the magnitude of the forces exerted on the TMV particles is dependent on the occurence of aggregations. Boedtker and Simmons (128) have studied the properties of TMV in solution by various physical means such as light scattering, flow birefringence, and viscosity. The method of light scattering is particularly sensitive to the presence of aggregates since the scattering is heavily weighted at low angles for the larger particles. Therefore, if aggregates are present the molecular weight and length will not be consistent with that determined by other methods. The light scattering data of Boedtker and Simmons as well as the earlier work of Oster (129) show that TMV does not form aggregates in the pH range 7 to 7.7 and under conditions of preparation similar to that employed in this study (see Chapter III, page 76). Since light scattering equipment was not available for the present study, another procedure was used which followed Steere's (130) method for preparing specimen grids to obtain representative sample populations. In this procedure, the TMV particles in a one percent solution of phosphotungstic acid are sprayed onto the specimen grids using a Vaponefrin nebulizer (No. 4662). The nebulizer produces very fine droplets of solution which, upon drying of the specimen grids, yield easily recognizable circles of the order of 5×10^{-3} cm or less in diameter. If aggregates are present in the TMV solution some of the droplets should contain a large number of particles and others only a few or none. Approximately 100 droplets were observed on several different specimen grids and from these observations there was no

evidence that the particles had formed aggregates. This method is suspect in that the particle size is decreased at the 5 percent level (Kolmogorov-Smirnov test) showing that the process of spraying leads to breakage of the TMV particles and possible disruption of aggregates. Even if aggregates are disrupted, it is doubtful that the particles would have time to be uniformly distributed throughout the solution as they are sprayed onto the specimen grids. Since the results from both the light scattering technique and the spray technique are in agreement, it can be assumed with confidence that no appreciable aggregation occurs in the solution. In view of these results the case considered in Chapter II in which the particles may be assumed to be isolated from each other appears to be more appropriate than assuming the presence of aggregates of the order of 10^4 particles which would be necessary to significantly increase the chance of breakage due to aggregation (see Appendix B, page 146).

Because of the above mentioned breakage, preparation of the specimen grids by spraying was not used in the study of the effects of exposure to acoustic transients. However, this method does provide a convenient way to determine the approximate concentration of the TMV particles. A solution of polystyrene latex spheres of known concentration was mixed with the TMV solution and the mixture sprayed onto specimen grids. The total number of polystyrene spheres and TMV particles in several droplets were counted. The ratio of TMV particles to polystyrene particles was used to estimate the concentration of TMV to be 4×10^{11} particles per cm^3.

The values of D listed in Table 3 give an indication of the

magnitude of the effect of the exposure to the acoustic transients and it is seen that in general the amount of breakage increases both with the number of exposures and the degree to which the laser beam was focused.

Figure 20 is a plot for fraction 4 showing the change in the percentage of 6000 A^{o}, 3000 A^{o}, 1500 A^{o}, and 750 A^{o} particles with the number of exposures resulting from a laser beam (focused to a diameter of 1 mm) and under water-backed conditions. It is observed that the relative number of longer particles decreases with the number of exposures while the number of shorter particles increases.

The theoretical values of the tensile force exerted at the center of the TMV monomer are given in Table 4. These values were obtained using equation (II-18), page 45. The power density of the laser beam (watts/cm^2) used in calculating the forces was obtained by dividing the incident laser power of 20 megawatts by the cross-sectional area of the absorbed beam. The volume coefficient of viscosity (3.1×10^{-3} Kg/m.sec) was used rather than the shear

Table 4

Estimated Forces Exerted on TMV

Diameter of Laser Beam (mm)	F_{avg} (dynes)	F_{max} (dynes)
20 ± 4	$5.15 \times 10^{-7} \leq F_{avg} \leq 2.06 \times 10^{-6}$	$8.12 \times 10^{-7} \leq F_{max} \leq 3.24 \times 10^{-6}$
4 ± 1	$2.12 \times 10^{-5} \leq F_{avg} \leq 5.89 \times 10^{-5}$	$3.32 \times 10^{-5} \leq F_{max} \leq 9.25 \times 10^{-5}$
1 ± 0.5	$2.36 \times 10^{-4} \leq F_{avg} \leq 2.12 \times 10^{-3}$	$3.70 \times 10^{-4} \leq F_{max} \leq 3.33 \times 10^{-3}$

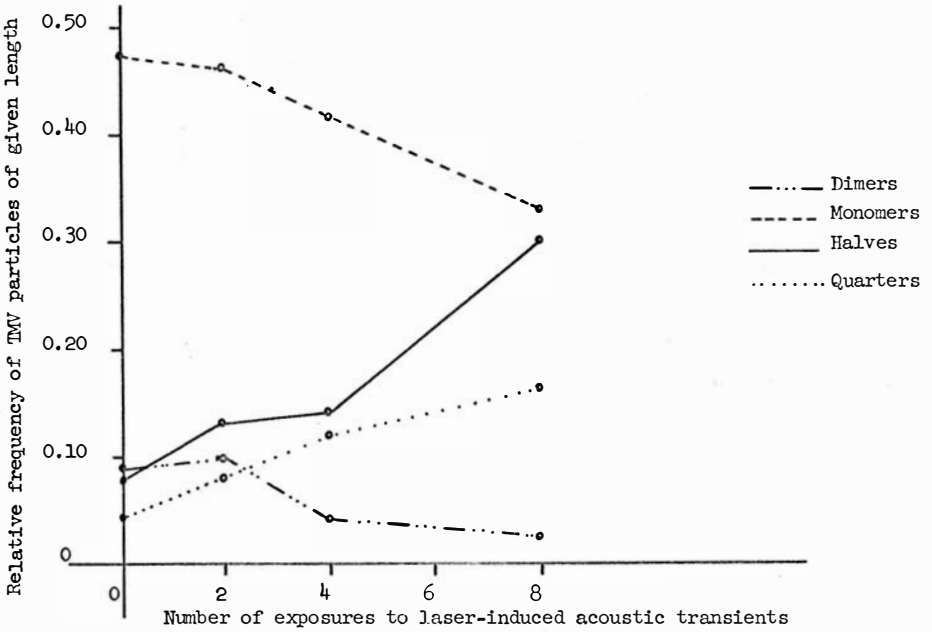

Fig. 20. Relative frequency of TMV particles of given length versus number of exposures to laser-induced acoustic transients (Fraction 4; laser focused to 1 mm dia.; water backed TMV solution)

coefficient, since expansion of the solvent occurred along the direction of propagation of the acoustic wave (131). As previously found (see page 93), the absorption coefficient for the incident laser light was 1000 cm^{-1}.

The values of the estimated forces exerted on TMV in Table 4 may be compared to the 2.64 to 3.65 x 10^{-4} dynes of force calculated as necessary to rupture the TMV particle based on the strength of primary chemical bonds (see page 52). Table 4 indicates that when the beam is focused to 4 mm in diameter or less, the forces produced by the pressure transients on the TMV particle are comparable in magnitude to the bond strength forces. However, when the beam is unfocused (approximately 2 cm diameter) the forces are not of comparable magnitude. When the irradiation chamber is water-backed so that the TMV solution is exposed to only one acoustic transient without reflection no significant breakage of the TMV particles is found until the beam is focused down to a diameter of 4 mm or less.

When the laser beam was focused to 1 mm diameter the percentage of monomer dropped from 48 to 33 percent after being exposed 8 times to the acoustic transient. This represents approximately a 3 percent breakage of monomers per exposure to the laser-induced transient. This figure is inexact since particles of other lengths are present which may also be broken by the acoustic transient. For example, if a large percentage of dimers are present they may be broken into monomers and the percentage of monomers may increase rather than decrease on exposure to the acoustic transient. It is further recognized that when the beam is focused to a small diameter a part of the TMV solution is exposed to greater acoustic pressures than

other parts as is shown in figure 11 where the shadow representing the pressure wave is darker at the center than at the ends. For comparison of the two cases in which the beam was focused to 1 mm and 4 mm, assume that a plane wave of this diameter is produced and that all of the monomers exposed to this wave are broken. Based on the area of TMV solution exposed to the acoustic wave, less than 1 percent of the TMV particles would be broken when the laser is focused to a diameter of 1 mm, whereas when the laser is focused to a diameter of 4 mm about 2 percent would be broken. However, the data show that 3 percent are broken in the 1 mm case and less than 1 percent in the 4 mm case. The first result is explained by the fact that the focused wave is spherical to some extent rather than plane. A quantitative study of the variation in intensity of the pressure wave across the plane of the absorber has not been possible since it has not proved feasible so far to design and calibrate small transducers (1 mm or less in diameter) for the determination of the amplitude distribution of the pressure transient. The second result may be explained by the effect of the orientation of the particles in the solution. Figure 21 shows the variation of the tension exerted on the particle as a function of the angle of orientation of the long axis of the particle with respect to the direction of propagation of the acoustic wave. Depending on the angle of orientation, the force on the particle may vary from zero when the particle is in the plane of the pressure wave to the maximum when the long axis of the particle is parallel to the direction of propagation of the wave. When the laser beam is focused to 1 mm diameter the orientation of the particles will have relatively little effect

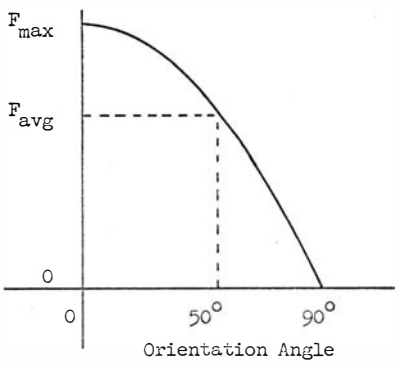

Fig. 21. Relative tension exerted at the center of the TMV particle versus the angle of orientation of the particle with respect to the direction of propagation of the acoustic wave

on the observed breakage since the force in this case is sufficient to break the particles in almost any orientation. However, when the laser beam is focused to 4 mm diameter the magnitude of the hydrodynamic forces is smaller by an order of magnitude than in the 1 mm case and orientation effects become more important so that only those particles with their long axes oriented within a small range of angles about the direction of propagation will be broken. For example, (see figure 21) only those particles which fall within an angle range of 0^{o} to 50^{o} will be exposed to a force greater than the average force, the average force being about 64 percent of the maximum force. Therefore, if only those particles which are exposed to the average force or greater are broken, then about 1 percent rather than 2 percent breakage would be expected. Thus, the observed breakage of less than 1 percent is consistent with the hypothesis that breakage will occur only in those particles favorably oriented with respect to the acoustic wave.

When the irradiation chamber is air-backed, breakage occurs at a much lower acoustic pressure than in the water-backed case. The experiments on fraction 5 in Table 3 indicate that the difference is not caused primarily by the increased number of reflections at the water-air interface. In this experiment an additional rubber gasket was used in the modified Rose chamber so that the TMV sample was surrounded on both sides by water. However the final water-filled gasket was air-backed so that the TMV solution was still exposed to the reflections from the exterior water-air interface after these reflections were transmitted back through the intervening water layer. Calculations on the attenuation and reflection of acoustic waves in water (see page 30) show that about 10 reflections could occur before the amplitude is decreased by a factor of 1/e (i.e., 37 percent). Since the number of reflections is very nearly the same for the two types of exposures of fraction 5, the difference must be because the wave is reflected from the boundary containing the TMV solution in one case and not in the other. It is known (see page 28) that when a positive pressure wave such as occurs in this study is reflected from a boundary between a medium of high acoustic impedance such as water and a medium of low acoustic impedance such as air a change in phase of approximately 180° occurs for a free boundary (132). The particle velocity changes from U to 2U on reflection at a perfectly free surface, resulting in an infinitely steep velocity gradient at the boundary. The plastic membrane which serves to separate the TMV solution from the air cannot be considered to provide a perfectly free surface; therefore, the velocity gradient at the surface has a finite but unknown magnitude.

If it is assumed that breakage of the TMV particles is due to the presence of this gradient, then the experimental results indicate that the magnitude of the gradient at the boundary is at least 10 times greater than the gradient within the solution. Although it is not possible to measure this gradient with the piezoelectric transducer, since its presence would destroy the boundary conditions being investigated, it would appear that this represents a logical explanation for the enhanced breakage at the air-water interface.

CHAPTER V. SUMMARY AND CONCLUSIONS

The mechanical effects of transient acoustic waves on tobacco mosaic virus (TMV), a geometrically well defined biological model, have been investigated and it has been determined that these transients produce breakage which significantly alters the frequency distributions of the particle lengths. A hydrodynamical analysis of the forces exerted on an elongated particle has been made based on methods developed by Oberbeck (133), Burgers (134), and Brenner (135) for determining the forces on ellipsoids of rotation and cylinders immersed in arbitrary flow fields.

The use of pressure transients in this study, rather than continuous waves, simplified the analysis of biological damage by eliminating certain factors such as temperature and high pressure waves caused by the collapse of bubbles (i.e., cavitation). The analysis may be simplified further by choosing the boundary conditions so that reflections are minimized. The importance of changes in acoustic impedance in the production of breakage of TMV particles has been noted. There was significantly more breakage when a reflection accompanied by a phase reversal occurs within the TMV solution. These findings emphasize the importance of boundary regions with large differences in acoustic impedance as regions more prone to produce acoustic damage.

The production of acoustic waves by transient heating was investigated theoretically and the effects of various boundary and initial conditions on the final form of the transient were determined and compared with experimental results. A schlieren system and a quartz piezoelectric transducer were used to detect the pressure

transients. Experimental values determined through the use of opposed transducers were compared with the theoretical values and found to be within 5 percent of each other.

A comparison was made of the infectivity of control and irradiated solutions on half leaves of the local lesion host, Nicotiana tobaccum, variety Xanthi. In agreement with the results from electron microscopy, a significant difference at the 5 percent level was found as determined by the t-test for paired variates.

Since calculations on the various bond strengths indicated that the breaking strength of the TMV particle was limited by the strength of the primary bonds rather than that of secondary bonds such as hydrogen bonds, the force necessary to break the TMV particle was estimated as equivalent to the weakest primary bond (carbon-carbon) in the RNA chain. This force was compared with the hydrodynamical forces exerted on the particles by the laser-induced acoustic transient. It was determined that a laser intensity of 1.6×10^{8} watts/cm^{2} incident on an absorbing dye solution (1000 cm^{-1} attenuation coefficient) was sufficient to cause significant virus breakage at the 5 percent level as determined by the Kolmogorov-Smirnov test.

Possible future applications of acoustic transients may include the use of these transients in determining the bonding strength of various chemical bonds for systems which have geometrical shapes amenable to hydrodynamical calculations. The use of acoustic transients offers a physical means of determining bond strengths for short duration forces. If systems are developed in which the

duration of the pulse can be varied the bond strengths as a function of time may be studied. In this regard, a study would be of value in which the biological effects of exposure to the pressure waves produced by underwater spark discharges (approximately 1 microsecond duration) are compared to the effects produced by absorption of a laser pulse. A direct comparison of the effects of pressures of the same amplitude but different rise and fall times would be of importance in further elucidating the role of the pressure gradient in producing biological damage.

LIST OF REFERENCES

1. Wood, R. H., and Loomis, A. L., "Physical and Biological Effects of High Frequency Sound Waves of Great Intensity", Physical Review 29: 373 (1927).

2. Maiman, T. H., "Stimulated Optical Radiation in Ruby", Nature 187: 493-4 (1959).

3. Gregg, E. C., Jr., "Ultrasonic Vibrations" in Biophysical Research Methods by F. M. Uber, pp. 301-342. Interscience Publishers, New York (1950).

4. Fry, W. J., "Intense Ultrasound in Investigations of the Central Nervous System" in Advances in Biological and Medical Physics by C. A. Tobias and J. H. Lawrence, vol. 6, pp. 281-348. Academic Press, New York (1958).

5. Grabar, P., "Biological Actions of Ultrasonic Waves" in Advances in Biological and Medical Physics by C. A. Tobias and J. H. Lawrence, vol. 3, pp. 191-246. Academic Press, New York (1953).

6. Hueter, T. F., and Bolt, R. H., Sonics, pp. 225-244. John Wiley and Sons, Inc., New York (1955).

7. Strasberg, M., "Onset of Ultrasonic Cavitation in Tap Water", The Journal of the Acoustical Society of America 31: 163-176 (1959).

8. Briggs, H. B., Johnson, J. B., and Mason, W. P., "Properties of Liquids at High Sound Pressure", The Journal of the Acoustical Society of America 19: 664-677 (1947).

9. Hueter, T. F., and Bolt, R. H., Sonics, pp. 225-244. John Wiley and Sons, Inc., New York (1955).

10. Miller, N., "Chemical Action of Sound Waves on Aqueous Solutions", Transactions Faraday Society 46: 546-550 (1950).

11. Hueter, T. F., and Bolt, R. H., Sonics, pp. 225-244. John Wiley and Sons, Inc., New York (1955).

12. Strasberg, M., "Onset of Ultrasonic Cavitation in Tap Water", The Journal of the Acoustical Society of America 31: 163-176 (1959).

13. Lehmann, J. F., and Herrick, J. F., "Biologic Reactions to Cavitation, A Consideration for Ultrasonic Therapy", Archives of Physical Medicine 34: 86-98 (1953).

14. Willard, G. W., "Ultrasonically Induced Cavitation in Water: a step-by-step process", The Journal of the Acoustical Society of America 25: 669-686. (1953).

15. Hueter, T. F., and Bolt, R. H., Sonics, pp. 225-244. John Wiley and Sons, Inc., New York (1955).

16. El'piner, I. E., Ultrasound, pp. 84. Consultants Bureau, New York (1964).

17. Jackson, F. J., and Nyborg, W. L., "Small Scale Acoustic Streaming Near a Locally Excited Membrane", The Journal of the Acoustical Society of America 30: 614-619 (1958).

18. Ackerman, E., Biophysical Science, pp. 220-232. Prentice Hall, Inc., Englewood Cliffs (1962).

19. Hawley, S. A., Macleod, R. M., and Dunn, F., "Degradation of DNA by Intense, Noncavitating Ultrasound", The Journal of the Acoustical Society of America 35: 1285-7 (1963).

20. Melville, H. W., and Murray, A. J. R., "The Ultrasonic Degradation of Polymers", Transactions of the Faraday Society 46: 996-1009 (1950).

21. Freifelder, D., and Davison, P. F., "Studies on the Sonic Degradation of Deoxyribonucleic Acid", Biophysical Journal 2: 235-247 (1962).

22. Doty, P., McGill, B. B., and Rice, S. A., "The Properties of Sonic Fragments of DNA", Proceedings of the National Academy of Science 44: 432-8 (1958).

23. Hughes, D. E., and Nyborg, W. L., "Cell Disruption by Ultrasound", Science 138: 108-114 (1962).

24. Weissler, A., Cooper, H. W., and Snyder, S., "Chemical Effect of Ultrasonic Waves", Journal of the American Chemical Society 72: 1769-1775 (1950).

25. Hodge, A. J., and Schmitt, F. O., "Interaction Properties of Sonically Fragmented Collagen Macromolecules", Proceedings of the National Academy of Science 44: 418-424 (1958).

26. Melville, H. W., and Murray, A. J. R., "The Ultrasonic Degradation of Polymers", Transactions of the Faraday Society 46: 996-1009 (1950).

27. Takahashi, W. N., and Christensen, R. J., "The Virucidal Action of High Frequency Sound Radiation", Science 79: 415-416 (1934).

28. Stanley, W. M., "The Action of High Frequency Sound Waves on Tobacco Mosaic Virus", Science 80: 339-341 (1934).

29. Oster, G., "Studies on the Sonic Treatment of Tobacco Mosaic Virus", Journal of General Physiology 31: 89-102 (1947).

30. Newton, N., "Some Effects of High Intensity Ultrasound on Tobacco Mosaic Virus", Science 114: 185-186 (1951).

31. Anderson, T. F., Boggs, S., and Winters, B. C., "The Relative Sensitivities of Bacterial Viruses to Intense Sonic Vibration", Science 108: 18 (1948).

32. Gooberman, G., "Ultrasonic Degradation of Polystyrene. Part I. A Proposed Mechanism for Degradation", Journal of Polymer Science 42: 25-46 (1960).

33. Frenkel, J., "Orientation and Rupture of Linear Macromolecules in Dilute Solutions Under the Influence of Viscous Flow", Acta Physicochimica U.R.S.S. 19: 51-76 (1944).

34. White, C. S., "Biological Effects of Blast", Technical Progress Report No. 1271 of the Defense Atomic Support Agency, Washington, D. C. (1961).

35. Frungel, F., High Speed Pulse Technology, pp. 519-527. Academic Press, New York (1965).

36. Allen, M., and Soike, K., "Sterilization by Electrohydraulic Treatment", Science 154: 155-157 (1966).

37. Frungel, F., High Speed Pulse Technology, pp 519-527. Academic Press, New York (1965).

38. Ham, W. T., Jr., Williams, R. C., Mueller, H. A., Guerry, D., III, Clarke, A. M., and Geeraets, W. J., "Effects of Laser Radiation on the Mammalian Eye", Transactions of the New York Academy of Science 28: 517-526 (1966).

39. Amar, L., Bruma, M., Desvignes, P., Leblanc, M., Perdriel, G., and Velghe, M., "Detection d'ondes Elastiques (Ultrasomores) sur l'os Occipital Induites par Impulsions Laser dans l'oeil d'un Lapin", Comptes Rendus Academie de Science 259: 3653-3655 (1964).

40. Carome, E. F., Clark, N. A., and Moelber, C. E., "Generation of Acoustic Signals in Liquids by Ruby Laser-Induced Thermal Stress Transients", Applied Physics Letters 4: 95-97 (1964).

41. Fine, S., Klein, E., Novak, W., Scott, R. E., Laor, Y., Simpson, L., Crissey, J., Donoghue, J., and Derr, V. E., "Interaction of Laser Radiation with Biologic Systems", Federation Proceedings 24: (Supplement No. 14), S35-S45 (1965).

42. Stanley, W. M., "Isolation of a Crystalline Protein Possessing the Properties of Tobacco Mosaic Virus", Science 81: 644-645 (1935).

43. Bernal, J. D., and Fankuchen, I., "X-ray and Crystallographic Studies of Plant Virus Preparations III", Journal of General Physiology 25: 147-165 (1941).

44. Franklin, R. E., and Klug, A., "The Nature of the Helical Groove on the Tobacco Mosaic Virus Particle", Biochemica et Biophysica Acta 19: 403-416 (1956).

45. Klug, A., and Caspar, D. L. D., "The Structure of Small Viruses", Advances in Virus Research 7: 225-325 (1960).

46. Schramm, G., Schumacher, G., and Zillig, W., "An Infectious Nucleoprotein from Tobacco Mosaic Virus", Nature 175: 548-550 (1955).

47. Nixon, H. L., and Wood, R. D., "The Structure of Tobacco Mosaic Virus Protein", Virology 10: 157-159 (1960).

48. Stevens, C. L., and Lauffer, M. A., "Polymerization-Depolymerization of Tobacco Mosaic Virus Protein", Biochemistry 4: 31-37 (1965).

49. Franklin, R. E., "Location of the Ribonucleic Acid in the Tobacco Mosaic Virus Particle", Nature 177: 928-930 (1956).

50. Hart, R. G., "Reactivation of Partially Degraded Tobacco Mosaic Virus", Nature 177: 130-131 (1956).

51. Franklin, R. E., and Commoner, B., "X-ray Diffraction by an Abnormal Protein (B8) Associated with Tobacco Mosaic Virus", Nature 175: 1076-1077 (1955).

52. Klug, A., and Caspar, D. L. D., "The Structure of Small Viruses", Advances in Virus Research 7: 225-325 (1960).

53. Williams, R. C., and Steere, R. L., "Electron Microscopic Observations on the Unit of Length of the Particles of Tobacco Mosaic Virus", Journal of the American Chemical Society 73: 2057-2061 (1951).

54. Brenner, S., and Horne, R. W., "A Negative Staining Method for High Resolution Electron Microscopy of Viruses", Biochemica et Biophysica Acta 34: 103-110 (1959).

55. Klug, A., and Caspar, D. L. D., "The Structure of Small Viruses", Advances in Virus Research 7: 225-325 (1960).

56. Boedtker, H., and Simmons, N. S., "The Preparation and Characterization of Essentially Uniform Tobacco Mosaic Virus Particles", Journal of the American Chemical Society 80: 2550-2556 (1956).

57. Carome, E. F., Clark, N. A., and Moelber, C. E., "Generation of Acoustic Signals in Liquids by Ruby Laser-Induced Thermal Stress Transients", Applied Physics Letters 4: 95-97 (1964).

58. White, R. M., "Generation of Elastic Waves by Transient Surface Heating", Journal of Applied Physics 34: 3559-3567 (1963).

59. Carome, E. F., Clark, N. A., and Moelber, C. E., "Generation of Acoustic Signals in Liquids by Ruby Laser-Induced Thermal Stress Transients", Applied Physics Letters 4: 95-97 (1964).

60. Michaels, J. E., "Thermally Induced Elastic Wave Propagation in Slender Bars", Proceedings of the Third United States National Congress of Applied Mechanics: 209-213 (1957).

61. Ready, J. F., "Effects Due to Absorption of Laser Radiation", Journal of Applied Physics 36: 462-467 (1965).

62. Carslaw, H. S., and Jaeger, J. C., Conduction of Heat in Solids, pp. 78-80. Oxford University Press, London (1959).

63. Hueter, T. F., and Bolt, R. H., Sonics, pp 416. John Wiley and Sons, Inc., New York (1955).

64. Lester, W. W., "On the Theory of the Propagation of Plane, Finite Amplitude Waves in a Dissipative Fluid", The Journal of the Acoustical Society of America 33: 1196-1199 (1961).

65. Mostafa, M. A. K., "A Mechanism of Degradation of Long Chain Molecules by Ultrasonic Waves", Journal of Polymer Science 33: 323-335 (1958).

66. Frenkel, J., "Orientation and Rupture of Linear Macromolecules in Dilute Solutions Under the Influence of Viscous Flow", Acta Physicochimica U.R.S.S. 19: 51-76 (1944).

67. Mostafa, M. A. K., "A Mechanism of Degradation of Long Chain Molecules by Ultrasonic Waves", Journal of Polymer Science 33: 323-335 (1958).

68. Mark, H., "Some Applications of Ultrasonics in High Polymer Research", The Journal of the Acoustical Society of America 16: 183-187 (1945).

69. Gooberman, G., "Ultrasonic Degradation of Polystyrene. Part I. A Proposed Mechanism for Degradation", Journal of Polymer Science 42: 25-46 (1960).

70. Milne-Thomson, L. M., Theoretical Hydrodynamics, p. 567. The McMillan Company, New York (1960).

71. Dryden, H. L., Murnaghan, F. D., and Bateman, H., Hydrodynamics, pp. 4-6. Dover Publications, Inc., New York (1956).

72. Happel, J., and Brenner, H., Low Reynolds Number Hydrodynamics, p. 53. Prentice Hall, Inc., Englewood Cliffs (1965).

73. Perry, R. H., Chilton, C. H., and Kirkpatrick, S. D., Editors, Perry's Chemical Engineers' Handbook, pp. 5-60. McGraw Hill, New York (1963).

74. Dryden, H. L., Murnaghan, F. D., and Bateman, H., Hydrodynamics, pp. 4-6. Dover Publications, Inc., New York (1956).

75. Lamb, H., Hydrodynamics, pp. 643-644. Dover Publications, Inc., New York (1945).

76. Dryden, H. L., Murnaghan, F. D., and Bateman, H., Hydrodynamics, p. 9. Dover Publications, Inc., New York (1956).

77. Einstein, A., Investigations on the Theory of the Brownian Movement, pp. 36-59. Dover Publications, Inc., New York (1958).

78. Lamb, H., Hydrodynamics, pp. 643-644. Dover Publications, Inc., New York (1945).

79. Jeffery, G. B., "The Motion of Ellipsoidal Particles Immersed in a Viscous Fluid", Proceedings of the Royal Society A 102: 161-179 (1922).

80. Burgers, J. M., "Stationary Streaming Caused by a Body in a Fluid with Friction", Proceedings of the Academy of Science, Amsterdam 23: 1082-1107 (1921).

81. Burgers, J. M., "On the Motion of Small Particles of Elongated Form Suspended in a Viscous Liquid", Koninklijke Nederlandse Akademie van Wetenschappen, Verhandelingen 16: 113-184 (1938).

82. Brenner, H., "The Stokes Resistance of an Arbitrary Particle - Part V", Chemical Engineering Science 21: 97-109 (1966).

83. Burgers, J. M., "On the Motion of Small Particles of Elongated Form Suspended in a Viscous Liquid", Koninklijke Nederlandse Akademie van Wetenschappen, Verhandelingen 16: 113-184 (1938).

84. Lamb, H., Hydrodynamics, pp. 597-598. Dover Publications, Inc., New York (1945).

85. Schramm, G., Schumacher, G., and Zillig, W., "An Infectious Nucleoprotein from Tobacco Mosaic Virus", Nature 175: 548-550 (1955).

86. Kauzmann, W., "Some Factors in the Interpretation of Protein Denaturation", Advances in Protein Chemistry 14: 1-63 (1959).

87. Setlow, R. B., and Pollard, E. C., Molecular Biophysics, p. 208. Addison-Wesley Publishing Company, Inc., Reading (1962).

88. Morse, P. M., "Diatomic Molecules According to the Wave Mechanics. II. Vibrational Levels", Physical Review 34: 57-64 (1929).

89. Pauling, L., The Nature of the Chemical Bond, p. 622. Cornell University Press, New York (1960).

90. Cottrell, T. L., The Strengths of Chemical Bonds, pp. 275-277. Academic Press, New York (1954).

91. Brand, J. C. D., and Speakman, J. C., Molecular Structure, pp. 247-252. Edward Arnold (Publisher) Ltd. London (1960).

92. deBoer, J. H., "The Influence of van der Waals' Forces and Primary Bonds on Binding Energy, Strength and Orientation, with Special Reference to Some Artificial Resins", Transactions of the Faraday Society 32: 10-38 (1936).

93. Irwin, G. R., "Fracture", Handbuch Der Physik, Flugge, S., editor, Vol. VI: 551-590. Springer-Verlag, Berlin (1959).

94. Morse, P. M., "Diatomic Molecules According to the Wave Mechanics. II. Vibrational Levels", Physical Review 34: 57-64 (1929).

95. Longuet-Higgins, H. C., "Intermolecular Forces", Discussions of the Faraday Society 40: 7-18 (1965).

96. Setlow, R. B., and Pollard, E. C., Molecular Biophysics, p. 63. Addison-Wesley Publishing Company, Inc., Reading (1962).

97. Maiman, T. H., "Stimulated Optical Radiation in Ruby", Nature 187 493-494 (1959).

98. Garbuny, M., Optical Physics, p. 363. Academic Press, Inc., New York (1965).

99. Garbuny, M., Optical Physics, p. 340. Academic Press, Inc., New York (1965).

100. Williams, R. C., and Mueller, H. A., "A Recording Sampling System for Measuring Laser Energy", Applied Optics 5: 135-138 (1966).

101. Cady, W. G., Piezoelectricity, Vol. I, pp. 220-221. Dover Publications, Inc., New York (1964).

102. Hueter, T. F., and Bolt, R. H., Sonics, p. 126. John Wiley and Sons, Inc., New York (1955).

103. Redwood, M., "Transient Performance of a Piezoelectric Transducer", The Journal of the Acoustical Society of America 33: 527-536 (1961).

104. Cady, W. G., Piezoelectricity, Vol. I, p. 414. Dover Publications, Inc., New York (1964).

105. Hueter, T. F., and Bolt, R. H., Sonics, p. 103. John Wiley and Sons, Inc., New York (1955).

106. Cady, W. G., Piezoelectricity, Vol. I, p. 220. Dover Publications, Inc., New York (1964).

107. Flint, G. W., Lasers and Their Effects - Annual Progress Report (Martin Marietta Corp., Orlando, Florida) (1966).

108. Rose, G., "A Separable and Multipurpose Tissue Culture Chamber", Texas Reports on Biology and Medicine 12: 1074-1083 (1954).

109. Siegel, A., "Artificial Production of Mutants of Tobacco Mosaic Virus", Advances in Virus Research 11: 25-60 (1965).

110. Steere, R. L., "The Purification of Plant Viruses", Advances in Virus Research 6: 1-73 (1959).

111. Commoner, B. F. L., Mercer, P. Merrill, and Zimmer, A. J., "Microanalytical Determination of the Rate of Tobacco Mosaic Virus Synthesis in Tobacco Leaf Tissue", Archives of Biochemistry 26: 271-286 (1950).

112. Steere, R. L., "The Purification of Plant Viruses", Advances in Virus Research 6: 1-73 (1959).

113. Steere, R. L., Private communication.

114. Steere, R. L., "Tobacco Mosaic Virus: Purifying and Sorting Associated Particles According to Length", Science 140: 1089-1090 (1963).

115. Hulett, H. R., and Loring, H. S., "Effect of Particle Length Distribution on Infectivity of Tobacco Mosaic Virus", Virology 25: 418-430 (1965).

116. Stanley, W. M., and Anderson, T. F., "A Study of Purified Viruses with the Electron Microscope", Journal of Biological Chemistry 139: 325-338 (1941).

117. Williams, R. C., "Electron Microscopy of Viruses", Advances in Virus Research 2: 183-239 (1954).

118. Brenner, S., and Horne, R. W., "A Negative Staining Method for High Resolution Electron Microscopy of Viruses", Biochemica et Biophysica Acta 34: 103-116 (1959).

119. Brenner, S., and Horne, R. W., "A Negative Staining Method for High Resolution Electron Microscopy of Viruses", Biochemica et Biophysica Acta 34: 103-116 (1959).

120. Williams, R. C., and Steere, R. L., "Electron Microscopic Observations on the Unit of Length of the Particles of Tobacco Mosaic Virus", The Journal of the American Chemical Society 73: 2057-2061 (1951).

121. Steere, R. L., "Electron Microscopy of Structural Detail in Frozen Biological Specimens", The Journal of Biophysical and Biochemical Cytology 3: 45-59 (1957).

122. Hall, C. E., "Lengths of Tobacco Mosaic Virus from Electron Microscopy", Journal of the American Chemical Society 80: 2556-2557 (1958).

123. Anderson, T. F., "Techniques for the Preservation of Three Dimensional Structure in Preparing Specimens for the Electron Microscope", Transactions of the New York Academy of Science 13: 130-134 (1949).

124. Horne, R. W., and Wildy, P., "Virus Structure Revealed by Negative Staining", Advances in Virus Research 10: 101-170 (1963).

125. Siegel, S., Nonparametric Statistics, pp. 127-136. McGraw Hill Book Company, Inc., New York (1956).

126. Kendall, M. G., and Stuart, A., The Advanced Theory of Statistics, Vol. 2, pp. 452-461. Charles Griffin and Co. Limited, London (1961).

127. Siegel, S., Nonparametric Statistics, p. 279. McGraw-Hill Book Company, Inc., New York (1956).

128. Boedtker, H., and Simmons, N. S., "The Preparation and Characterization of Essentially Uniform Tobacco Mosaic Virus Particles", Journal of the American Chemical Society 80: 2550-2556 (1956).

129. Oster, G., Doty, P. M., and Zimm, B. H., "Light Scattering Studies of Tobacco Mosaic Virus", Journal of the American Chemical Society 69: 1193-1197 (1947).

130. Williams, R. C., and Steere, R. L., "Electron Microscopic Observations on the Unit of Length of the Particles of Tobacco Mosaic Virus", The Journal of the American Chemical Society 73: 2057-2061 (1951).

131. Herzfeld, K. F., and Litovitz, T. A., Absorption and Dispersion of Ultrasonic Waves, pp. 34-38. Academic Press, Inc., New York (1959).

132. Cole, R. H., Underwater Explosions, pp. 51-55. Dover Publications, Inc., New York (1965).

133. Lamb, H., Hydrodynamics, pp. 643-644. Dover Publications, Inc., New York (1945).

134. Burgers, J. M., "On the Motion of Small Particles of Elongated Form Suspended in a Viscous Liquid", Koninklijke Nederlandse Adademie van Wetenschappen, Verhandelingen 16: 113-184 (1938).

135. Brenner, H., "The Stokes Resistance of an Arbitrary Particle - Part V", Chemical Engineering Science 21: 97-109 (1966).

136. Ready, J. F., "Effects Due to Absorption of Laser Radiation", Journal of Applied Physics 36: 462-467 (1965).

137. Milne-Thomson, L. M., Theoretical Hydrodynamics, The McMillan Company, New York (1960).

138. Milne-Thomson, L. M., Theoretical Hydrodynamics, p. 565. The McMillan Company, New York (1960).

139. Lamb, H., Hydrodynamics, pp. 643-644. Dover Publications, Inc., New York (1945).

140. Lamb, H., Hydrodynamics, p. 598. Dover Publications, Inc., New York (1945).

141. Brenner, H., "The Stokes Resistance of an Arbitrary Particle - Part V", Chemical Engineering Science 21: 97-109 (1966).

142. Brenner, H., "The Stokes Resistance of an Arbitrary Particle - Part IV", Chemical Engineering Science 19: 703-727 (1964).

143. Burgers, J. M., "On the Motion of Small Particles of Elongated Form Suspended in a Viscous Liquid", Koninklijke Nederlandse Akademie van Wetenschappen, Verhandelingen 16: 113-184 (1938).

144. Carome, E. F., Parks, P. E., and Mraz, S. J., "Propagation of Acoustic Transients in Water", The Journal of the Acoustical Society of America 36: 946-952 (1964).

APPENDIX A. PRODUCTION OF ACOUSTIC TRANSIENTS BY TRANSIENT HEATING

The stress $S(x,t)$ in the x-direction produced by a temperature rise $T(x,t)$ as discussed in Chapter I is given by:

$$S(x,t) = \rho v^2 \frac{\partial \xi}{\partial x} - BaT, \tag{A-1}$$

where

ρ = density,

ξ = particle displacement,

B = bulk modulus,

a = coefficient of thermal expansion, and

t = time.

Applying Newton's law, the wave equation obtained is

$$\rho \frac{\partial^2 \xi}{\partial t^2} = \frac{\partial S}{\partial x} = \rho v^2 \frac{\partial^2 \xi}{\partial x^2} - Ba \frac{\partial T}{\partial x} \quad \text{or} \tag{A-2}$$

$$\frac{\partial^2 \xi}{\partial x^2} - \frac{1}{v^2} \frac{\partial^2 \xi}{\partial t^2} = \frac{Ba}{\rho v^2} \frac{\partial T}{\partial x} .$$

In order to solve this equation some function of the temperature must be calculated or assumed. Consider the case of a semi-infinite medium with laser light incident on the surface. Assume the laser light has a uniform intensity over a period, τ, and that the light is absorbed exponentially. Further assume that the instantaneous temperature is directly proportional to the total amount of energy absorbed at each point of the medium up to that time, t. Letting I(t) be the intensity distribution from the laser, then

$$I(t) = I_o\Big[U(t) - U(t - \tau)\Big] \tag{A-3}$$

where

$U(t) = 0$ for $t < 0$,

$U(t) = 1$ for $t > 0$, and

I_o = energy per unit area per unit time.

The total energy per unit area at the end of time, t, is

$$\int_o^t I(t)dt = \int_o^t I_o\Big[U(t) - U(t - \tau)\Big]dt \qquad \text{(A-4)}$$

$$= tI_oU(t) - I_o(t - \tau)U(t - \tau).$$

The energy is absorbed exponentially so that the energy incident per unit area is equal at any point, x, to:

$$\int_o^x Edx = - I_o\Big[tU(t) - (t- \tau)U(t - \tau)\Big]e^{-\alpha x} \qquad \text{(A-5)}$$

where E is the energy absorbed per unit volume and α is the absorption coefficient. On differentiating the above expression, E becomes

$$E = \alpha I_o\Big[tU(t) - (t - \tau)U(t - \tau)\Big]e^{-\alpha x} \qquad \text{(A-6)}$$

Assuming the energy absorbed per unit mass is equal to cT where c is the specific heat, then the temperature, T, is given by:

$$T = \frac{\alpha I_o}{\rho c}\Big[tU(t) - (t - \tau)U(t - \tau)\Big]e^{-\alpha x}. \qquad \text{(A-7)}$$

The temperature distribution $tU(t) - (t - \tau)U(t - \tau)$ is a linearly rising function from $t = 0$ to $t = \tau$. At the point τ the temperature becomes constant and remains constant for times greater than τ. This form of the temperature distribution apparently gives a reasonably good approximation to the actual temperature distribution where thermal conduction can be neglected. In particular this form of the temperature distribution should apply to short

duration pulses (e.g., Q-switched laser pulses) in which the time for thermal conduction to dissipate the heat is long compared to the pulse duration. However, this is certainly an unrealistic temperature distribution in many cases as heat conduction cannot be neglected. Ready (136) has evaluated the heat equation for a Q-switched laser pulse by numerical methods. His results show a very steeply rising temperature which can be approximated as a linear rise. His results also show that the temperature falls off rapidly, although not as rapidly as it rises. The temperature decrease appears to be fairly linear down to about one-third the maximum temperature rise where it then decreases more slowly as ambient temperature is approached. Based on these observations, it appears that the temperature distribution can be represented by a linear rise and a linear fall which have different slopes, the approximation becoming poor as the temperature approaches ambient. However the phenomena of interest in this study is related to the maximum pressure produced and the steepness of the pressure gradients. Therefore, the fact that the approximation is not good near ambient temperature is of little concern.

Therefore the temperature distribution will be assumed to be of the form:

$$tU(t) - g(t - \tau)U(t - \tau) + (g - 1)(t - h\tau)U(t - h\tau)$$

where $h = g(g - 1)^{-1}$ and where g may vary from 1 to 2. T in equation (A-7) is now replaced by:

$$T = \frac{\alpha I_o}{\rho c}\left[tU(t) - g(t - \tau)U(t - \tau) + (g - 1)(t - h\tau)U(t - h\tau)\right]e^{-\alpha x}. \qquad \text{(A-8)}$$

The wave equation (A-2) now becomes:

$$\frac{\partial^2 \xi}{\partial x^2} - \frac{1}{v^2}\frac{\partial^2 \xi}{\partial t^2} = K\Big[tU(t) - g(t-\tau)U(t-\tau) + (g-1)(t-h\tau)U(t-h\tau)\Big]e^{-\alpha x} \qquad \text{(A-9)}$$

where

$$K = -\frac{Ba\alpha^2 I_o}{\rho^2 v^2 c}.$$

The initial and boundary conditions are

$$\xi(x,0) = 0,$$

$$\frac{\partial \xi}{\partial t}(x,0) = 0, \text{ and}$$

$$\xi(\infty,t) = 0.$$

One other boundary condition must be applied which depends on the restraints on the surface of the absorbing medium. If the surface is considered to be rigid, then the displacement, $\xi(0,t)$, at the boundary must be zero. If the surface is considered to be free, then the stress, $S(0,t)$, at the boundary must be zero. The conditions of neither of these cases are fully met in practice. However the equation will be solved using these boundary conditions, keeping in mind that the actual boundary conditions probably lie somewhere between these two extremes.

In order to solve the wave equation (A-9), use will be made of the Laplace transformation. Letting $F(x,s)$ equal the Laplace transform of $\xi(x,t)$ the transformed wave equation is given by:

$$\frac{\partial^2 F(x,s)}{\partial x^2} - \frac{s^2}{v^2}F(x,s) = \frac{K}{s^2}\Big[1 - ge^{-\tau s} + (g-1)e^{-h\tau s}\Big]e^{-\alpha x} = Q. \qquad \text{(A-10)}$$

Using the method of variation of parameters to solve equation

(A-10), assume a solution of the form

$$F = A(x)e^{-sx/v} + B(x)e^{sx/v} \quad . \tag{A-11}$$

Taking the derivative of F with respect to x,

$$\frac{\partial F}{\partial x} = \frac{\partial A}{\partial x}e^{-sx/v} + \frac{\partial B}{\partial x}e^{sx/v} - \frac{s}{v}Ae^{-sx/v} + \frac{s}{v}Be^{sx/v} \quad . \tag{A-12}$$

As usual, assume

$$\frac{\partial A}{\partial x}e^{-sx/v} + \frac{\partial B}{\partial x}e^{sx/v} = 0. \tag{A-13}$$

Now find the second derivative of F:

$$\frac{\partial^2 F}{\partial x^2} = -\frac{s}{v}\frac{\partial A}{\partial x}e^{-sx/v} + \frac{s}{v}\frac{\partial B}{\partial x}e^{sx/v} + \frac{s^2}{v^2}Ae^{-sx/v} + \frac{s^2}{v^2}Be^{sx/v}. \tag{A-14}$$

Substituting the expression for F and $\partial^2 F/\partial x^2$ in equation (A-10)

$$-\frac{s}{v}\frac{\partial A}{\partial x}e^{-sx/v} + \frac{s}{v}\frac{\partial B}{\partial x}e^{sx/v} = Q. \tag{A-15}$$

Equation (A-13) may now be substituted into (A-15) and the resulting equation solved for $\partial A/\partial x$ and $\partial B/\partial x$ giving

$$\frac{\partial B}{\partial x} = \frac{vQ}{2s}e^{-sx/v} \quad \text{and} \quad \frac{\partial A}{\partial x} = \frac{vQ}{2s}e^{sx/v} \quad . \tag{A-16}$$

Substituting these into equation (A-11) F is given by:

$$F = e^{-sx/v}\int_{c_1}^{x} -\frac{vQ}{2s}e^{sx/v}dx + e^{sx/v}\int_{c_2}^{x}\frac{vQ}{2s}e^{-sx/v}dx \tag{A-17}$$

$$= e^{-sx/v}\int_{c_1}^{x} -\frac{vK}{2s^3}e^{-\alpha x}\left[1 - ge^{-\tau s} + (g-1)e^{-h\tau s}\right]e^{sx/v}dx$$

$$+ e^{sx/v}\int_{c_2}^{x}\frac{vK}{2s^3}e^{-\alpha x}\left[1 - ge^{-\tau s} + (g-1)e^{-h\tau s}\right]e^{-sx/v}dx$$

$$= \frac{v^2K}{2s^3}\left[1 - ge^{-\tau s} + (g-1)e^{-h\tau s}\right]\left[-\frac{e^{-\alpha x}}{s + \alpha v}\right.$$

$$+ \frac{e^{-sx/v}}{s + \alpha v} e^{-c_2(s/v + \alpha)} - \frac{e^{-\alpha x}}{s - \alpha v} + \frac{e^{-sx/v}}{s - \alpha v} e^{c_1(s/v + \alpha)} \Bigg].$$

In order to evaluate the above expression for F the boundary condition on x must be applied. Substituting the conditions $\xi(\infty,t) = 0$ or $F(\infty,s) = 0$ into (A-17), it is found that $e^{sx/v}\, e^{-c_2(s/v + \alpha)}$ must approach zero as x approaches infinity. Equation (A-17) now becomes

$$F = - \frac{v^2 K}{2s^3}\Big[1 - g^{-s\tau} + (g - 1)e^{-h\tau s}\Big] \qquad \text{(A-18)}$$

$$\cdot\Big[\frac{2s}{s^2 - \alpha^2 v^2} e^{-\alpha x} - \frac{e^{-sx/v} e^{c(s/v + \alpha)}}{s - \alpha v}\Big].$$

To evaluate the final constant, the boundary condition at the surface must be used. In the rigid case $\xi(o,t) = 0$ and $F(o,t) = 0$. This condition substituted into (A-18) requires

$$e \frac{c(s/v + \alpha)}{s - \alpha v} = - \frac{2s}{s^2 - \alpha^2 v^2}. \qquad \text{(A-19)}$$

Therefore the final expression for F in the rigid surface case becomes

$$F = - \frac{v^2 K}{s^2(s^2 - \alpha^2 v^2)}\Big[1 - ge^{-\tau s} + (g - 1)e^{-h\tau s}\Big]\Big[e^{-\alpha x} - e^{-sx/v}\Big]. \qquad \text{(A-20)}$$

Using the fact that the inverse transform of

$$\frac{1}{s^2(s^2 - \alpha^2 v^2)} \qquad \text{is} \qquad \frac{\sinh \alpha v t}{(\alpha v)^3} - \frac{t}{(\alpha v)^2},$$

the inverse transform of F in equation (A-20) becomes:

$$\frac{\xi(x,t)}{\xi_o} = e^{-\alpha x}\Big[\sinh \alpha v t - \alpha v t\Big], \quad t \geq 0 \qquad \text{(A-21)}$$

$$- ge^{-\alpha x}\left[\sinh \alpha v(t - \tau) - \alpha v(t - \tau)\right], \quad t \geq \tau$$

$$+ (g - 1)e^{-\alpha x}\left\{\sinh\left[\alpha v(t - h\tau)\right] - \alpha v(t - h\tau)\right\}, \quad t \geq h\tau$$

$$- \sinh\left[\alpha v(t - x/v)\right] + \alpha v(t - x/v), \quad t \geq x/v$$

$$+ g\left\{\sinh\left[\alpha v(t - x/v - \tau)\right] - \alpha v(t - x/v - \tau)\right\}, \quad t \geq x/v + \tau$$

$$- (g - 1)\left\{\sinh\left[\alpha v(t - x/v - h\tau)\right] - \alpha v(t - x/v - h\tau)\right\}, \quad t \geq x/v + h\tau$$

where $\xi_o = \dfrac{BaI_o}{v^3\rho^2 c\alpha}$.

The stress, S, given by equation (A-1) becomes

$$-\frac{S}{S_o} = e^{-\alpha x}\left[\sinh(\alpha v t)\right], \quad t \geq 0 \qquad \text{(A-22)}$$

$$- ge^{-\alpha x}\left[\sinh \alpha v(t - \tau)\right], \quad t \geq \tau$$

$$+ (g - 1)e^{-\alpha x}\left[\sinh \alpha v(t - h\tau)\right], \quad t \geq h\tau$$

$$- \cosh \alpha v(t - x/v) + 1, \quad t \geq x/v$$

$$+ g\left\{\cosh\left[\alpha v(t - x/v - \tau)\right] - 1\right\}, \quad t \geq x/v + \tau$$

$$- (g - 1)\left\{\cosh\left[\alpha v(t - x/v - h\tau)\right] - 1\right\}, \quad t \geq x/v + h\tau$$

where $S_o = \dfrac{BaI_o}{v\rho c}$.

These expressions may be simplified when αx is large and the terms in $e^{-\alpha x}$ become small. Making this approximation and expressing $\xi(x,t)$ in terms of the delayed time $t' = t - x/v$, equation (A-21) becomes

$$2\frac{\xi(x,t')}{\xi_o} = e^{\alpha v t'} - ge^{\alpha v(t' - \tau)} \tag{A-23}$$

$$+ (g - 1)e^{\alpha v(t' - h\tau)}, \quad t' < 0$$

$$= e^{-\alpha v t'} - ge^{\alpha v(t' - \tau)}$$

$$+ (g - 1)\left[e^{\alpha v(t' - h\tau)}\right] + 2\alpha v t', \quad 0 < t' < \tau$$

$$= e^{-\alpha v t'} - ge^{-\alpha v(t' - \tau)} + (g - 1)e^{\alpha v(t' - h\tau)}$$

$$+ 2\alpha v t'(1 - g) + 2g\alpha v\tau, \quad \tau < t' < h\tau$$

$$= e^{-\alpha v t'} - ge^{-\alpha v(t' - \tau)} + (g - 1)e^{-\alpha v(t' - h\tau)},$$

$$t' \geq h\tau$$

Under the same approximation the stress, S, is given by

$$-\frac{2S}{S_o} = e^{\alpha v t'} - ge^{\alpha v(t' - \tau)} + (g - 1)e^{\alpha v(t' - h\tau)}, \quad t' < 0 \tag{A-24}$$

$$= 2 - e^{-\alpha v t'} - ge^{\alpha v(t' - \tau)} + (g - 1)e^{\alpha v(t' - h\tau)}, \quad 0 < t' < \tau$$

$$= 2(1 - g) - e^{-\alpha v t'} + ge^{-\alpha v(t' - \tau)}$$

$$+ (g - 1)e^{\alpha v(t' - h\tau)}, \quad \tau < t' < h\tau$$

$$= e^{-\alpha v t'} + ge^{-\alpha v(t' - \tau)} - (g - 1)e^{-\alpha v(t' - h\tau)}, \quad t' \geq h\tau.$$

Returning to equation (A-18) and applying the boundary conditions which apply to the free surface, $S(0,t) = 0$, it is seen that the stress equation (A-1) leads to the condition that

$$\left.\frac{\partial \xi}{\partial x}\right]_{x=o} = \frac{BaI_o}{\rho v^2} \tag{A-25}$$

$$\left.\frac{\partial F}{\partial x}\right]_{x=o} = \frac{K}{\alpha s^2}\left[1 - ge^{-\tau s} + (g - 1)e^{-h\tau s}\right].$$

Differentiating equation (A-18) and applying this boundary condition, one obtains:

$$-\frac{K}{\alpha s^2}\left[1 - ge^{-\tau s} + (g-1)e^{-h\tau s}\right] \qquad \text{(A-26)}$$

$$= -\frac{v^2K}{2s^3}\left[1 - ge^{-\tau s} + (g-1)e^{-h\tau s}\right]\left[-\frac{2\alpha s}{s^2 - \alpha^2v^2} + \frac{se^{c(s/v-\alpha)}}{v(s-\alpha)}\right].$$

Therefore

$$\frac{e^{c(s/v - \alpha)}}{s - \alpha} = \frac{2\alpha v}{s^2 - \alpha^2v^2} + \frac{2}{\alpha v},$$

and the final expression for F in the case of a free surface is

$$F = -\frac{K}{v^2(2s^3)}(1 - e^{-\tau s}) \qquad \text{(A-27)}$$
$$\cdot\left[\frac{2s}{s^2 - \alpha^2v^2}e^{-\alpha x} - e^{sx/v}\left(\frac{2\alpha v}{s^2 - \alpha^2v^2} + \frac{2}{\alpha v}\right)\right].$$

Taking the inverse transform (L^{-1}), then

$$L^{-1}\left[s^{-2}(s^2 - \alpha^2v^2)^{-1}\right] = (\alpha v)^{-3}\sinh(\alpha vt) - t(\alpha v)^{-2},$$

$$L^{-1}\left[s^{-3}(s^2 - \alpha^2v^2)^{-1}\right] = (\alpha v)^{-4}\left[\cosh(\alpha vt) - 1\right] - t^2(2\alpha^2v^2)^{-1}, \text{ and}$$

$$L^{-1}\left[s^{-3}\right] = \frac{t^2}{2}.$$

Using these relations, the transform of equation (A-27) becomes

$$-\frac{\xi}{\xi_o} = -e^{-\alpha x}\left[\sinh(\alpha vt) - \alpha vt\right], \; t \geq 0 \qquad \text{(A-28)}$$

$$+ ge^{-\alpha v}\left\{\sinh\left[\alpha v(t - \tau)\right] - \alpha v(t - \tau)\right\}, \; t \geq \tau$$

$$- (g-1)e^{-\alpha x}\left\{\sinh\left[\alpha v(t - h\tau)\right] - \alpha v(t - h\tau)\right\}, \; t \geq h\tau$$

$$+ \cosh\left[\alpha v(t - xv^{-1})\right] - 1, \; t \geq xv^{-1}$$

$$- g\left\{\cosh\left[\alpha v(t - x/v - \tau\right] - 1\right\},\ t \geq x/v + \tau$$

$$+ (g - 1)\left\{\cosh\left[\alpha v(t - x/v - h\tau)\right] - 1\right\},\ t \geq x/v + h\tau$$

where ξ_o is the same as in equation (A-17).

The stress, S, becomes for the free boundary case:

$$-\frac{S}{S_o} = e^{-\alpha x}\sinh(\alpha v t),\ t \geq 0 \qquad \text{(A-29)}$$

$$- ge^{-\alpha x}\sinh\left[\alpha v(t - \tau)\right],\ t \geq \tau$$

$$+ (g - 1)e^{-\alpha x}\sinh\left[\alpha v(t - h\tau)\right],\ t \geq h\tau$$

$$- \sinh\left[\alpha v(t - x/v)\right],\ t \geq x/v$$

$$+ g\sinh\left[\alpha v(t - x/v - \tau)\right],\ t \geq x/v + \tau$$

$$- (g - 1)\sinh\left[\alpha v(t - x/v - h\tau)\right],\ t \geq x/v + h\tau.$$

Simplifying equation (A-28) and (A-29) and using the same approximation as in equation (A-23) and (A-24) then

$$\frac{2\xi}{\xi_o} = e^{\alpha v t'} - ge^{\alpha v(t' - \tau)} + (g - 1)e^{\alpha v(t' - h\tau)},\ t' < 0 \qquad \text{(A-30)}$$

$$= 2 - e^{-\alpha v t'} - ge^{\alpha v(t' - \tau)} + (g - 1)e^{\alpha v(t' - h\tau)},\ 0 < t' < \tau$$

$$= 2(1 - g) - e^{-\alpha v t'} + ge^{-\alpha v(t' - \tau)} + (g - 1)e^{\alpha v(t' - h\tau)},\ \tau < t' < h\tau$$

$$= - e^{-\alpha v t'} + ge^{-\alpha v(t' - \tau)} - (g - 1)e^{-\alpha v(t' - h\tau)},\ t' > h\tau;$$

and

$$-\frac{2S}{S_o} = e^{\alpha v t'} - ge^{\alpha v(t' - \tau)} + (g - 1)e^{\alpha v(t' - h\tau)},\ t' < 0$$

$$= e^{-\alpha v t'} - ge^{\alpha v(t' - \tau)} + (g - 1)e^{\alpha v(t' - h\tau)},\ 0 < t' < \tau$$

$$= e^{-\alpha v t'} - ge^{-\alpha v(t' - \tau)} + (g - 1)e^{\alpha v(t' - h\tau)},\ \tau < t' < h\tau$$

$$= e^{-\alpha v t'} - ge^{-\alpha v(t' - \tau)} + (g - 1)e^{-\alpha v(t' - h\tau)},\ t' > h\tau.$$

In the experimental portion of this study the absorbing dye solution or carbon coated mylar film was backed with a rigid plate of plexiglass (see page 70) corresponding to the boundary conditions of equations (A-21) and (A-22). Figures 22 and 23 show the stress and displacement as determined using equations (A-21) and (A-22) for two cases, g = 1 and 1/3 and g = 1 respectively. The case for g = 1 corresponds to the case in which heat conduction is neglected. The case for g = 1 and 1/3 corresponds approximately to the form of the temperature distribution obtained by Ready for the absorption of laser light on tungsten (see page 119). Comparison of the two figures shows that when heat conduction is not negligible that the stress is first negative and then positive, whereas when heat conduction can be neglected the stress is never positive.

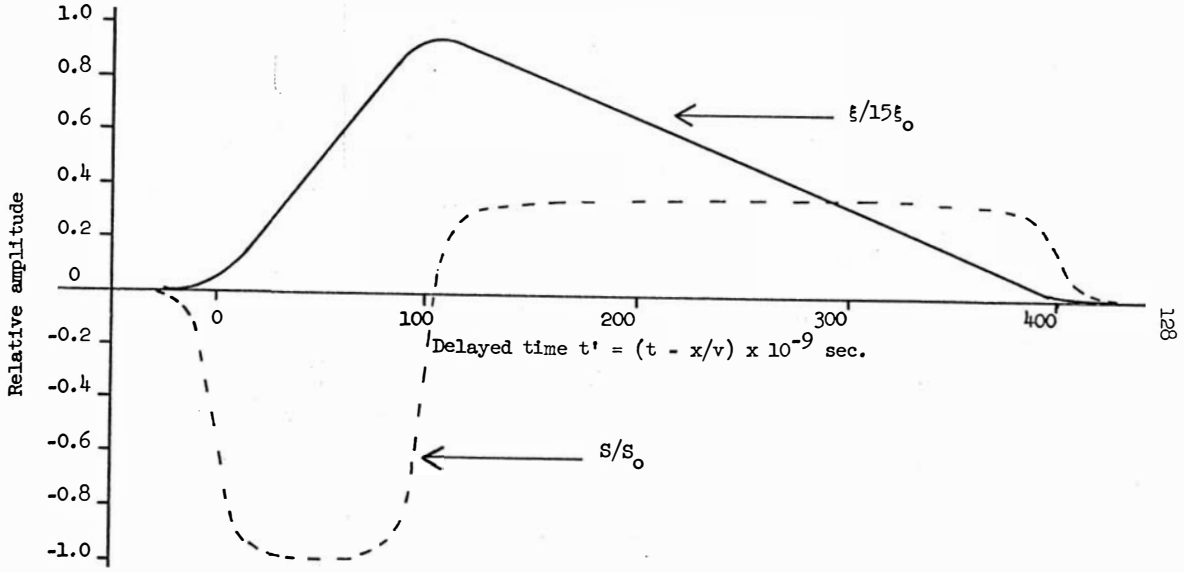

Fig. 22. Laser-induced particle displacement and stress for g = 1 1/3.
(Rigid boundary; $\tau = 10^{-7}$ sec.; $\alpha = 10^{3}$ per cm.)

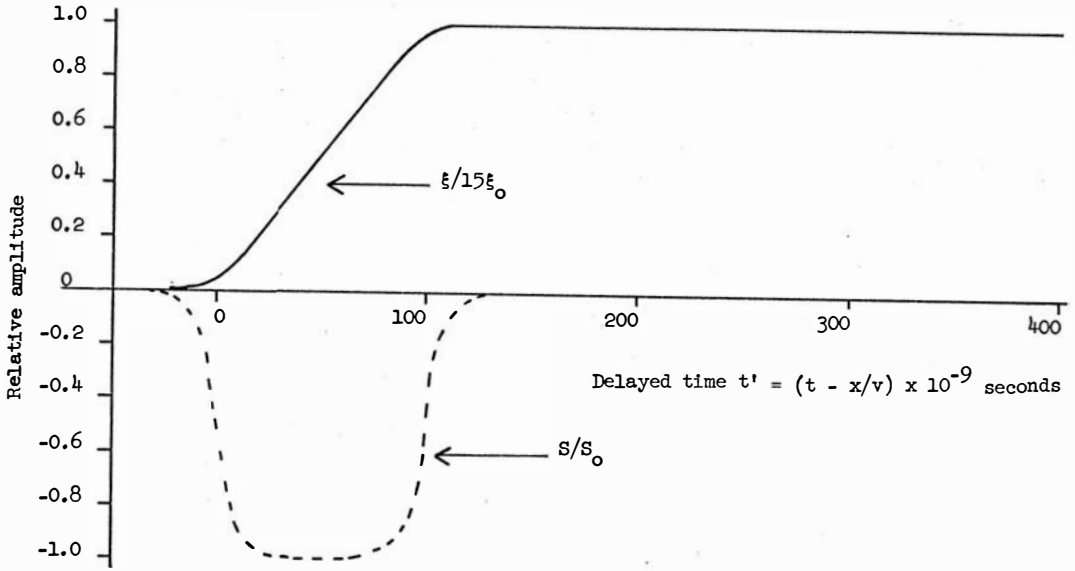

Fig. 23. Laser-induced particle displacement and stress for g = 1. (Rigid boundary; $\tau = 10^{-7}$ sec.; $\alpha = 10^{3}$ per cm.)

APPENDIX B. HYDRODYNAMICAL CALCULATIONS FOR AN ELLIPSOID OF ROTATION IN A FLOW FIELD WITH A LINEAR VELOCITY GRADIENT

1. The Force Experienced by the Ellipsoid

Much of the material considered in this appendix is covered in standard texts on hydrodynamics such as Theoretical Hydrodynamics by Milne-Thomson (137). The background material in this appendix is given for continuity, and standard texts should be consulted for additional details. The solution of the equation of motion (II-7) for the force on an ellipsoid will, however, be presented in full.

A consideration of the forces on a submerged particle requires a knowledge of the stress dyadic, $\tilde{S}$. An ideal fluid can support no shear forces, so that the stress dyadic may be written as

$$\tilde{S} = -p\tilde{I} \tag{B-1}$$

where

p = pressure and

$\tilde{I}$ = the idemfactor.

The stress, $\vec{S}$, on a differential unit area perpendicular to the unit vector, $\vec{n}$, is then given by

$$\vec{S} = \vec{n}\tilde{S} = -p\vec{n}. \tag{B-2}$$

In a viscous liquid the stress on a differential unit area is not necessarily normal to this area and in this case the stress dyadic, assuming one to exist, can be of the form

$$\tilde{S} = -p'\tilde{I} + \tilde{W} \tag{B-3}$$

where the dyadic, $-p'\tilde{I}$, has spherical symetry as in the case of an ideal fluid. The dyadic, $\tilde{W}$, depends directly on the viscosity.

The stresses on a particle surrounded by fluid are dependent

on the motion of the fluid about the particle. The general motion of a fluid particle may be written as a sum of three components. Consider an infinitesimal element of fluid whose center of gravity is at the point, P. For example, let the point, P, be the center of a sphere of infinitesimal radius, h, with $\vec{n}$ as the unit outward normal of a differential area on the surface of this sphere. If the fluid velocity at P is $\vec{q}$, then the velocity at a point on the surface of the sphere may be written as

$$\vec{q} + 1/2\ (\nabla \wedge \vec{q}) \wedge h\vec{n} + f(h\vec{n})$$

where $\vec{q}$ corresponds to a translation of the fluid element as a whole; $1/2\ (\nabla \wedge \vec{q}) \wedge h\vec{n}$ corresponds to the velocity of rotation of the element as a whole, the angular velocity being $1/2\ (\nabla \wedge \vec{q})$; and $f(h\vec{n})$ is a velocity relative to P in the direction of the normal to the surface of the sphere. The first two motions correspond to rigid body motions and the third motion is called a pure strain.

The viscosity hypothesis states that

$$\vec{n}\tilde{W} = 2\mu f(\vec{n}) \qquad \text{(B-4)}$$

where

$$f(\vec{n}) = (\vec{n}\,\nabla)\vec{q} + 1/2\ \vec{n} \wedge (\nabla \wedge \vec{q}) \qquad (138),$$

and where μ is the viscosity coefficient. $\tilde{W}$ may be written as

$$\mu(\nabla\,;\vec{q} + \vec{q}\,;\,\nabla)$$

where $\vec{q}\,;\nabla$ is the dyadic product conjugate to $\nabla;\vec{q}$.

Defining the pressure, p, as the scaler invariant of the stress (the negative of the mean value of the normal stress on a sphere of unit radius) then the stress dyadic becomes

$$\tilde{S} = -p\tilde{I} - 2/3\ \mu(\nabla\vec{q})\tilde{I} + \mu(\nabla;\vec{q} + \vec{q}\,;\,\nabla) \qquad \text{(B-5)}$$

and the stress on an element of differential area normal to the unit

vector $\vec{n}$ is given by

$$\vec{S} = \vec{n}\tilde{S} = - p\vec{n} - 2/3\ \vec{n}\mu(\nabla\vec{q}) + (2\vec{n}\mu\nabla)\vec{q} + \vec{n}\wedge\mu(\nabla\wedge\vec{q}). \qquad \text{(B-6)}$$

Consider the motion of a volume of fluid, V, within a surface, A. Using Newton's law

$$\int\rho\,\frac{D\vec{q}}{Dt}\,dV = \int\vec{n}\tilde{S}dA + \int\rho\vec{F}dV \qquad \text{(B-7)}$$

where $\vec{F}$ represents any external body forces such as gravity. Applying Gauss' theorem to convert the surface integral to a volume integral it is then possible to take the resulting expressions out of the integral signs since the volume of integration is arbitrary. The equation then becomes

$$\rho\,\frac{D\vec{q}}{Dt} = \rho\vec{F} + \nabla\tilde{S}. \qquad \text{(B-8)}$$

Substituting the stress dyadic (B-6) in the above equation and assuming the coefficient of viscosity to be constant and the fluid to be incompressible, the equation of motion becomes

$$\rho\,\frac{D\vec{q}}{Dt} = \rho\vec{F} - \nabla p + \mu\nabla^2\vec{q}. \qquad \text{(B-9)}$$

For small Reynolds numbers this equation may be simplified as discussed in Chapter II, page 37. The simplified equation is

$$\mu\nabla^2\vec{q} - \nabla p = 0 \qquad \text{(B-10)}$$

where $\vec{q}$ and p are functions of time, and where the continuity condition

$$\nabla\vec{q} = 0 \qquad \text{(B-11)}$$

must be satisfied. This equation is to be solved for a linear flow velocity and for an ellipsoidal particle.

Consider first the solution of the equation (B-10) for a particle in a uniform field of flow along the x axis. Assume the

particle to be an ellipsoid with one of its principal axes parallel to the x direction. Once the resistance along a principal axis is known, then by analogy the resistance for any orientation of the ellipsoid may be found.

The equation of an ellipsoid may be written as

$$\frac{x^2}{a^2} + \frac{y^2}{b^2} + \frac{z^2}{c^2} = 1 \qquad \text{(B-12)}$$

where a, b, and c are the semi-axes of the ellipsoid in the directions x, y, and z respectively. Before solving the vector equation (B-10) consider the solution to the scaler Laplace's equation

$$\nabla^2 \phi = 0. \qquad \text{(B-13)}$$

In order to solve this equation it is convenient to transform to ellipsoidal co-ordinates. Consider the three equations:

$$\frac{x^2}{a^2 + u_1} + \frac{y^2}{b^2 + u_1} + \frac{z^2}{c^2 + u_1} = 1 \quad (u_1 > -c^2) \qquad \text{(B-14)}$$

which represents a family of ellipsoids with parameter u_1;

$$\frac{x^2}{a^2 + u_2} + \frac{y^2}{b^2 + u_2} + \frac{z^2}{c^2 + u_2} = 1 \qquad (-c^2 > u_2 > -b^2) \qquad \text{(B-15)}$$

which represents a family of hyperboloids of one sheet with parameter u_2; and

$$\frac{x^2}{a^2 + u_3} + \frac{y^2}{b^2 + u_3} + \frac{z^2}{c^2 + u_3} = 1 \qquad (-b^2 > u_3 > -a^2) \qquad \text{(B-16)}$$

which represents a family of hyperboloids of 2 sheets with parameter u_3. The point (u_1, u_2, u_3) defined by the intersection of the above three surfaces is a point in ellipsoidal space with ellipsoidal co-

ordinates (u_1, u_2, u_3).

Laplace's equation (B-13) in the transformed space becomes

$$\nabla^2\phi = \frac{4}{(u_1 - u_2)(u_1 - u_3)(u_2 - u_3)}\left[(u_2 - u_3)R_{u_1}\frac{\partial}{\partial u_1}\left(R_{u_1}\frac{\partial\phi}{\partial u_1}\right)\right.$$

$$\left. + (u_3 - u_1)R_{u_2}\frac{\partial}{\partial u_2}\left(R_{u_2}\frac{\partial\phi}{\partial u_2}\right) + (u_1 - u_2)R_{u_3}\frac{\partial}{\partial u_3}\left(R_{u_3}\frac{\partial\phi}{\partial u_3}\right)\right]$$

$$= 0 \qquad \text{(B-17)}$$

where $R_u = \left[(u + a^2)(u + b^2)(u + c^2)\right]^{1/2}$.

This equation (B-17) may be solved by separation of variables. Since u_1 is the parameter of the family of ellipsoids, it is equal to zero on the boundary surface of the ellipsoidal particle. The variables u_2 and u_3 are parameters of the hyperboloids and as such serve to measure position on any ellipsoid where u_1 is equal to a constant. On the surface, $u_1 = 0$, ϕ must be independant of u_2 and u_3. Therefore it is appropriate to consider a solution of $\nabla^2\phi = 0$ depending only on u_1. Assuming $\phi = \phi(u_1)$, Laplace's equation becomes

$$\frac{\partial}{\partial u_1}\left(R\frac{\partial\phi}{\partial u_1}\right) = 0 \qquad \text{(B-18)}$$

where

$$R = R_{u_1} = \left[(u_1 + a^2)(u_1 + b^2)(u_1 + c^2)\right]^{1/2}.$$

An expression for ϕ which satisfies (B-18) is

$$\phi_1 = c_1\int_{u_1}^{\infty}\frac{du_1}{R}. \qquad \text{(B-19)}$$

Another solution may be obtained by observing that

$$\frac{x^2}{a^2 + u_1} + \frac{y^2}{b^2 + u_1} + \frac{z^2}{c^2 + u_1} = 1$$

and substituting this into equation (B-19) one obtains

$$\phi_2 = c_2 \int_{u_1}^{\infty} \left(\frac{x^2}{a^2 + u_1} + \frac{y^2}{b^2 + u_1} + \frac{z^2}{c^2 + u_1} \right) \frac{du_1}{R}. \qquad \text{(B-20)}$$

This problem which was first solved by Oberbeck is discussed by Lamb (139). Following the procedure indicated by Lamb the velocity field will be assumed to be of the form

$$u = A \frac{\partial^2 \phi_2}{\partial x^2} + B \left(x \frac{\partial \phi_1}{\partial x} - \phi_1 \right) + U, \qquad \text{(B-21)}$$

$$v = A \frac{\partial^2 \phi_2}{\partial x \partial y} + Bx \frac{\partial \phi_1}{\partial y}, \text{ and} \qquad \text{(B-22)}$$

$$w = A \frac{\partial^2 \phi_2}{\partial x \partial z} + Bx \frac{\partial \phi_1}{\partial z} \qquad \text{(B-23)}$$

where u, v, and w are the components of the velocity $\vec{q}$ in the x, y, and z directions respectively. The constants c_1 and c_2 have been absorbed into the constants A and B, so that ϕ_1 and ϕ_2 are given by equations (B-19) and (B-20) where the c's have been omitted. The partial derivitives in the above equations (B-21) - (B-23) may be expressed as

$$\frac{\partial \phi_2}{\partial x} = 2x\alpha, \qquad \frac{\partial \phi_2}{\partial y} = 2y\beta, \qquad \frac{\partial \phi_2}{\partial z} = 2z\gamma \qquad \text{(B-24)}$$

where

$$\frac{\partial^2 \phi_2}{\partial x^2} = 2\alpha, \qquad \frac{\partial^2 \phi_2}{\partial x \partial y} = 2x \frac{\partial \alpha}{\partial y}, \qquad \frac{\partial^2 \phi_2}{\partial x \partial z} = 2x \frac{\partial \alpha}{\partial z},$$

$$\alpha = \int_{u_1}^{\infty} \frac{du_1}{(a^2 + u_1)R}, \qquad \beta = \int_{u_1}^{\infty} \frac{du_1}{(b^2 + u_1)R}, \qquad \text{and } \gamma = \int_{u_1}^{\infty} \frac{du_1}{(c^2 + u_1)R}.$$

Equations (B-21) - (B-23) are seen to satisfy the equation of continuity since $\nabla^2\phi_1$ and $\nabla^2\phi_2$ are equal to zero. At large distances from the ellipsoid u_1 becomes large and α, β, γ, and ϕ_2 approach zero, giving u = U, v = 0, and w = 0 in accordance with the initial conditions of the problem.

The solution of interest must satisfy the vector equation (B-10) as well as the scaler Laplace's equation (B-13). Using equations (B-21) - (B-23) for the velocity components $\nabla^2\vec{q}$ may be evaluated and the function of p required to satisfy equation (B-10) determined. Making use of the facts that $\nabla^2\phi_1 = \nabla^2\phi_2 = \nabla^2 U = 0$ and that ϕ_1 is quadratic in x, then

$$\nabla^2 u = B\frac{\partial^2}{\partial x^2}\left(x\frac{\partial\phi_1}{\partial x}\right) = B\frac{\partial}{\partial x}\left(x\frac{\partial^2\phi_1}{\partial x^2} + \frac{\partial\phi_1}{\partial x}\right) = B\left(\frac{\partial^2\phi_1}{\partial x^2} + \frac{\partial^2\phi_1}{\partial x^2}\right) = 2B\frac{\partial^2\phi_1}{\partial x^2}. \tag{B-25}$$

By a similar procedure

$$\nabla^2 v = 2B\frac{\partial^2\phi_1}{\partial x\partial y} \qquad \text{and} \qquad \nabla^2 w = 2B\frac{\partial^2\phi_1}{\partial x\partial z}. \tag{B-26}$$

Therefore, equation (B-10) is satisfied by taking

$$p = 2B\mu\frac{\partial\phi_1}{\partial x} + \text{constant}. \tag{B-27}$$

In order to evaluate the constants A and B, use is made of boundary conditions at the surface of the particle which require u = v = w = 0. The conditions on v and w require that

$$2Ax \frac{\partial \alpha}{\partial y} + Bx \frac{\partial \phi_1}{\partial y} = 0, \text{ and} \tag{B-28}$$

$$2Ax \frac{\partial \alpha}{\partial z} + Bx \frac{\partial \phi_1}{\partial z} = 0. \tag{B-29}$$

The behavior of these equations must be investigated as u_1 is varied; therefore, consider the variation of y and z as u_1 is varied. For the variation of y, considering points along the y axis where x and z are equal to zero, then the equation (B-14) becomes

$$\frac{y^2}{b^2 + u_1} = 1. \tag{B-30}$$

On taking the partial derivitive of y with respect to u_1, this equation gives

$$\frac{\partial y}{\partial u_1} = \frac{1}{2y}, \tag{B-31}$$

but

$$\frac{\partial \alpha}{\partial u_1} = \frac{\partial y}{\partial u_1} \frac{\partial \alpha}{\partial y} = \frac{1}{2y} \frac{\partial \alpha}{\partial y},$$

or

$$\frac{\partial \alpha}{\partial y} = 2y \frac{\partial \alpha}{\partial u_1}. \tag{B-32}$$

In like manner

$$\frac{\partial \alpha}{\partial z} = 2z \frac{\partial \alpha}{\partial u_1}, \qquad \frac{\partial \phi_1}{\partial y} = 2y \frac{\partial \phi_1}{\partial u_1}, \quad \text{and} \quad \frac{\partial \phi_1}{\partial z} = 2z \frac{\partial \phi_1}{\partial u_1}. \tag{B-33}$$

Substituting equations (B-32) and (B-33) into (B-28) and (B-29), one equation is obtained,

$$2A \frac{\partial \alpha}{\partial u_1} + B \frac{\partial \phi_1}{\partial u_1} = 0. \tag{B-34}$$

Equation (B-34) is to be evaluated at $u_1 = 0$. Using equation (B-24) the $\frac{\partial \alpha}{\partial u_1}$ and $\frac{\partial \phi_1}{\partial u_1}$, evaluated at $u_1 = 0$, become

$$\left[\frac{\partial \alpha}{\partial u_1}\right]_{u_1=o} = \left[\frac{1}{(a^2 + u_1)R}\right]_{u_1=o} = \frac{1}{a^3 bc} \tag{B-35}$$

and

$$\left[\frac{\partial \phi_1}{\partial u_1}\right]_{u_1=o} = \left[\frac{1}{R}\right]_{u_1=o} = \frac{1}{abc} . \tag{B-36}$$

Substituting these values into equation (B-34) it is found that

$$A = -\frac{a^2 B}{2} . \tag{B-37}$$

Examining equations (B-21) and (B-24) for the condition that u is zero on the surface of the ellipsoid, it is found that

$$2\alpha_o A - B\phi_{1_o} + U = 0 \tag{B-38}$$

where the subscript, o, refers to evaluation at $u_1 = 0$. Making use of (B-37) and solving for A and B, one obtains

$$A = -\frac{a^2 U}{2(a^2 \alpha_o + \phi_{1_o})} \tag{B-39}$$

and

$$B = \frac{U}{a^2 \alpha_o + \phi_{1_o}} \tag{B-40}$$

In order to determine the force on the ellipsoid, use may be made of the solution for the force on a sphere. The force on the sphere is given by the well known Stokes formula:

$$\vec{F} = 6\pi\mu R\vec{U} \tag{B-41}$$

where

μ = coefficient of viscosity, and

R = radius of the sphere.

At large distances from the ellipsoid the velocity components must approach those of the sphere at large distances from the sphere. By comparing the solutions for the velocity components of the sphere and the ellipsoid, it is possible to determine an equivalent radius for the ellipsoid. The velocity components for flow about a sphere as given by Lamb (140) are:

$$u = U + \left(B' - \frac{A'r^2}{6\mu}\right)\frac{\partial}{\partial x}\frac{x}{r^3} + \frac{2A'}{3\mu r}, \tag{B-42}$$

$$v = \left(B' - \frac{A'r^2}{6\mu}\right)\frac{\partial}{\partial y}\frac{x}{r^3}, \text{ and} \tag{B-43}$$

$$w = \left(B' - \frac{A'r^2}{6\mu}\right)\frac{\partial}{\partial z}\frac{x}{r^3} \tag{B-44}$$

where

$$B' = -1/4\ UR^3, \text{ and}$$

$$A' = -3/2\ \mu UR.$$

For large distances from the ellipsoid, u_1 becomes much greater than the semi-axes of the ellipse a, b, and c. ϕ_1 (B-19) becomes

$$\phi_1 = \int_{u_1}^{\infty} u_1^{-3/2} du_1 = 2u^{-1/2}. \tag{B-45}$$

But as u becomes large, r^2 approaches u_1, and therefore, $\phi_1 = \frac{2}{r}$.

Using the same limiting procedure ϕ_2 (B-20) becomes

$$\phi_2 = \int_{u_1}^{\infty}\left(\frac{x^2}{u_1} + \frac{y^2}{u_1} + \frac{z^2}{u_1}\right)u_1^{-3/2}du_1 = r^2\int_{u_1}^{\infty} u_1^{-5/2}du_1 = \frac{2}{3}\,\frac{1}{r}\,. \quad \text{(B-46)}$$

Using these limiting values for ϕ_1 and ϕ_2 equation (B-21) for u becomes

$$u = \frac{2}{3}A\left(\frac{3x^2}{r^5} - \frac{1}{r^3}\right) - 2B\left(\frac{x^2}{r^3} + \frac{1}{r}\right) + U. \quad \text{(B-47)}$$

Expanding the above expression, using the fact that

$$\frac{\partial}{\partial x}\left(\frac{1}{r}\right) = -\frac{x}{r^3} \qquad \text{and} \qquad \frac{\partial^2}{\partial x^2}\left(\frac{1}{r}\right) = \frac{3x^2}{r^5} - \frac{1}{r^3},$$

and comparing coefficients for the terms in $\frac{x^2}{r^3}$, one obtains

$$\frac{3A'}{6\mu} = -2B \qquad \text{or} \qquad 1/2\left(-\frac{3}{2}UR\right) = -2B$$

giving

$$R = \frac{8B}{3U}\,. \quad \text{(B-48)}$$

This R is the radius of a sphere which is equivalent hydrodynamically to the ellipsoid. Substituting (B-40) and (B-48) into the equation for the Stokes force (B-41), the force on the ellipsoidal particle is given by

$$\vec{F} = \frac{16\pi\mu\vec{U}}{\phi_{1_o} + a^2\alpha_o} = \frac{4\pi\mu\vec{U}a}{\ln 2(a/b) - 0.5} \quad \text{(B-49)}$$

In an analogous manner the force may be found when other axes are oriented along the direction of fluid flow.

As discussed by Brenner (141), the resultant resistance experienced by an ellipsoid of any orientation with respect to the flow field may be expressed as

$$\vec{F} = \mu \tilde{K} \vec{U}_o \tag{B-50}$$

where $\tilde{K}$ is the translation dyadic which for the ellipsoid is given by:

$$\tilde{K} = 16\pi \frac{\vec{i};\vec{i}}{\phi_{1_o} + a^2\alpha_o} + \frac{\vec{j};\vec{j}}{\phi_{1_o} + b^2\beta_o} + \frac{\vec{k};\vec{k}}{\phi_{1_o} + c^2\gamma_o} \tag{B-51}$$

and $\vec{U}_o$ is the uniform velocity the fluid would have in the absence of the particle.

The above relation gives the force on a stationary ellipsoid immersed in a fluid with a uniform flow $\vec{U}$ at a large distance from the ellipsoid. It is desired, however, to find the force on a particle immersed in a flow field with a linear velocity gradient. A plausible approach is to assume that the flow field can be expanded in a Taylors series about the origin (located at the center of the particle). Brenner (142) has rigorously justified the use of the Taylors expansion and has obtained

$$\vec{F} = \mu \tilde{K} \vec{U}_o + \vec{r}_o;(\nabla\vec{U})_o + \frac{(r_o r_o)}{2!};(\nabla\nabla\vec{U})_o + \cdots \tag{B-52}$$

The second term in the above expansion is zero since $\nabla\vec{U}$ is zero for an incompressible fluid. The third term and higher terms are also zero if $\vec{U}$ is assumed to be linear with respect to the spatial coordinates over the length of the TMV particle. This is true since the third and higher order terms involve second order or greater spatial derivatives. The equation for the force on a particle suspended in a uniform velocity gradient is therefore given by

$$\vec{F} = \mu \tilde{K} \vec{U}_o \tag{B-53}$$

where $\vec{U}_o$ is the value the assumed velocity field would have at the

origin if the particle were not present.

The particle immersed in a velocity gradient will also experience a torque tending to align the particle with the flow field. If it is assumed that the long axis of the particle lies along the x axis, then the torque experienced by the particle lying in the x-y plane (the plane of the velocity gradient) is

$$\vec{L} = 2\int_o^a \vec{i}x \wedge d\vec{F} \tag{B-54}$$

where

$$d\vec{F} = \mu\tilde{K}d\vec{U} = \mu\tilde{K}\left(\vec{i}\,\frac{\partial U_i}{\partial x} + \vec{j}\,\frac{\partial U_j}{\partial x}\right)dx.$$

Expanding;

$$\vec{L} = 2\vec{k}\mu\tilde{K}\int_o^a x\,\frac{\partial U_j}{\partial x}\,dx \tag{B-55}$$

where $U_j = U \sin\theta$ and θ is the angle between the x axis and the direction of propagation of the velocity gradient.

For comparison with Oberbecks solution to the forces experienced by an ellipsoid in a uniform flow field, a brief discussion of Burgers (143) application of the Oseen approximation to ellipsoids and cylinders will be given. Burgers assumes that the particle under consideration may be replaced by a system of forces distributed along the points which were originally situated on the axis of the body. He gives an expression for the components of velocity produced by these forces. The intensity of the forces are then determined by applying the boundary condition that the resultant velocity must vanish on the surface of the particle. In actual practice, Burgers requires the mean value of the resultant velocity

to vanish when taken over an arbitrary section of the surface made by a plane perpendicular to the axis under consideration. For a prolate ellipsoid with its axis along the direction of propagation of the uniform flow, Burgers deduces that the u component of velocity produced by the force, $f(\xi)d\xi$, at a point on the surface of the body, situated on the section made by a plane x = constant is given by:

$$du = \frac{f(\xi)d\xi}{8\pi\mu}\left[\frac{1}{\left\{(x-\xi)^2 + b^2\right\}^{1/2}} + \frac{(x-\xi)^2}{\left\{(x-\xi)^2 + b^2\right\}^{1/2}}\right] \tag{B-56}$$

where b is the radius of the section considered. For a cylinder, rather than an ellipsoid, b is a constant. The boundary condition on the surface of the particle requires that

$$U + u = U + \int_{-a}^{a} du = 0 \tag{B-57}$$

where U is the uniform velocity of the flow field in the absence of the particle, u is the component of the perturbed velocity along the x direction, and a is the semi-axis of the ellipsoid. When the expression for du is substituted in the above equation, an integral equation involving $f(\xi)$ is obtained which cannot be solved explicitly. Therefore $f(\xi)$ is assumed to be of the form:

$$f(\xi) = -8\pi\mu U\left[A_o + A_1(\xi/a)^2 + A_2(\xi/2)^4\right] \tag{B-58}$$

The integration in equation (B-57) can now be performed leading to:

$$2\left[A_o + A_1(x/2)^2 + A_2(x/a)^4\right]\ln 4(a^2 - x^2)/b^2 \tag{B-59}$$

$$- (2A_o - 2A_1 - A_2) - (8A_1 - 2A_2)(x/a)^2 - (31/3)A_2(x/a)^4 - 1 = 0.$$

Applying the condition that

$$\frac{x^2}{a^2} + \frac{b^2}{b_o^2} = 1 \tag{B-60}$$

where b_o is the semiminor axis of the ellipsoid. Equation (B-59) is found to be satisfied by taking

$$A_o = \frac{1}{2\ln(4a^2/b_o^2) - 2}, \quad A_1 = 0, \quad \text{and } A_2 = 0. \tag{B-61}$$

The resultant force per unit length is thus found to be

$$f(\xi) = -\frac{4\pi\mu U}{\ln 4(a/b) - 1} = -\frac{2\pi\mu U}{\ln 2(a/b) - 0.5}. \tag{B-62}$$

The total force is therefore:

$$F = -\int_{-a}^{a} f(\xi)du = \frac{4\pi\mu Ua}{\ln 2(a/b) - 0.5}. \tag{B-63}$$

which is the same as equation (B-49) determined by Oberbeck's method. For the case of a cylindrical body, Burgers replaces $\ln 4(a^2 - x^2)/b^2$ in equation (B-59) by the approximation

$$\ln 4(a/b)^2 - (x/a)^2 - 1/2\,(x/a)^4.$$

The coefficients of $(x/a)^0$, $(x/a)^2$, and $(x/a)^4$ are then equated to zero and the resulting expression solved for A_o, A_1, and A_2. The approximation leads to

$$A_o + (1/3)A_1 + (1/5)A_2 = \frac{1}{4\left[\ln 2(a/b) - 0.72\right]}$$

and

$$F = \frac{4\pi\mu Ua}{\ln 2(a/b) - 0.72}. \tag{B-64}$$

The two formulas derived for F, (B-49) and (B-64) assuming an ellipsoid or a cylinder for the shape of the particle, give results

which differ less than 7 percent for a particle with an axial ratio of 20.

2. Translational and Rotational Motion of the Ellipsoid

In equations(B-53) and (B-55) for the force and torque on a suspended particle, the velocity U is the relative velocity of the fluid medium with respect to the particle. It is necessary, therefore, to determine if the particle will move with the field or if it can be assumed to be essentially stationary. The translational motion may be investigated by applying Newton's second law to give

$$m\left(\frac{dU_p}{dt}\right) = f(U_s - U_p) \qquad \text{(B-65)}$$

where U_p is the velocity of the TMV particle, U_s is the solvent velocity and f is the frictional coefficient ($\mu\tilde{K}$). Assuming that U_s increases linearly with time over a period of about 30 nanoseconds, corresponding to the laser-induced transient, then equation (B-65) becomes

$$m\frac{dU_p}{dt} + fU_p = fkt \qquad \text{(B-66)}$$

where k is a constant. This equation may be solved using the variation of parameters technique. A solution of the form

$$U_p = A(t)e^{-(f/m)t} \qquad \text{(B-67)}$$

is assumed and substituted into equation (B-66), giving

$$\frac{dA(t)}{dt} = \frac{fkt}{m}\ e^{ft/m}. \qquad \text{(B-68)}$$

Solving for A(t) and substituting this result into (B-67)

$$U_p = k(t - m/f) + Ce^{-(f/m)t} \qquad \text{(B-69)}$$

where C is a constant of integration. Applying the initial condition that $U_p = 0$ at $t = 0$, gives

$$U_p = k(t - m/f) + (mk/f)e^{-(f/m)t}. \qquad \text{(B-70)}$$

This relation shows that when m/f is small in comparison with t the velocity of the particle is approximately equal to the velocity of the solvent. For a 3000 A^o length TMV particle m/f is found to be 7.2×10^{-11}. Therefore a single TMV particle can be assumed to follow the motion of the solvent, that is the relative velocity between the solvent and the particle may be assumed to be zero at the center of mass of the particle. In order for m/f to approach the magnitude of 30 nanoseconds the mass must increase by a factor of approximately 400. If the mass is assumed to increase due to the formation of aggregates the value of the frictional coefficient will also change depending on the form of the aggregate. Assuming spherical aggregates with a volume twice the sum of the volumes of the individual particle, the mass must be increased by a factor of approximately 10^4 in order to increase m/f by a factor of 400.

The angular velocity (ω_p) of the particle may be investigated in a similar manner. Using (B-55) let

$$I \frac{d\omega_p}{dt} = L = 2f\int_o^a x \frac{\partial U_j dx}{\partial x} \qquad \text{(B-71)}$$

where

I = moment of inertia,

$U_j = (U_s)_j - (U_p)_j$, and

U_s and U_p = the solvent and particle velocities respectively.

But $(U_p)_j = x\omega_p$ and since ω_p is independent of x for a stiff rod,

then

$$\frac{\partial(U_p)_j}{\partial x} = \omega_p. \tag{B-72}$$

On evaluating the portion of the integral containing ω_p and transferring this to the left, equation (B-71) becomes

$$I\frac{d\omega_p}{dt} + fa^2\omega_p = 2f\int_0^a x\frac{\partial(U_s)_j}{\partial x}\,dx. \tag{B-73}$$

However,

$$\frac{\partial(U_s)_j}{\partial x} = \sin\theta\cos\theta\frac{\partial U_s}{\partial x'} \tag{B-74}$$

where θ is the angle between the direction of propagation, x', of the acoustic transient and the x axis of the particle. If $\frac{\partial U_s}{\partial x}$ is assumed to be constant over a period of about 30 nanoseconds, then equation (B-73) may be written as

$$I\frac{d\omega_p}{dt} + fa^2\omega_p = fa^2Kt \tag{B-75}$$

where K is a function of x' equal to $\sin\theta\cos\theta\frac{\partial k(x')}{\partial x'}$ and where U_s was taken to be kt as in the translational case.

Equation (B-75) is identical in form to equation (B-66). On comparison with equation (B-70) the solution may be written as

$$\omega_p = K(t - I/fa^2) + (IK/fa^2)e^{-It/fa^2}. \tag{B-76}$$

The moment of inertia, I, for a rod of semi-axis, a, is given by

$$I = a^2m/3 \quad \text{and} \quad I/fa^2 = m/3f. \tag{B-77}$$

Therefore equation (B-76) becomes

$$\omega_p = K(t - m/3f) + (Km/3f)e^{-mt/3f}. \tag{B-78}$$

For m/f small, then ω_p is approximately given by:

$$\omega_p = Kt. \tag{B-79}$$

An approximate value of K may be obtained by using equations (A-21) and (A-28) derived in Appendix A. The amount of angular rotation $\Delta\theta$ is given by $1/2\ Kt^2$ which for a K of $2 \times 10^{13}/sec^2$ (evaluated for S_o of 10 atm and t of 30 nanoseconds) is found to be 9×10^{-5} radians.

The results of these calculations on the translational and rotational motion of a single TMV particle indicate that the particle may be assumed to move with the average velocity of the solvent and that the angular orientation will be essentially unaltered during the time of exposure to the acoustic transient. It should be noted that for longer pulse durations (order of 1 microsecond) such as occur in spark discharge phenomena (see page 16, Chapter I) that the particle will be completely oriented with the flow field.

APPENDIX C. THE TRANSIENT STRESS RESPONSE OF A PIEZOELECTRIC CRYSTAL

Piezoelectric substances are substances which are capable of reversibly transforming mechanical energy into electrical energy. Consider the application of an electric field, E, to a suitable cut piece of piezoelectric material such as a thin disk with conducting electrodes on the faces of the disk. For a crystal free of external stresses, a strain, X, will be produced when the electric field is applied to the electrodes of the disk. The strain is given by

$$X_k = d_{kj} E_j \tag{C-1}$$

where

X_k is the strain in the k^{th} direction,

d_{kj} is the piezoelectric strain constant, and

E_j is the electric field strength applied in the j^{th} direction.

For a clamped crystal (restrained so that no change in length is possible) the stress developed when an electric field is applied is defined by:

$$S_h = e_{hj} E_j \tag{C-2}$$

where

S_h is the stress in the h^{th} direction and

e_{hj} is the peizoelectric stress constant.

Many crystals such as quartz possess certain crystallographic axes in which the stress and strain constants are a maximum. For the study of plane compressional waves disks may be cut with faces perpendicular to these axes. X-cut quartz crystals which are of this type were used in this study. For crystals of this axial orientation the piezoelectric stress and strain constants of interest are d_{11} and e_{11}. Since these are the only constants of interest, the sub-

scripts will be dropped. The stress then becomes S = Ee and the strain, X = Ed. The transformation of mechanical to electrical responses depend on the same constants, the charge per unit area on the crystal faces being Q/A = Sd for shunted electrodes. Making use of equation (C-2) the stress associated with plane compressional waves propagating in the x direction in the transducer may be written as

$$S = c\left(\frac{\partial \xi}{\partial x}\right) - eE = c\left(\frac{\partial \xi}{\partial x}\right) - hD \qquad \text{(C-3)}$$

where

c = the elastic constant,

ξ = the displacement along the x direction,

$h = e/\epsilon$,

ϵ = the dielectric constant, and

D = the electric displacement.

The electric field may be expressed as:

$$E = -h\left(\frac{\partial \xi}{\partial x}\right) + D/\epsilon. \qquad \text{(C-4)}$$

Applying Newton's law to equation (C-3) then,

$$\frac{\partial^2 \xi}{\partial t^2} = v^2 \frac{\partial^2 \xi}{\partial x^2} - (h/\rho) \frac{\partial D}{\partial x}. \qquad \text{(C-5)}$$

But since there is no free charge inside the transducer, then by Gauss' law

$$\nabla D = 0 \qquad \text{(C-6)}$$

and for a plane wave $\frac{\partial D_y}{\partial y} = \frac{\partial D_z}{\partial z} = 0$ and therefore $\frac{\partial D_x}{\partial x} = 0$.

Equation (C-5) therefore becomes

$$\frac{\partial^2 \xi}{\partial t^2} = v^2 \frac{\partial^2 \xi}{\partial x^2} \qquad \text{(C-7)}$$

which is recognized as the one dimensional wave equation.

It is required to find the transient voltage response of a piezoelectric crystal to a stress step of amplitude S_o incident on the transducer face at time t = 0. It is assumed that the pressure pulse is incident from water and that the transducer is air backed. Let Z_1, Z_d, and Z_2 be the characteristic impedances of water, transducer and air respectively. Taking the Laplace transform (L) of (C-7)

$$\frac{\partial^2 \xi'}{\partial x^2} = (s^2/v^2)\xi' \qquad \text{(C-8)}$$

where $\xi' = L(\xi)$. The solution of (C-8) is

$$\xi' = Ae^{-sx/v} + Be^{sx/v}. \qquad \text{(C-9)}$$

The constants A and B may be evaluated by applying the boundary conditions. From equation (C-3)

$$S' = Z_d s(Ae^{-sx/v} + Be^{sx/v}) - hQ'/M \qquad \text{(C-10)}$$

where

M = area of the transducer face,

Q' = L(Q) = D'M, the charge on the transducer, and

$Z_d = \rho v$.

The stress and the displacement must be continuous at the front (x=0) and back (x=p) surfaces of the transducer. This requires that

$$(S_1)_o = (S)_o; \qquad (S_2)_1 = (S)_1 = 0 \text{ and } (\xi_1)_o = (\xi)_o \qquad \text{(C-11)}$$

where the subscripts 1 and 2 refer to water and air respectively. The constant B_2 will be equal to zero if the air is assumed to be semi-infinite in extent (no reflection). Applying conditions (C-11), then

$$A + B = A_1 + B_1 \tag{C-12}$$

$$sZ_d(-A + B) - \frac{hQ'}{M} = sZ_1(-A_1 + B_1) \tag{C-13}$$

$$sZ_d(-Ae^{-sp/v} + Be^{sp/v}) - \frac{hQ'}{M} = 0. \tag{C-14}$$

Form (C-12) - (C-14) A is found to be

$$A = \frac{-2sZ_1A_1 + (hQ'/M)\left[1 + (Z_1/Z_d - 1)e^{-sp/v}\right]}{s(Z_d - Z_1)(e^{-2sp/v} - 1)} \tag{C-15}$$

and

$$B = \frac{hQ'}{sZ_dM}e^{-sp/v} + Ae^{-2sp/v}. \tag{C-16}$$

On rearranging equation (C-15), A becomes

$$A = \frac{sA_1(1 - r_o) + (hQ'/M)\left[\frac{r_o}{Z_d}e^{-sp/v} - \frac{1}{Z_d + Z_1}\right]}{s(1 - r_oe^{-2sp/v})} \tag{C-17}$$

where

$$r_o = \frac{Z_d - Z_1}{Z_d + Z_1}.$$

Making use of equation (C-4) and noting that the voltage, V', across the crystal is equal to

$$V' = \int E'dx = -h(\xi'_p - \xi'_o) + Q'/C \tag{C-18}$$

where $C = \epsilon M/p$, the capacitance of the transducer, then

$$V' = hA(1 - e^{-sp/v}) + hB(1 - e^{sp/v}) - V'/sRC. \tag{C-19}$$

where

$Q' = -V'/sR$, and

R = the input resistance of the oscilloscope.

Substituting A and B from equations (C-17) and (C-16) into equation

(C-19) then,

$$V' = \frac{(-hS_i/Z_1)(1 - r_o)(1 - 2e^{-sx/v} + e^{-2sx/v})}{(s - a)(s - b)(1 - x)} \qquad (C\text{-}20)$$

where

$$x = \frac{(s^2 + s/RC)(r_o e^{-2sp/v}) - \frac{h^2(2Z_d + Z_1)}{Z_d R(Z_d + Z_1)M} - \frac{4Z_d e^{-sp/v}}{2Z_d + Z_1} + \frac{(2Z_d - Z_1)e^{-2sp/v}}{2Z_d + Z_1}}{(s - a)(s - b)}$$

and

$$a \text{ and } b = -1/RC \pm \left[(1/2RC)^2 + h^2(2 + Z_1/Z_d)RM(Z_d + Z_1)\right]^{1/2}$$

S_i in the above formula is the amplitude of the stress input at $t = 0$, obtained by noting that $S(0) = S_i/s = -sZ_1A_1$. The factor $(1 - x)^{-1}$ may be expanded according to the binomial expression as $1 + x + x^2 + \ldots$. where the terms containing x all refer to times greater than the time of travel for the acoustic pulse through the transducer (indicated by the occurrence of s in the exponential terms) and thus refer to reflected waves in the transducer. Since only the initial part of the transient response of the detector will be measured, the terms in x may be neglected. The equation of interest is then:

$$V' = -\frac{(hS_i/Z_1)(1 - r)}{(s - a)(s - b)} . \qquad (C\text{-}21)$$

Taking the Laplace inverse of this equation

$$V = -\left[2S_i h/(Z_d + Z_1)\right](e^{-at} - e^{-bt})/(b - a). \qquad (C\text{-}22)$$

For a and b small (about 10^{-8} per second) then

$$V = -2S_i ht/(Z_d + Z_1). \qquad (C\text{-}23)$$

This expression was derived for a step function pressure input but it may be shown that for any type of input the detector voltage is proportional to the time integral of the incident stress wave. This follows from the fact that the electric field is directly proportional to the strain (see equation C-1) giving the voltage across the detector as the space integral of the strain. Since the space profile of the strain is of the same form as the time profile of the incident stress the voltage will be proportional to the time integral of the incident stress (144).

Following the same procedure as used above in deriving equation (C-23), the stress response to a given voltage input to the transducer may be determined. The result is that the stress follows the applied voltage as

$$S = \frac{heZ_1 V}{p(Z_1 + Z_d)} \qquad \text{(C-24)}$$

where

V = the applied voltage, and

e = the piezoelectric stress constant.

The stress wave output of a given piezoelectric transducer may thus be predicted from a knowledge of the voltage input to the transducer.